analytical chemistry

Review

pubs.acs.org/ac

Fluorescence, Phosphorescence, and Chemiluminescence

Noureen Siraj,[†] Bilal El-Zahab,[‡] Suzana Hamdan,[†] Tony E. Karam,[†] Louis H. Haber,[†] Min Li,[§] Sayo O. Fakayode,[∥] Susmita Das,[⊥] Bertha Valle,[⊗] Robert M. Strongin,[○] Gabor Patonay,[#] Herman O. Sintim,[×] Gary A. Baker,[$] Aleeta Powe,[¶] Mark Lowry,[○] Jan O. Karolin,[&] Chris D. Geddes,[&] and Isiah M. Warner*[,†]

[†]Department of Chemistry, Louisiana State University, Baton Rouge, Louisiana 70803, United States
[‡]Department of Mechanical and Materials Engineering, Florida International University, Miami, Florida 33174, United States
[§]Process Development Center, Albemarle Corporation, Baton Rouge, Louisiana 70805, United States
[∥]Department of Chemistry, Winston-Salem State University, Winston-Salem, North Carolina 27110, United States
[⊥]Department of Civil Engineering, Adamas Institute of Technology, Barasat, Kolkata 700126, West Bengal India
[⊗]Department of Chemistry, Texas Southern University, Houston, Texas 77004, United States
[○]Department of Chemistry, Portland State University, Portland, Oregon 97207, United States
[#]Department of Chemistry, Georgia State University, Atlanta, Georgia 30302-4098, United States
[×]Department of Chemistry and Biochemistry, University of Maryland, College Park, Maryland 20742, United States
[$]Department of Chemistry, University of Missouri Columbia, Columbia, Missouri 65211-7600, United States
[¶]Department of Chemistry, University of Louisville, Louisville, Kentucky 40208, United States
[&]Institute of Fluorescence, University of Maryland Baltimore County, Baltimore, Maryland 21202, United States

CONTENTS

Fluorescence, Phosphorescence, and Chemiluminescence cover a wide array of topics. One can simply examine the number of topics that arise from photon induced excitation and emission as summarized in Figure 1 to understand the magnitude of this overall topic. Thus, as in previous years, we are not able to provide extensive coverage of all developments of relevance to this extremely broad area of research. Instead, we have attempted to focus on important advances of general interest and relevance to the field of analytical chemistry. In addition,

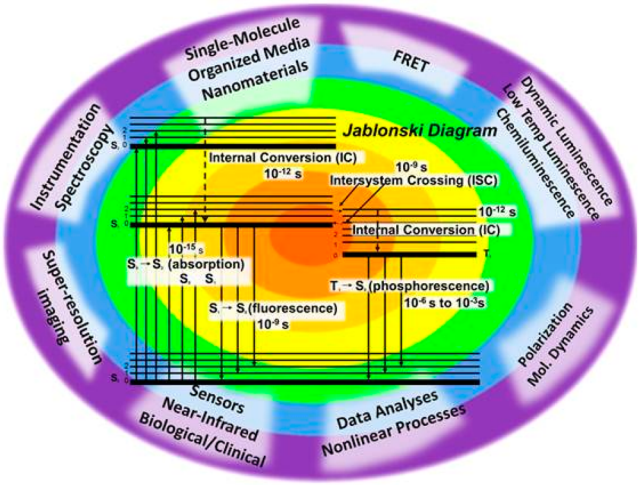

Figure 1. Jablonski diagram for photoluminescence and examples of applications.

Special Issue: Fundamental and Applied Reviews in Analytical Chemistry 2016

DOI: 10.1021/acs.analchem.5b04109
Anal. Chem. 2016, 88, 170−202

rather than cover extensions of previous advances, we have attempted to balance inclusion of a sufficient number of highly relevant, high-impact references to adequately survey the field with ample descriptions of individual citations for better clarification. If you feel that we have omitted an important article published during the above referenced time period, please forward the reference to the journal for inclusion in the next review.

As a result of a change in date for this review, this review is not in its normal biennial sequence. For that reason, this review primarily covers the past two years (June 2013 to June 2015) plus select articles since the last review in 2012.[1] A computer search of *Chemical Abstracts* provided most of the references for this review. A search for documents written in English containing the terms "fluorescence or phosphorescence or chemiluminescence" and terms used in the topics covered was used. Each section was individually screened by a single author in order to be able to capture the most important advances for a particular topic. Key word searches for each topic provided subtopics of manageable sizes. Other citations were found through individual searches by the various authors who wrote a particular section of this review. In an effort to more effectively accomplish this goal, we have included authors who are knowledgeable in the various subtopics of this review.

Coverage is limited to articles that describe new developments in the theory and practice of molecular luminescence for chemical analysis in the ultraviolet, visible, and near-infrared region. We have reorganized the various topics and included several new sections in this review. Discussions of cited work are intended to be critical and focused as in previous reviews. In general, citations are limited to journal articles and do not include patents, proceedings, reports, and dissertations. In an effort to reduce the length of this review to less than 300 citations, we have attempted to limit duplicate citations between sections by retaining the same reference number for a given citation which is cited under more than one heading. In this effort, the citation retains the number assigned for the first citation in this review.

BOOKS, REVIEWS, AND CHAPTERS OF GENERAL INTEREST

Over the last 2 years (2013−2015), a number of books can be referenced on the mechanisms, developments, and applications of fluorescence. These books are either comprehensive or tutorial and cover a broad spectrum of areas including fundamental principles and novel applications or focus on specific areas in which fluorescence techniques are employed. For example, *Introduction to Fluorescence,* edited by Jameson, introduces fundamentals of the fluorescence phenomenon and provides detailed examples of fluorescence applications in the molecular life sciences, including biochemistry, biophysics, clinical chemistry and diagnostics, pharmaceutical science, and cell and molecular biology.[2] *Fluorescence Spectroscopy and Microscopy: Methods and Protocols (Methods in Molecular Biology)* edited by Engelborghs and Visser covers topics in four broad categories: steady-state fluorescence spectroscopy, time-resolved fluorescence spectroscopy, fluorescent probe development, and the various subcategories of fluorescence microscopy, such as fluorescence recovery after photobleaching (FRAP), live cell FRET imaging (FRETim), fluorescence lifetime imaging (FLIM), fluorescence fluctuation spectroscopy (FFS), and single-molecule fluorescence spectroscopy (smFS).[3]

A number of books encompassing a variety of applications of fluorescence microscopy techniques in biological fields have also been published recently. For example, *Fluorescence Microscopy: From Principles to Biological Applications* edited by Kubitscheck provides a comprehensive introduction to advanced fluorescence microscopy methods and their applications.[4] *Fluorescence Lifetime Spectroscopy and Imaging: Principles and Applications in Biomedical Diagnostics* edited by Marcu and French explores advances in time-resolved fluorescence techniques and the role of this approach in a wide range of biological and clinical applications.[5]

Other comprehensive books of broad interest have also been published that cover fluorescence applications and fundamentals. A *Handbook of Single Molecule Fluorescence Spectroscopy* edited by Gell, Brockwell, and Smith provides discussion on the potential use of single molecule detection for nanotechnology and quantum information processing. This handbook provides an introduction to single molecule investigations using fluorescence techniques and places special emphasis on the practicalities of achieving single molecule resolution, analyzing the resulting data, and exploring applications in biophysics.[6] *Fundamentals of Fluorescence Microscopy: Exploring Life with Light* edited by Mondal and Disapro introduces optical imaging concepts and then provides considerable depth on advanced imaging systems and their applications. Additionally, these books also cover molecular orbital theory as an important basis for presenting molecular physics and gaining a complete understanding of light−matter interactions at the geometrical focus.[7] *Luminescence: The Instrumental Key to the Future of Nanotechnology* edited by Gilmore emphasizes the nanoscale semiconductor field by amalgamating a broad multidisciplinary arena including applications for energy conservation, materials performance enhancement, electronic circuitry, video displays, lighting, photovoltaics, quantum computing, memory, chemo- and biosensors, pharmaceuticals, and medical diagnostics inter alia.[8] The *Handbook of Fluorescent Dyes and Probes* edited by Sabnis provides up-to-date resource of information on more than 150 fluorescent dyes and probes. This comprehensive volume is available and covers all available dyes and probes known to date in the literature for uses in various fields.[9]

In addition to the above-mentioned books and book chapters, some useful review articles have been published since 2013, which summarize and critically review the developments and novel applications of fluorescence techniques in areas of biological, medicinal, and analytical chemistry. Coverage here is limited to a small number of reviews of broader interest. Many other reviews that focus on narrower and more specific topics are included in various sections of this manuscript. For example, a review article is reported on utilization of different single molecular fluorescence tools for development of DNA devices and for structural dynamic investigations of biomolecules and DNA molecules.[10] In a tutorial review article, recent advances made in development and applications of NIR fluorescent probes have been highlighted. This review focuses on NIR fluorescent probes that have been devised to sense various biologically important species, including ROS/RNS, metal ions, anions, enzymes, and other related species as well as intracellular pH changes.[11]

SPECIALIZED FLUORESCENCE TECHNIQUES

Many somewhat specialized fluorescence techniques are intense areas of research in the relatively recent past. However, in today's fast paced multidisciplinary research environment, these

DOI: 10.1021/acs.analchem.5b04109
Anal. Chem. 2016, 88, 170−202

same techniques are becoming quite common tools for researchers of widely varying interests and expertise. Single molecule fluorescence, fluorescence correlation spectroscopy (FCS), and Forster resonance energy transfer (FRET) are three examples of such techniques. An in depth review of each of these techniques is not possible in this relatively short section. However, some relevant reviews and advanced examples of discoveries using these tools can be found in other sections of this Review and in the literature at large. Rather than focus on various applications or specific results, this section will briefly highlight a small subset of articles and reviews that acknowledge some technical challenges in using these tools and/or offer some guidance on how results gained using these techniques can be further improved. Although these techniques are related and occasionally overlap, the discussion below is divided into three subsections: (1) single molecule fluorescence, (2) fluorescence correlation spectroscopy (FCS), and (3) Forster resonance energy transfer (FRET).

Single Molecule Fluorescence. Recent advances in commercial imaging systems have allowed the use of single molecule fluorescence as a useful tool for many researchers of varying backgrounds. One such example involves the use single molecule and single-particle fluorescence microscopy by traditionally trained synthetic chemists to investigate chemical systems by exploring the mechanisms of organic reactions, spatial distribution of chemical reactivity on surfaces, and the phase of active catalysts. In a recent Perspectives article, Cordes et al. discuss the requisite photophysical and chemical properties of fluorescent reporters and highlight the primary challenges in applying single-molecule techniques to chemical questions, with a goal of encouraging its broader use to observe chemical reactions molecule by molecule.[12]

Single molecule fluorescence microscopy has a wide range of uses, one of which involves biological investigations inside living cells with millisecond- and nanometer-scale resolution. The power of single-molecule-based methods and its increasing accessibility have led to many exciting results. However, optimizing new single-molecule experiments can be challenging, in particular when super-resolution imaging and tracking are applied to living cells. In a recent review, Haas et al. summarize common obstacles to live-cell single-molecule microscopy and also describe methods developed and applied to overcoming these challenges.[13]

Shivanandan et al. have reviewed the challenges in quantitative single molecule localization microscopy (SMLM), a highly useful tool for quantitative biological experiments ranging from molecular biology to neuroscience.[14] This review includes a discussion of applications of SMLM in quantitative biology, as well as some of the challenges involved and some solutions that have been proposed. In another work, Endesfelder et al. discuss some key principles of single-molecule super-resolution techniques; pointing out pitfalls, highlighting recent developments, and identifying opportunities for the future.[15]

Sauer and co-workers suggest that achieving super resolution is now public domain as a result of the availability of commercial instruments and open-source reconstruction software.[16] They also note that localization microscopy remains prone to user errors. For example, high emitter densities with inappropriate photoswitching rates can give rise to the appearance of artificial membrane clusters. Thus, single-molecule movies recorded to reconstruct these images must be carefully investigated when investigating membrane organization and cluster analysis. In other work, Coltharp et al. describe typical workflows and precautions for quantitative analysis of single-molecule superresolution images.[17] Their guidelines include potential pitfalls and essential control experiments.

Sage et al. report the quantitative evaluation of software packages for single-molecule localization microscopy (SMLM), noting that the quality of super-resolution images obtained by SMLM depends largely on the software used to detect and accurately localize point sources.[18] They focus on the computational aspects of super-resolution microscopy in order to devleop metrics that reflect various trade-offs of SMLM software packages in an effort to help users choose the best software for their needs.

Recent advances in single-molecule switching nanoscopy have greatly accelerated data acquisition speed and have improved temporal resolution of super-resolution imaging. However, Lin et al. noted that this technique had not been quantified as to whether an increase in speed comes with compromised image quality.[19] They provide guidelines for optimizing the factors that affect spatial and temporal resolution so that single-molecule switching nanoscopy at high speeds can achieve the same image quality as imaging at conventional speeds. In other work, Moerner and co-workers report that the rotational mobility of single molecules affects localization accuracy in super-resolution fluorescence microscopy.[20]

Long et al. have investigated the effects of fixed pattern noise (FPN) in semiconductor complementary metal oxide (sCMOS) cameras that had previously obstructed their widespread use in single molecule localization microscopy.[21] Surprisingly, they found that FPN leads to almost no effect on localization precision and that localization bias is usually <2 nm and thus can be neglected for most localization microscopy experiments.

Bleed-through or misidentification of probe species in multicolor localization microscopy is known to create false colocalization and to artificially increase certain types of correlation between two imaged species, affecting the reliability of information provided by colocalization and quantified correlation. Yet, surprisingly, the effect of bleed-through on correlation and methods for its correction had not previously been systematically studied at typical rates of bleed-through in multicolor imaging. Kim et al. recently presented a method of bleed-through correction that can be applied to all types of localization microscopy (PALM, STORM, dSTORM, GSDIM, etc.), provided the rate of bleed-through can be reliably determined.[22] In another work, McGorty et al. have described the correction of depth-dependent aberrations in 3D single-molecule localization and super-resolution microscopy.[23] They demonstrate that their method can maintain z localization accuracy over a large range of imaging depths between 0 and 2.5 μm past the coverslip.

Allen et al. have noted and addressed the importance of proper sample preparation in single molecule localization-based optical nanoscopy.[24] They have presented in-depth analyses of all aspects of sample preparation for single molecule super-resolution, including both live and fixed cell preparation, choice of fluorophore, fixation and staining techniques, and imaging buffer considerations. In a realated study, Whelan et al. have discussed potentially overlooked preparative artifacts in single molecule localization microscopy (SMLM).[25] In this study, they presented three well-optimized fixation protocols for staining microtubules, mitochondria, and actin with a discussion on various artifacts related to images obtained from samples prepared using these protocols.

DOI: 10.1021/acs.analchem.5b04109
Anal. Chem. 2016, 88, 170−202

Fluorescence Correlation Spectroscopy. Fluorescence correlation spectroscopy (FCS) is a powerful tool for accurate determination of translational diffusion coefficients. In an IUPAC Technical Report, Enderlein considered several of the most common sources of optical aberrations and their impact on the outcome of conventional FCS measurements.[26] A new variant of FCS, dual-focus FCS, which is robust against most of the considered aberrations, was also described in this report.

Sanguigno et al. noted that FCS experiments performed on flat elements, such as membranes, show unusually high relative errors as compared to experiments in aqueous solution.[27] FCS measurements on flat surfaces have generally been interpreted with certain hypotheses; the membrane is assumed to be perfectly flat, motionless, and aligned with the optical axes. The authors investigated the robustness of these hypotheses, in an attempt to understand how misalignments and thermal fluctuations affect temporal correlation of intensity fluctuation collected during measurements on membranes.

Imaging FCS using array detectors has been used to quantify the number, mobility, and organization of biomolecules in cells and organisms. However, Wohland and co-workers have noted that there have not been any systematic studies on the errors in these estimates that are introduced due to instrumental and experimental factors.[28] They further investigate the limitations that current state-of-the-art detectors place on time resolution, signal-to-noise ratio, and total measurement time. This was achieved by using a combination of simulations and experiments on lipid bilayers to provide characteristic performance parameters and guidelines that govern accuracy and precision of diffusion coefficient and concentration measurements in camera-based FCS. Guidelines are provided for an efficient experimental design for camera-based FCS to extract information on mobility, concentration, and heterogeneity.

Although FCS is a powerful tool for investigation of molecular dynamics using fluorescent proteins as molecularly specific labels, Wohland and co-workers note that FCS data analyses and interpretation using fluorescent proteins remain a challenge due to typically low signal-to-noise ratio of FCS data and correlated noise in autocorrelated data sets.[29] Fitting procedures that ignore these two important issues can provide similarly good fits for multiple competing models. Bayesian model selection accounts for the highly correlated noise that is present in FCS data sets and additionally penalizes model complexity to prevent over interpretation of FCS data. Thus, the authors applied Bayesian model selection to evaluate FCS data from fluorescent proteins assayed in vitro and in vivo. They found that Bayesian model selection was a robust procedure for determining appropriate transport and photophysical models for fluorescent proteins when suitable models are provided. In other studies, Schwille and co-workers present a graphical user interface (PyCorrFit) for fitting theoretical model functions to experimental FCS data.[30] The program features a set of tools specialized in FCS data evaluation.

FCS is typically used at nanomolar concentrations and this limitation is generally thought to be fundamentally related to the technique itself. However, Laurence et al. report that the limitation to nanomolar concentrations is not fundamental but instead due to detector limits as well as laser fluctuations.[31] Use of a high count rate detector system and application of laser fluctuation corrections allowed FCS measurements up to 38 μM with the same signal-to-noise as at lower concentrations without the need for nanoconfinement approaches previously used to increase the concentration range of FCS.

Forster Resonance Energy Transfer. The physical process of Förster resonance energy transfer (FRET) was elucidated more than 6 decades ago and has since become a powerful tool for biomedical research. A wide range of FRET approaches have been described with each having corresponding advantages and disadvantages. Ma et al. have recently reviewed FRET applications in protein studies.[32] They summarize the basic components of FRET techniques, established quantification methods, as well as potential pitfalls and illustrated all of these by example applications.

Conjugation between streptavidin (SA) and biotin has been widely used to link donors and acceptors for investigating distance-dependent FRET, but a contradictory finding has recently been reported that FRET of a common system of (QD-SA)-(biotin-DNA-dye) (donor, quantum dot (QD); acceptor, small organic fluorescent dye; and linker, deoxyribose nucleic acid (DNA) molecule via SA-biotin conjugation) lost its dependence on the number of DNA base pairs when using a phosphate-buffered saline (PBS) solution. Thus, Saremi et al. have reported a re-evaluation of biotin streptavidin conjugation in FRET applications in an effort to resolve these conflicting results.[33] They have found that the conflict was caused by the ionic strength of the adopted buffer solutions. FRET was found to lose the DNA length dependence at relatively high ionic strengths.

Warner and co-workers have recently explored the FRET phenomena in organic nanomaterials for potential applications in sensor and optoelectronic devices.[34] In this regard, special types of organic salts with relatively low melting points, given the acronym Group of Uniform Material Based of Organic Salts (GUMBOS), are employed. Two cyanine-based GUMBOS of variable methane chain length were used to synthesize binary nanomaterials (nanoGUMBOS). FRET between binary cyanine nanoGUMBOS of altered methane chain exhibited emission in the visible to near-infrared region of the electromagnetic spectrum, demonstrating potential applications in optoelectronics. These binary organic nanomaterials also exhibited high thermal- and photostability. Moreover, this approach demonstrated that tuning emission spectra produced by use of FRET can be easily achieved by changing the mole ratio of donor and acceptor during nanomaterials formation. In another study from this group, carbazole based GUMBOS were synthesized that displayed intramolecular FRET.[35] These carbazole-based GUMBOS exhibited multiple emissions from the second excited singlet state (S_2), first excited singlet state (S_1), as well as from an intramolecular charge transfer state. This study suggests a significant overlap between the S_2 emission and S_1 absorption such that intramolecular FRET is observed.

Ensemble FRET results can be analyzed in a variety of ways, and due to experimental artifacts, the results obtained from different analyses are not always consistent. In an effort to determine optimal analysis for use in nanodrop fluorometry, Kelliher, et al. performed both ensemble and single-molecule studies of FRET on oligomers of double-stranded DNA and compared the single-molecule results to those obtained using various ensemble FRET analyses.[36] It was found that analyzing the increase of acceptor fluorescence is less likely to introduce errors, as compared with analyzing the fluorescence intensity of the donor in the absence and presence of the acceptor. In another study, Kruger et al. describe single molecule FRET data analysis procedures for FRET efficence determination.[37] They outline the parameters needed for FRET efficiency

DOI: 10.1021/acs.analchem.5b04109
Anal. Chem. 2016, 88, 170−202

calculation and illustrate that the shape of the FRET distribution changes depending on what parameters are included in the data analysis procedure using single molecule FRET data obtained on G-quadruplex DNA structures that exhibit large conformation diversity.

Alternating-laser excitation (ALEX) combined with single-molecule FRET has been found to be a power technique to study biological interactions. Hohlbein et al. recently presented a comprehensive overview of the concept and current applications of ALEX. They discuss how to obtain fully corrected distance information across the entire FRET range and present new ideas for applications of ALEX which they claim will push the limits of single molecule FRET-based experiments in terms of temporal and spatial resolution for the study of complex biological systems.[38]

Finally, Cho et al. have used FRET to devise a rapid, general and cost-efficient super-resolution imaging method which can be directly employed using a simple fluorescent imaging system with general fluorophores.[39] Fluorescent donor molecules that label specific target structures are stochastically quenched by diffusing acceptor molecules, thereby temporally separating otherwise spatially overlapped fluorescence signals and allowing super-resolution imaging. The authors expect that the new method will be an attractive option for super-resolution imaging due to the simplicity of the approach.

Imaging and Super-Resolution Imaging (Conventional and Lifetime). A series of fluorophores has been reported that undergoes two-photon excitation at ∼900 and emits in the red wavelength region (≥600 nm). These dyes afford relatively diminished autofluorescence and solvent sensitivity. One of the new probes enables in vivo imaging of amyloid-β plaques in an Alzheimer's disease mouse model.[40] In other recent research involving Alzheimer's, a curcumin analogue dubbed CRANAD-3 was synthesized that is capable of detecting both soluble and insoluble Aβ species. This embodies a unique example of near-infrared fluorescence used in monitoring Alzheimer's disease therapy. This in vivo imaging technology will thus also enable drug development.[41]

Zhou and co-workers have reported a ratiometric two-photon fluorescent probe for imaging living cells and tissues in real time using a through-bond energy transfer (TBET) strategy. This probe consists of naphthalene and rhodamine derivatives linked via π-conjugation. In live cells and tissues, the probe exhibits excellent ratiometric imaging resolution and deep-tissue imaging depth (180 μm).[42] A unique two-photon probe method for targeted imaging of live pancreatic islet cells was recently reported. The probe, TP-α, was used successfully for 3D imaging of live islets via direct staining of alpha cells.[43]

A cyclooxygenase-2 (COX-2)-specific fluorescence probe (ANQ-IMC-6) has been designed and synthesized to image cancer cells and Golgi-related events. COX-2 is an enzyme biomarker in virtually all cancer cell lines. The quenched probe unfolds and strongly fluoresces upon binding COX-2 in the Golgi apparatus of cancer cells. The differentiation of tumor and normal cells via flow cytometry as well as via one- and two-photon fluorescence imaging, has been demonstrated.[44] A promising approach for detecting tumors during surgery has been reported employing functionalized single-walled carbon nanotubes (SWNTs). SWNTs exhibit intrinsic fluorescence in the second-window near-infrared NIR2 spectral region. In the cited study they enabled a gynecological surgeon to identify and excise submillimeter tumors. In comparison to conventional NIR dyes, the functionalized SWNT material exhibited improved S/N and photostability as well as better tumor-to-background uptake.[45]

McCarley and co-workers have recently synthesized a novel probe based on trimethyl-locked quinone propionic acid (Q_3PA) attached via linker to a naphthalimide for cellular imaging of a cancer enzyme.[46] An overexpressed cancer enzyme present in the cytosol of human tumor cell, NAD(P)H/quinone oxidoreductase-1, selectively reduces Q_3PA and produced bright emission of naphthalimide (reporter) which is used to image cancer cells. The quantum yield of the reporter, formed after reduction by the cancer enzyme, is 95 times more fluorescent than the probe. In another study, the turn on fluorescent probe based on a naphthalimide derivative was synthesized for rapid and selective imaging of biological thiols composed of glutathione, cysteine, and homocysteine.[47]

Tumor pH-sensitive magnetic nanogrenades (termed PMNs) have been developed and used as cancer theranostic agents. PMNs are comprised of self-assembled iron oxide nanoparticles and pH-responsive ligands. They target tumors via surface-charge switching triggered by the acidic tumor microenvironment. In acidic subcellular compartments, they are in a highly active state that turns on MR contrast, fluorescence, and photodynamic therapeutic activity. Therapeutic efficacy was achieved in heterogeneous drug-resistant tumors.[48] In another example of probes possessing both MR and optical imaging modalities, the Meade group synthesized multimeric contrast agents possessing three Gd(III) chelates and an IR-783 dye. Biodistribution of a PEGylated derivative resulted in observable fluorescence in xenograft MCF7 tumors and renal clearance via MR imaging.[49]

A new theranostic prodrug that undergoes hydrogen peroxide-mediated boronate oxidation features activation of a fluorophore for detection and release of the anticancer agent, SN-38. The prodrug showed effective antitumor activity in a mouse model of metastatic lung disease. This technology is proposed for use in imaging and treatment of metastatic tumors, as these characteristically possess high levels of reactive oxygen species.[50]

Gold quantum dots exhibit potentially favorable optical and magnetic properties as compared to gold nanoparticles. However, biocompatibility and aqueous stability issues have limited their use in imaging. New silica encapsulated gold quantum dots have been synthesized that are called "quantum rattles." They are stable in aqueous solutions, and cytotoxicity studies are promising. In vivo studies show that they lead to improved drug delivery and reduced tumor burden via photothermal therapy. They couple three imaging modalities: near-infrared fluorescence, photoacoustic, and magnetic resonance imaging.[51]

The RAF serine/threonine kinases regulate cell growth through the MAPK pathway. It is known that protein multimers play a role in RAF activation and tumor responses to RAF inhibitors. However, the stoichiometry and cellular location of specific protein multimers involved in RAF activation have not been reported previously. Nan and co-workers used photo-activated localization microscopy (PALM) along with quantitative spatial analysis to directly visualize protein multimers in cells. This study embodies direct confirmation of the existence of RAF dimers and higher-order multimers as well as their involvement in cell signaling.[52]

The prediction of photophysical properties of fluorophores for superresolution microscopy has been addressed via a new stochastic approach. This method allows enumeration of

DOI: 10.1021/acs.analchem.5b04109
Anal. Chem. 2016, 88, 170−202

fluorophores in simulated data and determination of the kinetic rates governing stochastic photophysics.[53] A Rosetta-based computation was used to design a fluorophore ligase that accepts the red dye resorufin. The resorufin ligase catalyzes a site-specific covalent attachment of resorufin to various cellular proteins in mammalian cell lines and in primary cultured neurons. This enables specific imaging of cellular proteins by conventional, as well as superresolution, microscopies.[54]

A challenge in superresolution microscopy is imaging the 3D nanoscale morphology of an entire cell. Multifocus microscopy for volumetric multicolor superresolution imaging was simultaneously images nine focal planes and captures the distribution of single molecules. The superresolution imaging of 3D organization was demonstrated with the mammalian mitochondrial network and yeast microtubules during cell division.[55] Another current challenge in super-resolution microscopy is quantitative mapping and characterization of biomolecular species that reside deep inside cells, such as the nucleus. A reflected light-sheet superresolution microscopy method enables imaging inside the mammalian nucleus and molecular counting with single-copy accuracy. The investigators used this technology to probe the spatial organization of transcription by RNA polymerase II molecules and to quantify the extent of their nuclear clustering.[56]

Superresolution imaging of various nanocatalysts has been shown to afford unique understanding of single particle spatiotemporal fluctuations and reactivity patterns. The knowledge gained from such studies guides the design and synthesis of superior heterogeneous nanocatalysts.[57] Quinoxaline-based semiconducting polymer dots (Pdots) were reported that exhibit near-infrared fluorescence, ultrahigh brightness, large Stokes shifts, and cellular targeting capability with low cytotoxicity. The average per-particle brightness is at least 6 times higher than commercial quantum dots. The utility of these Pdots was demonstrated via an in vivo microangiography imaging study using living zebrafish embryos.[58] In a related study, the authors describe squaraine-based semiconducting polymer dots narrow bandwidth, high QY, and large Stokes shifts.[59]

Bright cyan and orange luminescent proteins (nanolanterns) have been developed for imaging. These proteins enable multicolor imaging of the rapid dynamics of endosomes and peroxisomes, the slow dynamics of focal adhesions, and the simultaneous monitoring of multiple gene expression or Ca(2+) dynamics in different cellular compartments in a single cell.[60] In a rare example of the application of advanced imaging and analytical tools to quantitatively measure pathogenicity in vivo, a unique approach for the investigation of host−pathogen processes based on medium-throughput 3D fluorescence imaging was developed. This technology was used for analysis of Shigella infection in a large tissue volume, including observation of the targeting of colonic crypts of the guinea pig colonic mucosa. This enables visualization of host−pathogen interactions during the progression of infection in a robust, versatile manner.[61]

The Glass group has recently reported the design of tunable fluorescent molecular logic gates for direct visualization of neurotransmitter trafficking. These gates are designed to afford a turn-on fluorescence response upon corelease of glutamate and zinc from secretory vesicles via exocytosis.[62] Chang and co-workers have reported the use of a turn-on probe to image labile iron(II) in live cells. This probe enables visualization of changes in iron stores upon iron supplementation or depletion and can be used to monitor reversible dynamics of iron pools with vitamin C stimulation or via the hormone hepcidin.[63]

INSTRUMENTATION AND LASER BASED FLUORESCENCE TECHNIQUES

Lasers have become integral components of many experimental techniques aimed at detailed investigations of fluorescence from samples. In this section, we focus primarily on samples in solution, such as fluorophores dissolved in a solvent or nanoparticles in colloidal suspension. Related topics including fluorescence-based microscopy or fluorescence from gas-phase samples can be found in a previously reported review.[64] Standard fluorescence measurements, whereby a sample is optically excited and the resulting emitted luminescence spectrum is detected, can often be accomplished using relatively low-intensity light conditions provided by a lamp, often coupled with a grating-based monochromator for wavelength selection of the excitation. However, laser-based methods are often used when greater optical excitation intensities are required, such as in cases of nonlinear fluorescence measurements, or when ultrafast temporal resolution of the fluorescence response is needed.

We use fluorescence and photoluminescence interchangeably to refer to both emission processes in this section. Photon−matter interactions can be described by linear and nonlinear optical processes. Nonlinear optical processes can be described by use of nonlinear contribution to polarization of a sample caused by an intense incident laser beam. Nonlinear fluorescence is a powerful technique for investigating the emission from excited-states that are not accessible with steady-state fluorescence measurements. Additionally, the emission intensity in time-resolved emission spectroscopy of a fluorophore is monitored at different time delays after excitation using laser pulses with short temporal pulse widths, allowing for precise temporal resolution. Evaluation of the fluorescence decay lifetimes provided valuable information on excited-state dynamics and molecular interactions with the surrounding environment. The nonlinear emission techniques can also be successfully implemented in microscopy investigations.[65] However, in this review we focus our discussion on ultrafast fluorescence measurements and nonlinear fluorescence spectroscopy of samples in solution.

When light interacts with a sample, such as molecules or materials, the electric field of the light $\tilde{E}(t)$ produces a polarization of the sample $\tilde{P}(t)$ given by a generalized equation,

$$\tilde{P}(t) = \chi^{(1)}\tilde{E}(t) + \chi^{(2)}\tilde{E}^2(t) + \chi^{(3)}\tilde{E}^3(t) + \ldots = \tilde{P}^{(1)}(t) + \tilde{P}^{(2)}(t) + \tilde{P}^{(3)}(t) + \ldots \quad (1)$$

where, $\chi^{(1)}$ is the linear or first-order susceptibility, while $\chi^{(2)}$ and $\chi^{(3)}$ are the second-order and third-order susceptibilities, respectively. The terms $\tilde{P}^{(1)}(t)$, $\tilde{P}^{(2)}(t)$, and $\tilde{P}^{(3)}(t)$ are the first-order, second-order, and third-order polarizations, respectively. In principle, this power series continues to additional higher-order terms that are usually negligibly small. Under low light intensities, this process is normally completely dominated by first-order or linear spectroscopic interactions such that polarization of the sample is linearly proportional to the incident optical electric field and the overall number of photons absorbed or scattered is linearly proportional to the incent optical intensity, where the intensity is proportional to the optical electric field squared. However, under higher intensity

DOI: 10.1021/acs.analchem.5b04109
Anal. Chem. 2016, 88, 170−202

light, or in samples with larger higher-order susceptibilities, the second-, third-, or higher-order optical interactions are not negligible and may even provide a substantial optical signal.

First-order polarization of a sample can either scatter at the incident optical frequency or absorb a single photon energy leading to an excited state of the sample that relaxes back to the ground state by either radiative or nonradiative processes. Likewise, second-order polarization of the sample can either scatter at twice the incident optical frequency, in a process known as second harmonic generation,[66,67] or the sample can absorb the energy corresponding to two incident photons leading to a higher excited state of the sample and subsequent relaxation to the ground state through radiative and nonradiative processes. Second-order and higher-order optical processes are nonlinear processes and comprise the field of nonlinear spectroscopy.

Two-photon absorption is a nonlinear process induced by intense laser radiation where two-photons of equal or different energies can be simultaneously absorbed causing an electronic excitation to an excited-state. Nonlinear fluorescence processes typically require pulsed laser sources with sufficient intensity to induce a two- or multiphoton excitation. Once two-photon or multiphoton absorption occurs, the fluorescence spectra can be acquired in the normal way using a spectrometer and a detector, and the parameters of the sample or excitation source such as the relative concentrations, laser power, or laser wavelength can be varied for systematic investigations of the light-sample interactions.

Additional information on nonlinear fluorescence signals can be obtained using emission anisotropy measurements.[68] In addition to angular distribution of the emission dipole direction of the molecule or material, the anisotropy parameter also contains information on the lifetime of the excited state, as long-lived excited states have more time to reorient toward a more isotropic distribution before emission takes place. The same process can be used for measuring the anisotropy from nonlinear fluorescence, where the excitation can be a two-photon multiphoton absorption. As an example, multiphoton induced emission anisotropy have been performed on biological molecules.[69] These measurements can provide valuable insight into the characteristics and properties of molecules, proteins, and DNA molecules since the emission is very sensitive to the environmental and conformational changes of these molecules.

Ultrafast fluorescence spectroscopy has been widely used for study of fluorescence processes at femtosecond to nanosecond temporal resolution. This can be accomplished through use of a single pulsed laser, where time-resolved fluorescence is measured using various detection methods such as time-correlated single photon counting[70] and streak camera,[71] with temporal resolutions on the order of picoseconds to nanoseconds.

A new ultrafast fluorescence spectroscopic technique has been recently reported, which is inspired from frequency-resolved optical gating (FROG) and transient grating spectroscopy methods. This technique provides the advantage of broadband detection of optical Kerr gating and low backgrounds, based on creating a transient grating with an ultrafast probe pulse that diffracts the fluorescence time-resolved detection.[72] The optical setup consists of a femtosecond laser beam that passes through a beam splitter to separate the pump and probe beams with a optical delay line for controlling the pump−probe temporal delay. The pump pulse excites the sample, leading to fluorescence emission, while the probe beam is split into two beams that focus on a Kerr gating medium. The generated photoluminescence light is then overlapped with the two ultrafast gate pulses in the $\chi^{(3)}$ Kerr gating medium, where the refractive index is modulated by the optical Kerr effect, leading to the diffraction of the signal for time-resolved detection with ultrafast temporal resolution.

Various nonlinear and ultrafast fluorescence processes can be investigated using intense pulsed lasers. Nonlinear fluorescence is used to probe two-photon or multiphoton induced processes in various samples. Nonlinear anisotropy experiments provide complementary measurements for the study of molecular orientation and rotational dynamics of various fluorophores. Additionally, ultrafast fluorescence spectroscopy can be used to probe the excited-state relaxation processes with ultrafast temporal resolution in various samples for applications such as nanomedicine, solar energy, and optoelectronics.

Nonlinear Emission Processes in Fluorescence Spectroscopy. Nonlinear emission responses of fluorophores and fluorescent nanoparticles provide valuable information about relevant spectroscopy, excited-states, conformational properties, and photodynamics, including excited-state relaxation, electron transfer, and energy transfer dynamics from a wide variety of samples. Nonlinear emission can be investigated for samples in solid-state,[73] biological tissue,[40] and colloidal suspensions.[74] In this section, we focus our discussion and review on important experimental results of nonlinear emission processes from various samples in solution, including organic molecules in solution, dissolved polymers, ionic liquids, biological materials, and colloidal nanoparticles. Techniques such as two-photon fluorescence, multiphoton fluorescence, and up-conversion fluorescence will be discussed, along with corresponding anisotropy measurements. Time-resolved measurements will also be discussed, including time-resolved up-conversion fluorescence, two-pulse emission modulation measurements, time-resolved fluorescence anisotropy, and transient absorption. These measurements provide valuable insights into the excited-state dynamics, charge and energy transfer, conformational dynamics, and optical gain of these samples for advances in potential applications such as photonics, drug delivery, cancer therapy, photovoltaics, and optoelectronics.

In the nonlinear optical process of two-photon induced photoluminescence, according to eq 1, the signal will depend on the square of the incident light intensity. Therefore, two-photon fluorescence signals typically grow quadratically as a function of the incident excitation light intensity. For this reason, two-photon fluorescence and other nonlinear spectroscopic investigations are often performed using intense pulses of light, with excitation pulse widths usually on the nanosecond to femtosecond time scales. By varying the excitation wavelength, nonlinear spectroscopy, including two-photon absorption and two-photon fluorescence, of a wide range of samples can be studied in detail to understand the molecular interactions under intense incident light. As an example, a series of studies on the two-photon absorption properties and subsequent two-photon fluorescence of a series of cyanoacetic acid triphenylamine derivatives in toluene were recently reported.[75] Here, the electron donor groups employed are the triphenylamine moiety, cyanoacetic acid moiety as electron acceptor groups, and vinylene or phenylethyne as the π-bridge. It has been shown that the two-photon absorption cross section is affected by the length of the π conjugation chain in the infrared region, which leads to enhanced two-photon excited fluorescence. Additionally, comparing the one-photon induced fluorescence to corresponding two-photon induced fluorescence,

DOI: 10.1021/acs.analchem.5b04109
Anal. Chem. 2016, 88, 170−202

along with the corresponding one-photon and two-photon absorption spectra, allows for a more detailed understanding of a molecule's interactions with light. Spectral shifts often occur between linear and nonlinear responses due to different spectroscopic symmetry, selection rules, and Franck−Condon factors. These studies can provide information on how nonlinear optical response varies with sample composition and can set the stage for additional time-resolved nonlinear optical measurements for determining the quantum mechanical energy relaxation dynamics in molecules and materials.

Nonlinear fluorescence measurements also provide detailed spectroscopic information for investigations on a variety of different nanoparticle samples in colloidal suspension. A recent study on plasmonic nanoparticles reports on the effect of various solvents on two-photon fluorescence of gold nanorods.[76] These measurements were performed in different organic solvents such as DMF, DEG, CH_3OH, C_2H_5OH, CH_3CN, DMSO, and DMF and the results were compared to gold nanorods in water. Here it was observed that two-photon induced emission is significantly quenched in organic solvents compared to water. Figure 2 is a plot of relative intensity of the two-photon

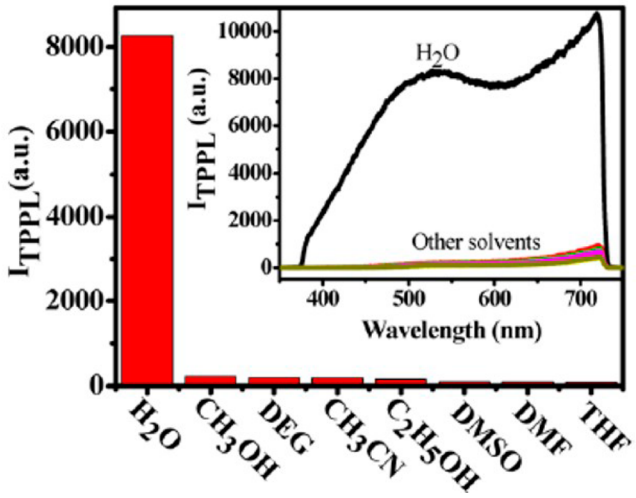

Figure 2. Relative intensity of two-photon fluorescence peaks of gold nanorods dispersed in various solvents. Inset: Two-photon fluorescence spectra of gold nanorods dispersed in water and the other organic solvents under study. Reproduced from Zhao, T.; Jiang, X.-F.; Gao, N.; Li, S.; Zhou, N.; Ma, R.; Xu, Q.-H. *J. Phys. Chem. B* **2013**, *117*, 15576−15583 (ref 76). Copyright 2013 American Chemical Society.

fluorescence spectra of gold nanorods dispersed in different solvents. Such measurements often enable subsequent measurements, such as transient absorption studies or time-resolved fluorescence measurements, which allows investigators to determine the mechanism for quenching or enhancements in nanoparticle samples. Here, time-resolved transient absorption measurements determined that electron transfer from the gold to the polymer is the primary process that leads to the fluorescence quenching. Nonlinear fluorescence measurements provide important nonlinear optical characterizations for a wide variety of nanomaterials.

In recent years, great interest has emerged regarding lanthanide-doped colloidal nanoparticles for potential applications in biological imaging and single molecule tracking. When excited using near-infrared radiation, these doped nanoparticles emit stable luminescence in the visible spectrum through the nonlinear process called up-conversion, which is strong, stable corollary to two-photon fluorescence. The narrow and spectrally pure emission of up-converting $NaYF_4$ nanocrystals can be achieved through multiple doping with lanthanide ions.[77] Through this method, it is possible to develop different doped nanoparticles with controlled, spectrally pure up-converted emission spectra. Figure 3 is a display of the emission spectra

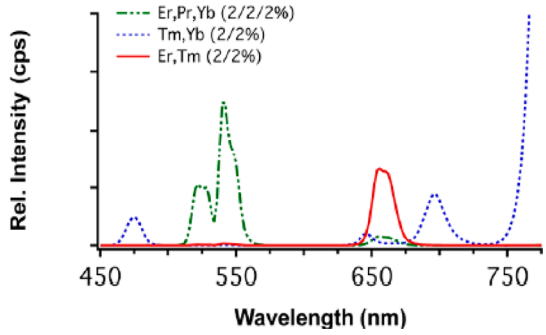

Figure 3. Emission spectra of $NaYF_4$ nanocrystals doped with Er^{3+}/Pr^{3+}/Yb^{3+} (2/2/2 mol %), Ym^{3+}/Tb^{3+} (2/2 mol %), and Er^{3+}/Tm^{3+} (2/2 mol %). Reproduced from Chan, E. M.; Han, G.; Goldberg, J. D.; Gargas, D. J.; Ostrowski, A. D.; Schuck, P. J.; Cohen, B. E.; Milliron, D. J. *Nano Lett.* **2012**, *12*, 3839−3845 (ref 77). Copyright 2012 American Chemical Society.

of lanthanide doped-$NaYF_4$ nanocrystals after excitation with 980 nm pulses. The spectrally pure and highly tunable emission achieved is via different energy transfer pathways between different lanthanide ions doped into the nanoparticle crystal matrix, which makes these nanomaterials suitable for diverse optical applications. The effect of varying the temperature on the up-conversion emission of Er-doped single-crystal perovskite $PbTiO_3$ nanofibers was also investigated,[78] where the high tetragonality and spontaneous polarization of perovskite can be controlled by changing the temperature. This method allows for additional control of the intensity of the luminescence. These lanthanide-doped nanoparticles can be studied and optimized for biological imaging applications using nonlinear fluorescence spectroscopy.

Time-resolved fluorescence is a widely used technique for study of chemical, structural, and electronic dynamics in a variety of samples such as proteins, molecular dyes, and nanomaterials. In time-resolved fluorescence, an excitation pulse, often from an ultrafast laser, provides sample excitation, and the fluorescence signal or spectrum is measured as a function of the delay time. Temporal resolution faster than the excited-state lifetime is needed to track the evolution of the signal strength, spectrum, or anisotropy on the appropriate time scale. Several instrumental techniques can be implemented for these measurements, including time-correlated single-photon counting and time-dependent fluorescence up-conversion. Time-resolved fluorescence up-conversion was used to investigate the dynamics of higher-lying excited-states in cyanine dyes to probe energy transfer from cyanine excited-states only accessible through two-photon excitation for applications in two-photon photosensitizers.[79] Here, the time-resolved fluorescence signal is up-converted in a nonlinear crystal using a probe pulse for subpicosecond temporal resolution of the fluorescent signal. It was shown that these dynamics strongly depend on the dye structure and the conjugation length.

DOI: 10.1021/acs.analchem.5b04109
Anal. Chem. 2016, 88, 170−202

Time-resolved fluorescence up-conversion was also used to investigate the dynamics of carrier recombination at the surface of CdS_xSe_{1-x} nanocrystals.[80] These nanocrystals possess a quasi-type-II electronic band alignment characterized by confinement of only a single carrier. This process hinders charge recombination due to formation of surface trap states, which can reduce fluorescence quantum yields. The temporal delay between excitation of the carriers and beginning of emission from the nanocrystals known as rise time τ_{rise}, provide valuable information on the surface charge trapping. Figure 4a

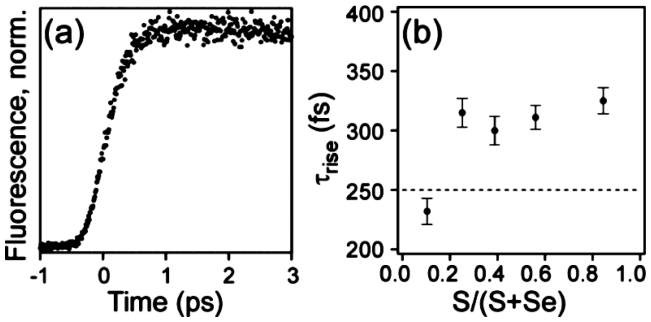

Figure 4. (a) Fluorescence upconversion time-profiles of $CdS_{0.39}Se_{0.61}$. (b) The rise time obtained from the time-resolved upconversion measurements of CdS_xSe_{1-x} nanocrystals at different sulfur composition. Reproduced from Keene, J. D.; McBride, J. R.; Orfield, N. J.; Rosenthal, S. J. *ACS Nano* **2014**, *8*, 10665−10673 (ref 80). Copyright 2014 American Chemical Society.

shows a representative fluorescence upconversion time profile of $CdS_{0.39}Se_{0.61}$. The change in τ_{rise} at different sulfur composition of the nanocrystal is illustrated in Figure 4b. By increasing the sulfur composition, the hole-trapping process was eliminated and an increase in the hole relaxation lifetime to the valence band is observed.

Gold nanorods and coupled gold nanospheres exhibit strong two-photon induced emission[81] that can be utilized in numerous applications such as two-photon sensing and imaging. However, more information on the mechanism behind this strong two-photon photoluminescence is essential for development and optimization of such applications. Femtosecond two-pulse emission modulation spectroscopy was used to further investigate these phenomena.[82] It was shown that decay times for the profiles of the cross contribution are 4.0 ± 0.2 ps and 3.1 ± 0.1 ps for gold nanorods and coupled gold nanospheres, respectively. These values are in agreement with the lifetimes of the intermediate states obtained from time-resolved transmittance measurements. These results prove that strong two-photon induced emission is due to sequential absorption of two-photons from the ground-state to the excited-state mediated by a real intermediate state. Figure 5 is a time profile obtained from two-pulse emission modulation of coupled gold nanospheres obtained by spatially and temporally overlapping two femtosecond laser beams centered at 800 nm.

Time-resolved fluorescence anisotropy is another powerful method to probe energy transfer dynamics between fluorophores at different molecular orientations. Here, the fluorescence anisotropy is measured using an up-conversion nonlinear crystal using a probe beam, at different polarizations. Ultrafast fluorescence up-conversion anisotropy was used to investigate the solvent-dependent energy transfer in different dendrimers composed of triarylamine groups connected by triazole linkers.[83] These measurements show that the anisotropy

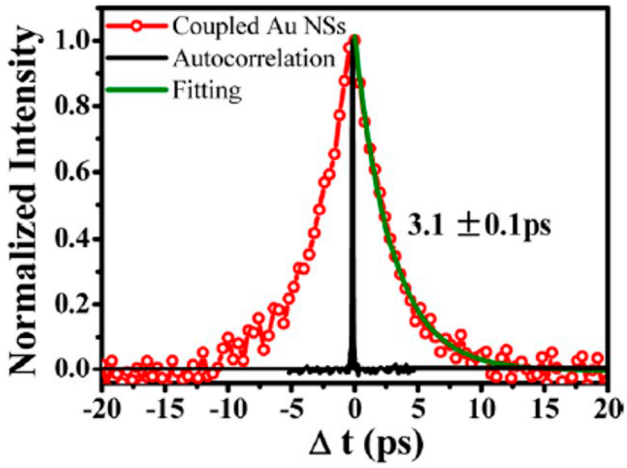

Figure 5. Time-profile obtained from the two-pulse emission modulation measurements of coupled gold nanospheres. Reproduced from Jiang, X.-F.; Pan, Y.; Jiang, C.; Zhao, T.; Yuan, P.; Venkatesan, T.; Xu, Q.-H. *J. Phys. Chem. Lett.* **2013**, *4*, 1634−1638 (ref 82). Copyright 2013 American Chemical Society.

decay is controlled by the two competitive processes of solvation effect and incoherent energy transfer between the different dendrimer branches.

The implementation of pulsed lasers allows for study of nonlinear optical phenomena that are not accessible with normal, continuous light sources. Nonlinear emission is widely used as the basis of various spectroscopy techniques such as two-photon fluorescence, multiphoton fluorescence, and up-conversion fluorescence, along with corresponding anisotropy measurements. These powerful techniques can be employed to investigate the nonlinear emission response of various materials such as organic fluorophores, polymers, molecules in the gas phase, solid-state samples, and nanomaterials. Nonlinear emission spectroscopy in colloidal samples is used to investigate the properties of various organic and polymer materials, nanomaterials, ionic liquids, and biological materials. The different spectroscopy techniques used are essential for characterization of excited-states phenomena that are not accessible by steady-state emission studies. Additionally, fluorescence anisotropy is used to probe the conformational changes of molecules and polymers. Time-resolved spectroscopy, including time-resolved upconversion, two-pulse emission modulation, and time-resolved fluorescence anisotropy measurements using femtosecond excitation pulses offers valuable tools to study the excited-state decay dynamics in various systems. These nonlinear and time-resolved fluorescence measurements provide fundamental studies on the excited states and dynamics of molecules and nanomaterials for developing new applications in fields such as nanomedicine, molecular sensing, photovoltaics, and optoelectronics.

TOTAL LUMINESCENCE AND SYNCHRONOUS EXCITATION SPECTROSCOPIES AND RELATED TECHNIQUES

Total luminescence (TL) and synchronous fluorescence spectroscopy (SFS) have garnered tremendous activity over the past 2 years, resulting in a large number of research articles published in this area. Total luminescence spectroscopy monitors intensity as a function of many experimental parameters, including excitation and emission wavelengths, the polarization

DOI: 10.1021/acs.analchem.5b04109
Anal. Chem. 2016, 88, 170−202

(both linearly and circularly polarized light), and luminescence decay time.

In many articles, the basic forms of TL spectra are often termed as an excitation emission matrix (EEM) or a three-dimensional spectrum. Total luminescence provides rich information about excited states, molecular interactions, and microenvironments. Synchronous fluorescence spectroscopy (SFS) is a measure of fluorescence intensity through synchronous scanning of both the excitation and emission monochromators.

Pavitra et al. have synthesized a series of Dy^{3+} ion single-doped and Dy^{3+}/Eu^{3+} ion codoped white-light emitting SrY_2O_4 nanocrystalline phosphors using a citrate sol−gel method. The cathodoluminescence (CL) spectra confirmed that the penetration depth is inversely proportional to the total atomic weight and atomic number of the compound. Measurement of cathodoluminescence (CL) spectra confirmed that the penetration depth is inversely proportional to the total atomic weight and atomic number of the compound.[84]

Lu et al. have prepared monodispersed, nanometer-size, periodic mesoporous organosilicas for effective screening of drugs and therapeutic protocols for diseases. These multi-fluorescent nanoparticles have intrinsically different and finely tunable pore surface polarities governed by the type and amount of fluorophore inside the framework.[85]

Some spectroscopy and imaging techniques have proved valuable for early detection of cancer. For example, the Miroslay group used EEM and total SFS of normal and malignant breast tissue specimens to serve as data inputs in the development of a Support Vector Machine (SVM) based diagnostic tool. Various input combinations were tested for classification accuracy using SVM prediction against histopathology results. Using SFS data, SVM provided 100% sensitivity and specificity for several data input combinations.[86] Also, based upon SFS, the group reported differences in the luminescence responses of pigmented human skin and nonpigmented human skin. The differences in fluorescent characteristics were more distinct in SFS spectra than in conventional emission and excitation spectra.[87]

Rajasekaran et al. characterized and distinguished urine samples from normal and cancer patients via use of SFS. Different ratio parameters were calculated from the values of synchronous luminescence spectra and the parameters were used as input variables for a multiple linear discriminant analysis across normal and cancer groups. The stepwise analysis classifies 90.3% of the original grouped cases correctly.[88]

Abdel-Aziz et al. used beta-cyclodextrin and Calix(8)arene as fluorescence enhancers in a novel SFS technique to quantify benzo(a)pyrene in contaminated water samples. The method showed a detection limit of 380.00 pg/mL, which is well below the maximum level set by the Environmental Protection Agency.[89]

During this review period, much research has been done on detection of metals in various matrices. For example, Change et al. found that the photoluminescence (PL) of 11-mercaptoundecanoic acid (11-MUA)-protected gold nanodots (Au NDs) was highly dependent on capping ligands and the ligand density. Because PL of the Au NDs-ligand species increased upon increasing the ligand density and chain length, they could be used as probes for detection of total mercury ions (organic and inorganic).[90]

Wang et al. have synthesized luminescent hybrid porous polymers (LHPP) with high thermal stability that could be used as sensors for chemical explosives. Their luminescent properties were quenched by nitroaromatic explosives and could be tuned by altering the reacting species and reaction conditions.[91]

LUMINESCENCE TECHNIQUES RELEVANT TO BIOLOGICAL AND CLINICAL MEASUREMENTS

Various luminescent techniques for detection of cells or biological analytes have been introduced during this review period. As one example, chemiluminescence-based techniques have been reported for detection of several bioanalytes. Zhang and co-workers have developed an interesting rolling circle for amplification-induced detection of DNA methyltransferase.[92] Ju et al. have used an array-based chemiluminescence imaging method to detect protein targets in a high-throughput format. In this regard, they used a proximity-dependent DNAzyme to produce chemiluminescent signals.[93] Ultrasensitive detection of DNA, via chemiluminescence, has been reported by Li and Gao.[94] These authors combined exonuclease-assisted signal amplification and a carbon nanotube-assisted background reduction approach to facilitate sensitive detection of DNA. Chemiluminescence resonance energy transfer has also been used to detect various analytes. Wu and co-workers have developed an immunoassay for detection of the ovarian cancer biomarker, CA-125, via chemiluminescence resonance energy transfer to graphene quantum dots.[95] Bi et al. have reported single-nucleotide polymorphism detection based on ligation chain reaction and utilizing chemiluminescence resonance transfer imaging on magnetic particles.[96]

During this review period, several fluorescent dyes and probes have been developed for bioanalyte detection or imaging. Li et al. have developed a new near-infrared fluorescence probe, with emission greater than 700 nm, for detection of nitroreductase in zebrafish.[97] Divalent zinc ion is known to play an important role in biology, including neurotransmission, apoptosis, and cellular metabolism. Therefore, there is great interest in probes that can detect zinc in biological environments. The Lippard group has reported a reaction-based fluorescent sensor for detection of mobile Zn^{2+}.[98] In addition, Peng et al. have reported detection of Zn^{2+} by use of dye-assembled up-conversion nanoparticles.[99]

Many luminescent techniques have been developed for preoperative cancer imaging, e.g., radiodiagnosis with 18-Fluorine-[100] or Technetium (99 mTc)-[101]based probes. In contrast, only a few intraoperative imaging techniques exist for cancer detection in real time. Real time intraoperative detection of breast cancer has been achieved by Tummers et al. using a near IR fluorophore, i.e., methylene blue.[102] Using indocyanine green, Yuen and co-workers have demonstrated detection of sentinel lymph nodes as well as lymphatic vessels during open prostatectomy.[103] Metildi and co-workers have reported use of activatable cell penetrating peptides (ACPPs) in fluorescence-guided surgery of pancreatic cancer using orthotopic mouse models.[104] Yano et al. have developed a telomerase-specific oncolytic adenovirus (OBP-401) that expresses green fluorescent protein (GFP) and have used this GFP-expressing adenovirus to label pancreatic cancer for fluorescence-guided surgery in a mice tumor model.[105]

LOW-TEMPERATURE LUMINESCENCE

Low-temperature luminescence and related studies continue to be areas of active research during this review period. This is

DOI: 10.1021/acs.analchem.5b04109
Anal. Chem. 2016, 88, 170−202

evidenced by the number of quality publications since the last review. Many papers involving the utility of low-temperature luminescence and related studies for characterization of lanthanide and actinide transition elements, inorganic and organic complexes, and rare-earth ion doped materials were published. Novel stannate phosphors, orthorhombic $CaSnO_3$ phosphors doped with Er^{3+}, Nd^{3+}, and Sm^{3+} were synthesized by conventional solid-state methods a under N_2/H_2 gas flow and subjected to visible and near-IR photoluminescence (PL) studies.[106] The dopant ions were observed to be incorporated well into $CaSnO_3$ and are responsible for PL emissions in the temperature range of 10−300 K. The observed PL peaks at 490, 546, 656, 696, 894, 1065, and 1344 nm for $CaSnO_3$:Nd^{3+} phosphor was ascribed to the f−f transition of Nd^{3+} ion. Emissions at 564, 600−607, 646−656, and 714 nm were detected for $CaSnO_3$:Sm^{3+} samples. The strongest emission, observed at 600 nm, was ascribed to $^4G_{5/2} \rightarrow {}^6H_{7/2}$ of Sm^{3+}. Emission lines at 528, 548, 662, and 852 nm were also observed for $CaSnO_3$:Er^{3+}, corresponding to Er^{3+} intra4f^n shell transitions. In a related study, the influence of temperature on PL properties of $LiMgPO_4$ doped with Eu^{3+} and Eu^{2+} has been published.[107] Luminescence emission was observed to be highly dependent on the excitation wavelength. Two broad PL emission bands, peaking at 380 and 490 nm were also observed. These emissions were related to $4f^65d^1 \rightarrow 4f^7$ (8S7/2) luminescence of Eu^{2+} and to europium-trapped excitation, respectively, and/or to several sharp lines between the 580 and 710 nm region, ascribed to the 5D0 → 7FJ (J = 0, 1, 2, 3 and 4) transitions in Eu^{3+}. Increased temperature was also observed to increase intensity of the Eu^{2+} luminescence. It was also reported that the charge compensation mechanism for Eu^{3+} and Li^+ as well as Eu^{2+} replacing Li^+ in the $LiMgPO_4$ is a long distance compensation that allowed for the existence of some of the europium ions either as Eu^{3+} at low temperature or as Eu^{2+} at high temperature. It was concluded that Eu^{2+} in the Li^+ site with long distance compensation yields only $4f^65d^6 \rightarrow 4f^6$ luminescence. In contrast, Eu^{2+} in the Li^+ site with short distance compensation yields $4f^65d^6 \rightarrow 4f^6$ luminescence and europium-trapped exciton emission.

A novel compound, dysprosium-based multifunctional ionic liquid crystals, has been synthesized and its spectral properties at various temperatures have been characterized.[108] The influence of phase transitions on luminescence as a result of changes in temperature for this dysprosium based ionic liquid crystal has also been studied. Luminescence characteristics of two emission transitions (4F9/2 to 6H15/2 and from 4F9/2 to 6H13/2) at various temperature (20−100 °C) were investigated. The change in luminescence intensity at different temperatures was categorized into three groups: (i) solid crystalline state, (ii) liquid crystalline state, and (iii) isotropic liquid state, which shows change in phase (Figure 6).

The unusual red phosphor, $Sr_2P_2O_7$:Bi^{2+}, exhibiting luminescence properties at low (10−300 K) and high (300−500 K) temperatures was reported.[109] Incorporation of Bi^{2+} ions into $Sr_2P_2O_7$ resulted in the emissions at ∼660 and ∼698 nm at room temperature and are encoded, as Bi(1) and Bi(2) due to the substitutions for two different crystallographic sites, i.e., Sr(1) and Sr(2), respectively, in the compound. At lower dopant concentrations, a preferential substitution into Sr(2) sites partially due to size matching was observed. On the contrary, more Bi^{2+} ions were found to occupy the Sr(1) sites at higher concentrations, resulting in distinct changes of emission intensity ratios of Bi(2) to Bi(1). Increased environmental

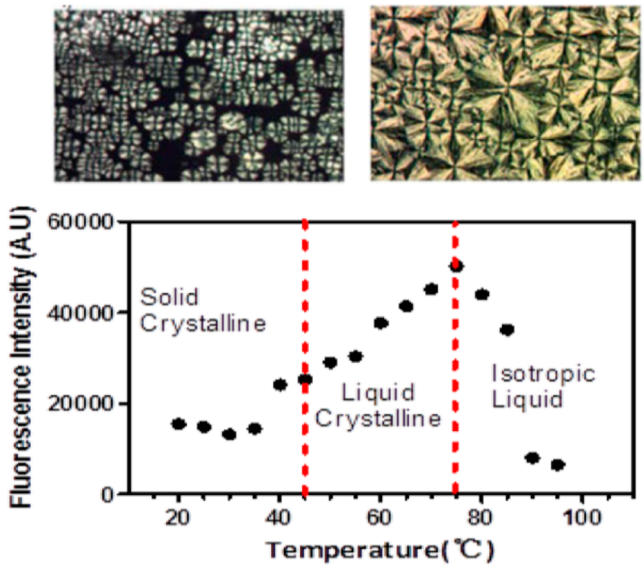

Figure 6. Temperature-dependent luminescence intensity from 4F9/2 to 6H15/2 transition (blue light emission, excitation at 366 nm) of [(−)EphC16H33]5 [Dy(SCN)8] ionic liquid crystal in ethanol and their micrographs obtained from polarized optical microscope. Reproduced from Lu, C.; Das, S.; Siraj, N.; Magut, P. K. S.; Li, M.; Warner, I. M. *J. Phys. Chem. A* **2015**, *119*, 4780−4786 (ref 108). Copyright 2015 American Chemical Society.

temperatures also resulted in increased thermal quenching, which was suppressed by increasing the Bi^{2+} concentration. The Bi(1) emission at ∼660 nm showed antithermal-quenching, particularly, at higher temperatures, with blue shift of the overall emission band and almost no change in lifetimes. This study is envisioned as promoting a future design of heavily doped phosphors for white light emitting diodes (WLEDs) with better resistance to thermal quenching. In a related study, the result of color-tunable luminescent organoclay-based hybrid materials, with potential applications in WLED and thermosensors was reported.[110] These hybrid composites (both as powder and transparent film) were prepared by simple mixing of an organic sensitizer, aminoclay (a.c.), and lanthanide (Ln^{3+}) in aqueous solution and subjected to PL analysis. It was observed that the emission color of a compound can be fine-tuned by changing various parameters, including the molar ratio of Eu^{3+} to Tb^{3+}, the excitation wavelength, and the temperature. The study resulted in white light with satisfactory color coordinates. The emission intensity ratio of the $^5D_4 \rightarrow {}^7F_5$ transition (Tb^{3+}) to the $^5D_0 \rightarrow {}^7F_2$ transition (Eu^{3+}) of the composite containing both Eu^{3+} and Tb^{3+} was also observed to be linearly related to temperature at 78−288 K. These characteristics make the composite particularly suitable for optoelectronic devices such as thermosensors and WLEDs.

Another study has reported on thermoluminescence (TL) spectral properties of samples of natural albite, $NaAlSi_3O_8$ in Brazil.[111] The mineral was a solid solution of K-feldspar (4600 ppm, K) and Ca-feldspar (1100 ppm, Ca). The TL spectra of natural and preannealed albite at high temperatures showed a very intense band around 275 nm and weaker bands around 400 and 560 nm. Other TL properties were investigated through monochromatic (275 and 400 nm) glow curves. The electron paramagnetic resonance (EPR) spectrum measured at low temperature (77 K) showed the typical 11 lines signal due to an Al−O^-−Al center superposed on the Fe^{3+} signal

DOI: 10.1021/acs.analchem.5b04109
Anal. Chem. 2016, 88, 170−202

around g = 2.0. However, the EPR spectra above 260 K showed only the g = 2.0 signal due to the Fe^{3+} ions. The results of temperature dependent PL of MgZnO epitaxial layers with high Mg content was investigated to gain a better insight of the influence of carrier localization on PL dynamics was published.[112] The result of the study showed a double blue-shift of the PL peak position with increases in temperature. The randomly distributed carrier localization centers in the MgZnO films resulted in two energy separated Gaussian-shape density-of-states tails in the vicinity of the fundamental band gap edge. The filling of these tail states by the thermally activated carriers with increased temperature resulted in a temperature-induced double blue-shift of the PL peak position. Magnesium content and crystal structure of the MgZnO epitaxial layers were observed to have considerable influence on double blue-shift of the PL peak position.

Layered rare-earth terbium hydroxides (NO_3-LTbH) co-doped with Gd^{3+} (NO_3-LTbH:Gd) also prepared by hydrothermal method using modified sensitizers (L) were reported.[113] Compared with the NO_3-LTbH precursor, the sensitizer-modified NO_3-LTbH:Gd was found to exhibit high luminescence intensity and high luminescence quantum efficiency (Φ = 33%) due to the synergistic effect of codoped Gd^{3+} and intercalated sensitizers in the organic−inorganic hybrid materials. The results of the study indicated that the synergistic effect of significant Tb^{3+} luminescence enhancement was caused by Gd^{3+} inducing a cascaded energy transfer from the host to Tb^{3+} via organic sensitizers. The LTbH:Gd was also observed to have multiple roles, including energy-transfer bridges that connect the sensitizers and Tb^{3+} (in host) to enhance the characteristic emission of Tb^{3+} and the phosphorescence of sensitizers, while also act as host matrixes for the sensitizers. A $SrWO_4$ single crystal was successfully synthesized using the Czochralski pulling method.[114] Luminescence spectrum under X-ray excitation of a bulk $SrWO_4$ single crystal was observed to show a broad emission band from 300 to 700 nm at room temperature. The decay time spectrum was reported to contain two components of 2.6 ns (5.7%) and 522 ns (94.3%) at room temperature. A change in the light yield and decay time was observed between 10 and 300 K. Most importantly, the luminescence yield of $SrWO_4$ at 125 K was found to be 8 times higher than at room temp. It is of significant interest to note that the $SrWO_4$ decay time gets longer by a factor of 51 as the temperature decreases down to 10 K.

In another study, luminescence properties of the promising cryogenic scintillator Li_2MoO_4 were investigated in the temperature region of 2−300 K during this review period.[115] In this study, the Li_2MoO_4 single crystals were grown using the conventional Czochralski method and the low-temperature gradient Czochralski technique. The bandgap of Li_2MoO_4 was established using the luminescence excitation and reflectivity spectra. Three luminescence bands with the maxima at 1.98, 2.08, and 2.25 eV were observed in the emission spectra of Li_2MoO_4 crystals. Two high-intensity peaks were also observed at 22 and 42 K in the thermoluminescence curves of both studied crystals due to the thermal release of self-trapped charge carriers. The coexistence of self-trapped electrons was believed to be the major factor responsible for poor scintillation light yield of Li_2MoO_4 at low temperatures. The first observation of low temperature luminescence of CoO crystals under synchrotron irradiation was also reported.[116] At 8 K, the PL of CoO was characterized by smaller bandwidth and higher intensity relative to the corresponding PL band of NiO. Interestingly, the PL excitation spectra of CoO and NiO were found to be identical. The position of the band related to charge transfer from oxygen ions to the 3d-shell of cobalt ions was also determined, with the excitation energy observed to be 3.5 eV.

In another study, sulfide and oxysulfide bulk glasses Ga−La−S−O, Ge−Ga−S, and Ge−Ga−As−S doped, or codoped, with various rare-earth (RE^{3+}) ions was investigated for their room temperature transmission and low-temperature PL.[117] Photoluminescence spectra were collected using external excitation into the Urbach tail of the fundamental absorption edge of the host glass. The results from this study indicated that low temperature PL spectra were dominated by the broad-band luminescence of the host glass, with relatively sharp superimposed emission bands due to radiative transitions within 4f shells of RE^{3+} ions. The dips in the host glass luminescence due to 4f−4f up-transitions of RE^{3+} ions were also observed in the Ge−Ga−S and Ge−Ga−As−S systems, providing direct experimental evidence of energy transfer between the host glass and respective RE^{3+} dopants.

The use of low temperature PL for optical characterization of several nanoparticles, nanomaterials, carbon nanotubes, and quantum dot materials has also attracted considerable attention. For example, results of temperature-dependent luminescence of structurally precise $Au_{25}(SC_8H_9)_{18}$ and $Au_{38}(SC_{12}H_{25})_{24}$ monolayer-protected cluster (MPC) nanoparticles at low temperature ranging from 4.5 to 200 K following electronic excitation using 3.1 eV pulsed lasers have been published.[118] The integrated PL intensity for $Au_{25}(SC_8H_9)_{18}$ was observed to be highly temperature dependent. A considerably high increase of approximately 70% PL intensity was observed as the sample temperature increased from 4.5 to 45 K. The PL intensity was also found to be statistically invariant for temperatures between 45 and 65 K. However, PL was quenched at temperatures >65 K. Quantitative analysis of PL emission energies and peak widths obtained at sample temperatures >45 K indicated that MPC nonradiative relaxation dynamics are mediated by coupling to low-frequency vibrations associated with the ligand shell that passivated the nanoclusters, which accounted for the low emission yields at high sample temperatures. Contributions from two different vibrational modes were further observed: Au(I)−S stretching (200 cm^{-1}) and Au(0)−Au(I) stretching (90 cm^{-1}). In addition, the magnitude of electronic−vibration coupling was observed to be state-specific and consistently larger for the high-energy portions of the PL spectra. The PL of single-wall carbon nanotubes with a varying spectral profiles ranging from ultranarrow lines in suspended nanotubes to broad and asymmetry line shapes at low temperature was also reported.[119] This study provided a complete set of PL profiles in matrix embedded nanotubes including unprecedented narrow emission lines. It was also reported that the diversity of the low temperature luminescence profiles in nanotubes originated in tiny modifications of their low-energy acoustic phonon modes. It was also reported that when low-energy modes are locally suppressed, a sharp photoluminescence line as narrow as 0.7 meV is restored. Multipeak luminescence profiles with specific temperature dependence also showed the presence of confined phonon modes.

In another study, hydride vapor phase epitaxy (HVPE) was utilized to grow low-defect GaN.[120] The undoped films were grown on sapphire and was subsequently subjected to steady-state and time-resolved PL analysis. One of the observed

DOI: 10.1021/acs.analchem.5b04109
Anal. Chem. 2016, 88, 170−202

dominant PL bands in high-quality GaN grown by HVPE was the green luminescence (GL) band, with a maximum at 2.4 eV. This PL band was easily recognized in time-resolved PL measurements due to its exponential decay even at low temperatures (<50 K), with a characteristic lifetime of 1−2 μs. The PL lifetime for the GL band was reported to increase by an order of magnitude as the temperature increases from 70 to 280 K. The authors explained this unusual phenomenon on the assumption that the electron-capture coefficient for the GL-related defect decreases with temperature as $T^{-2.6}$.

A ligand-assisted reprecipitation strategy for fabrication of brightly luminescent and color-tunable colloidal $CH_3NH_3PbX_3$ (X = Br, I, Cl) quantum dots with absorption quantum yield up to 70% at room temperature and low-excitation fluencies has been described.[121] The quantum dots average diameter size was found to influence the PL quantum yield of quantum dots. For example, $CH_3NH_3PbBr_3$ quantum dots of average diameter 3.3 nm were observed to have a more intense PL quantum yield than the corresponding micrometer-sized bulk particles (2−8 μm). This observation was due to the increase of exciton binding energy as a result of size reduction and proper chemistry passivation of the Br-rich surface. Wide-color gamut WLEDs using green emissive $CH_3NH_3PbBr_3$ quantum dots and red emissive K_2SiF_6:Mn^{4+} as color converters were also fabricated to further provide enhanced color quality for display technology. The colloidal $CH_3NH_3PbX_3$ quantum dots are expected to exhibit interesting nanoscale excitonic properties, with potential practical applications in lasers, electroluminescence devices, and optical sensors

Photoluminescence studies of $CdSiO_3$:Cr^{3+} (1−9 mol %) nanophosphor was also synthesized by a low-temperature solution combustion technique and subjected to low PL analysis.[122] The PXRD results revealed that the samples produced well formed with monoclinic crystals. With the average crystallite sizes established by Scherrer's method, Williamson−Hall (W−H) plots and size-strain plot were found to be in the range of 20−45 nm, with the energy band gap range of 5.42−5.47 eV. The nanophosphor PL analysis showed an intense emission peak at 691 nm for the excitation wavelength of 361 nm, corresponding to $^2E_g \rightarrow {}^4A_{2g}$ transition of the R-line of chromium. Racah parameters were used to describe the effects of electron−electron repulsion within the crystal lattice. The PL intensity was found to increase with increased in Cr^{3+} concentration. The highest PL intensity was observed from the 7 mol % doped sample. However, a decrease in PL intensity due to cross relaxation as result of concentration quenching was observed with further increases in Cr^{3+} concentration. The chromaticity coordinates and correlated color temperatures of all the phosphors were also observed to be located in the red region, with a high potential for the fabrication of the red component of WLEDs.

Low-temperature synthesis and characterization of microstructural, morphologic, and optical properties of Mn-doped ZnO nanorod array films via chemical bath deposition on glass substrates was also reported.[123] X-ray diffraction patterns showed sharp, intense peaks, demonstrating the highly crystalline nature of the film. Energy dispersive X-ray (EDAX) and scanning electron microscopy (SEM) were further utilized to confirm the presence of Mn^{2+} ions in ZnO nanorods. Scanning electron microscopy analysis suggested that Mn-doped ZnO nanorods were well aligned and distributed throughout the surface. A room- temperature PL showed the presence of one broad defects-related band in the visible region in the range 440−640 nm. In another study, low-temperature luminescence, luminescence excitation, and luminescence imaging spectroscopies were explored to investigate the optical and electronic properties of GaAs/AlGaAs quantum well tube (QWT) heterostructured nanowires (NWs).[124] The result of the study indicated that GaAs QWTs with widths >5 nm have electronic states which are delocalized and continuous along the length of the NW. However, a decrease in the NW QWT width from 5 to 1.5 nm resulted in only a single electronic state bound to the well, with no optical excitations to a confined excited state. These quantum-dot-like states broaden at higher temperatures and quench at temperatures >80 K. The lifetimes of these localized states were also observed to vary from dot to dot from 160 to 400 ps. The study concluded that the presence of delocalized states and then localized states as the QWTs become more confined, may provide opportunities and challenges for possible incorporation into quantum-confined device structures.

A two-step strategy for synthesis and fabrication of 3D flower-like Co_3O_4 hierarchical microstructures, from 3D flower-like α-$Co(OH)_2$ microstructures assembled by hexagonal porous nanoplates was published.[125] The 3D flower-like α-$Co(OH)_2$ microstructures were synthesized by use of a facile surfactant-free low temperature hydrothermal process and fabricated by annealing the obtained 3D flower-like α-$Co(OH)_2$ microstructures. The results of X-ray diffraction and Raman spectrum analyses have revealed that the hierarchical microstructures formed from 3D flower-like α-$Co(OH)_2$ microstructures are composed of pure cubic phase Co_3O_4. However, SEM analysis showed Co_3O_4 microstructures to exhibit 3D flower-like hierarchical structures assembled by hexagonal porous nanoplates. Photoluminescence study indicated that these novel 3D flower-like Co_3O_4 hierarchical microstructures displayed a strong broad emission in the visible range of 650 to 800 nm with a peak at around 710 nm (1.75 eV), which was very close to the indirect optical band gap of 1.60 eV for a Co_3O_4 thin film. The results of this study further showed that the PL emission likely originates from an indirect optical band gap emission. The broad PL emission was associated with a wide size distribution of porous nanoplates in 3D hierarchical microstructures. Accordingly, these 3D flower-like Co_3O_4 hierarchical microstructures, with unique optical properties, will likely have applications in visible light emitting materials.

Investigation of low temperature PL of several organic compounds and transition element organic complexes also generated considerable interest during the review period. For example, the luminescence of high-quality solvent-free PCBM ([6,6]-phenyl-C_{61}-butyric acid Me ester) crystals between room temperature and 4 K was reported.[126] The PL spectra of PCBM crystals were observed to become increasingly well-structured as the temperature is lowered, with extremely well-resolved emission lines (and a minimum line width of ∼1.3 meV at 1.73 eV). The observed structured emission was attributed to a vibronic coupling model such as Franck−Condon, Jahn−Teller, and Herzberg−Teller effects. It was also reported that the optical transitions are not formally forbidden from the low-lying excited states of PCBM. However, the high symmetry of the electronically active fullerene core limits the intensity of the 0−0 transition. The simulation studies also suggested that the emissive state of PCBM can be considered as a mixture of the T_{1g} and H_g excited states of C_{60}. Consequently, the H_g state was reported to play a more considerable role in the relaxed excited state of PCBM than in that of C_{60}. In another study, the

DOI: 10.1021/acs.analchem.5b04109
Anal. Chem. 2016, 88, 170−202

reported synthesis of a series of three Pt(II) complexes with doubly cyclometalating terdentate ligands L1, $L1H_2$ = 3,6-bis-(*p*-anizolyl)-2-carboranyl-pyridine, with di-Et sulfide (1), triphenylphosphine (2), and *t*-butylisonitrile (3) as ancillary ligands forming organic light emitting diodes was published.[127] X-ray diffraction studies of 1 and 2 show coordination of the L1 ligand in a C−N−C mode in which the bulky and rigid o-carborane fragment was cyclometalated via a C atom. The new Pt(II) pincer complexes displayed very high luminescence quantum yields at decay times of several tens of microseconds even in solutions under ambient conditions. Using the low temperature (T = 1.3 K) emission decay behavior, the emission was assigned to a ligand centered triplet excited state (^{3}LC) with small metal-to-ligand charge-transfer singlet and triplet (^{1,3}MLCT) admixtures. Phosphorescence was observed to be quenched by molecular oxygen. Therefore, optical sensors operating under a wide range of oxygen pressures can be developed. The new materials can also have potential utility as emitter materials for diverse optoelectronic applications because of their high luminescence quantum yields.

Dynamic Luminescence Measurements. Over the past review period, dynamic luminescence measurements have generated considerable new research in many areas including, but not limited to, bioimaging techniques, proteins dynamics, luminescence lifetimes, and quenching mechanisms. In this regard, various luminescent nanoscale probes have been explored for advancing in vivo imaging of biological entities. Near infrared-emitting long-persistent luminescent nanoparticles (LPLNPs) $Zn_{2.94}Ga_{1.96}Ge_2O_{10}:Cr^{3+},Pr^{3+}$ were synthesized via a citrate sol−gel method combined with calcination, for long-term in vivo tumor imaging.[128] These luminescent nanoparticles exhibit a high signal-to-noise ratio and deep tissue penetration without the need for excitation during imaging. An intense near-infrared emission and a long-lived afterglow (over 15 days) distinguish these biocompatible nanoparticles from persistent luminescent nanoscale counterparts.[128] Lanthanide-doped luminescent upconversion nanoparticles were also synthesized for imaging biological tissues.[129,130] The design of Nd^{3+}-sensitized upconversion core−shell nanoparticles was efficient in minimizing the laser-induced overheating effect, usually observed in Yb^{3+}-doped upconversion nanoparticles. This structural design allows for energy transfer from Nd^{3+} (sensitizer excited at 795 nm) to Yb^{3+} and Yb^{3+} to the activator A^{3+} (Tm, Er, Ho), while maintaining a spatial separation between Nd^{3+} in the shell and A^{3+} in the core of nanoparticles.[129,130] Advanced noninvasive in vivo imaging was achieved through improvement of spatio-temporal resolution in fluorescence microscopy, where ultra-thin light sheets from 2D optical lattices were introduced into the microscope.[131] This technique was applied to imaging of various intracellular dynamic processes with a reduced level of photobleaching; these nanoscale processes include three-dimensional tracking of microtubule growth during mitosis, cellular processes during the development of embryos, and cell−cell or cell−matrix interactions (Figure 7).

Single-molecule fluorescence imaging exhibits an amplified signal when employing a SunTag system to recruit 24 copies of green fluorescent proteins (GFP) coupled with antibodies to a polypeptide.[132] To test the tagging system in gene transcription, a nuclease-deficient mutant of Cas9 protein (dCas9) was first labeled with SunTag and coexpressed with antibody-GFP for imaging. SunTag was then fused with the herpes virus transcriptional activation domain VP16 and a subsequent strong activation of gene expression was observed.[132] In a different approach, single-molecule fluorescence spectroscopy was used to study the folding mechanisms of α-helical proteins.[133,134] The transition path time and the folding time were experimentally measured using a photon-by-photon analysis of fluorescence trajectories and a measurement of Forster resonance energy transfer (FRET) efficiencies of the dye-labeled protein. It was shown that the kinetics of folding and unfolding processes are affected by parameters such as temperature, pH, and viscosities of media.[133,134] Protein conformational changes were monitored by incorporating the fluorescent amino acid acridon-2-ylalanine (Acd) into proteins expressed in *Escherichia coli*.[135] Studies of fluorescence lifetimes of Acd showed that it is quenched by tryptophan and tyrosine through a photoinduced electron transfer (PET); however, Acd can also act as a Forster resonance energy transfer (FRET) acceptor from tryptophan and 7-methoxycoumarinylalanine (Mcm) fluorophore. PET, FRET, and luminescence resonance energy transfer (LRET) between Acd and Eu^{3+} lanthanide were all used as tools to monitor protein folding and binding interactions.[135] Detection of protein−peptide interactions in live bacteria was enabled by using a luminescent probe (DBT-2EEGWRESAI) which consists of two tax-interacting protein-1 (TIP-1)-specific ligands (EEGWRESAI) and one 4,7-di-(thiophen-2-yl)-2,1,3-benzothiadiazole (DBT) molecule, bound using a "click" chemistry.[136] The probe fluoresces via a turn-on mechanism in the far-red/near-infrared (FR/NIR) region upon interaction with protein (TIP-1) and polyprotein (ULD-TIP-1 tetramer). In this study, DBT fluorescence is activated due to the hydrophobic microenvironment provided by the self-assembly of the probe−protein complex into spherical or network-like nanoscale assemblies.[136]

Rapid measurement of luminescence lifetimes in the microsecond region has been performed on polystyrene microspheres encapsulated with lanthanide-complexes and coumarin salt.[137] Luminescence resonance energy transfer (LRET) occurs between the acceptor dye (coumarin) and Eu^{3+} lanthanide complex donor. The lanthanide lifetimes are tuned by modifying the dye−lanthanide distance, thereby creating

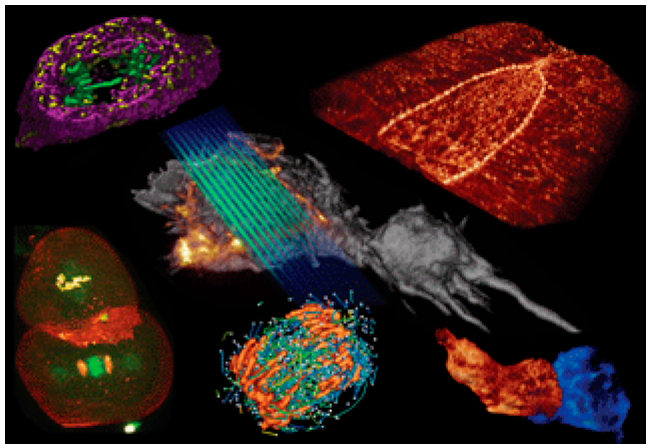

Figure 7. Lattice light-sheet microscopy. An ultrathin structured light sheet (blue-green, center) excites fluorescence (orange) in successive planes as it sweeps through a specimen (gray) to generate a 3D image. The speed, noninvasiveness, and high spatial resolution of this approach make it a promising tool for in vivo 3D imaging of fast dynamic processes in cells and embryos, as shown here in five surrounding examples. Reproduced with permission from AAAS (ref 131).

DOI: 10.1021/acs.analchem.5b04109
Anal. Chem. 2016, 88, 170−202

time-domain suspension arrays. These arrays were applied for simultaneous detection of different pathogen DNA single strands by conjugating Eu-LRET microspheres with different lifetimes to the target DNAs.[137] A time-correlated single-photon counting (TCSPC) board has been developed to concurrently record the decay of intrinsic fluorescence related to oxidized flavine adenine dinucleotide (FAD) and the phosphorescence decay from the oxygen sensitive ruthenium-complex K_{r341}, in living cells.[138] The TCSPC technique (TCSPC board TimeHarp 260) was integrated into fluorescence and phosphorescence lifetime imaging (FLIM/PLIM), a tool highly useful for tissue analysis. In this approach, the presence of dopamine induces protein binding and causes a decrease in FAD fluorescence lifetime; however, dopamine increases the phosphorescence decay time of K_{r341} loaded in cells due to oxygen consumption.[138] These luminescence lifetime studies proved that multiplexing concepts are feasible in the presence of a mixture of fluorophores as long as the luminescence decay times are significantly different.

Dynamic photoluminescence quenching and decrease in lifetime of carbon dots (CDs) have been demonstrated in the presence of Fe^{3+}. The quenching was found to be temperature-dependent due to increased collisions between Fe^{3+} and CDs at high temperatures. It was also noted that photoluminescence of CDs was substantially quenched in the presence of the H_2O_2/Fe^{2+} system due to oxidation of Fe^{2+} into Fe^{3+} and possible destruction of emissive groups by hydroxyl radicals. This temperature-dependent quenching behavior allows use of these materials as H_2O_2 sensors.[139] Luminescence of the bis(2,9-dimethyl-1,10-phenanthroline)copper(I) ($[Cu(dmp)_2]^+$) complex was observed to be quenched depending on the solvent (donating or nondonating solvents).[140] Studies show that luminescence quenching in this case is not due to the formation of metal-centered exciplex as has been previously postulated but rather due to interactions of the complex with solvent molecules. This interaction contributes to a change in energy band gap between the ground state and ^{3}MLCT (metal-to-ligand-charge-transfer) excited state, thus affecting luminescence lifetime. In this study, static and time-resolved X-ray absorption spectroscopy combined with molecular dynamics simulations were used to understand the photoluminescence quenching mechanism.[140]

SENSORS

Sensors that rely on fluorescent molecules or nanoparticles to report the presence or concentrations of an analyte of interest continue to be an active research area during this review period. With nearly 800 publications during this review period, this research has focused on various analytes including ions, explosives, and others. In this review, we have selected a small number of articles that represent the most interesting findings in terms of analytes, sensing systems, and observed response times and limits of detection.

Detection of explosives, particularly nitroaromatics, continues to be important subject matter during this review period. In a study by Zhang et al., a metal−organic framework (MOF) based sensor has been developed.[141] The MOF framework was found to provide recyclability and stability. This sensor depends on the electron accepting property of the NO_2 groups on the nitroaromatic explosives, which results in fluorescence quenching attributed to photoinduced electron transfer and resonance energy transfer. The researchers also observed that TNT detection was possible by use of the naked eye and that distinction between different nitroaromatic explosives was possible by detecting shifts in the PL spectra due to different number of NO_2 groups on various nitroaromatic molecules. In another study from Li et al., a visual method for detection of trinitrophenol using luminescent graphene quantum dots has been reported.[142] These sensors emitted blue at 450 nm after excitation with a UV light of 365 nm, while the analyte quenched this fluorescence due to resonance energy transfer. The reported limit of detection was 0.091 μmol L^{-1} and analysis was possible in aqueous samples. While many manuscripts in this review period covered detection of nitroaromatic compounds, Ganiga et al. have developed a nanosensor system for detection of the explosives pentaerythritol tetranitrate (PETN) and cyclotrimethylenetrinitramine (RDX).[143] This sensor was FRET-based as a result of initial quenching of the fluorescence of diphenylamine with CdS quantum dots. The analyte interaction with diphenylamine afforded a decrease in FRET intensity at 585 nm and an increase in fluorescence of diphenylamine at 355 nm. The authors reported a respective detection limit of 10 and 20 nM for PETN and RDX.

Fluorescence sensors based on ionic liquids and GUMBOS have been reported by Warner and co-workers. As an example, a novel ionic liquid based fluorescent sensor, i.e., bistrihexadecyl phosphonium fluorescein ($[P_{66614}]_2[Fl]$), has been synthesized for selective and sensitive detection (LOD ∼ 300 ng/mL) of albumin in aqueous medium.[144] This IL sensor exhibited strong interactions with albumins (BSA and HSA). The basis of sensing is that the IL sensor, ($[P_{66614}]_2[Fl]$, is converted from an aggregated state into a monomeric form upon interaction with albumin. The result is a drastic increase in fluorescence intensity of the IL sensor due to formation of the more fluorescent monomer. This change in fluorescence intensity of the IL probe for albumin primarily depends upon the amount of protein sample in the aqueous medium. In a different study, similar types of ILs, $[P_{66614}]_2[FL]$ and $[P_{66614}][FL]$ were employed in nanodroplet form as a pH sensor (Figure 8).[145]

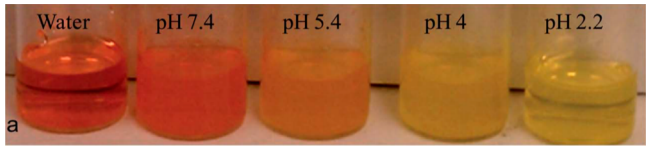

Figure 8. pH dependent color change of $[TTP]_2[FL]$ nanodroplets, Reproduced from Das, S.; Magut, P. K.; de Rooy, S. L.; Hasan, F.; Warner, I. M. *RSC Adv.*, **2013**, *3*, 21054−21061 (ref 145), with permission of the Royal Society of Chemistry.

Contrasting stacking patterns in the nanodroplets at different pH values produced drastic changes in spectral characteristic. In addition, significant color changes were visually observed when the IL-nanosensor was prepared under different pH conditions.

Similar to our last review, considerable attention has been given to development of fluorescent sensors for detection of ionic species. Reports on zinc and copper sensors were the most abundant, obviously driven by their utility in intracellular imaging. In a study by Palanimuthu et al., the authors reported on a glyoxal bis(4-methyl-4-phenyl-3-thiosemicarbazone) ligand based sensor permeating the MCF-7 cells and binding to Zn^{2+} in cell organelles.[146] The fluorescence intensity peaked at ∼550 nm and showed impressive selectivity to Zn^{2+} as compared to other metal ions tested. Lin et al. have also

DOI: 10.1021/acs.analchem.5b04109
Anal. Chem. 2016, 88, 170−202

developed a sensor for labile Zn^{2+} in the endoplasmic reticulum using benzoresorufin.[147] Benzoresorufin was functionalized with dipicolyl- or picolyl-amine groups and displayed an *in vitro* 8.4-fold fluorescence emission enhancement after complexing with Zn^{2+}, with similar results obtained in vivo in natural stem cells. The spontaneous localization of the sensor in the endoplasmic reticulum of different cell types allowed for zinc level monitoring specific to that organelle. This behavior was useful for studying the connection between various cellular phenomena and Zn^{2+} in the endoplasmic reticulum. The detection of potassium ions using a fluorescent sensor has been reported by Liu and coauthors.[148] By improving the fluorescence intensity of thioflavin T after binding to G-quadruplex, the authors developed a K^+ sensor with a detection limit of 1 mM. The fluorescence enhancement in this sensor was produced by rotational restrictions of the benzothiazole and dimethylaminobenzene rings in the excited state G-quadruplex-thioflavin T complex. The authors proposed a molecular rotor mechanism and confirmed this hypothesis by using a nonrotor analogue of thioflavin T.

A fluorescent sensor based on a metal-ion indicator displacement assay has been developed for detection of sulfur mustard simulants in water.[149] Allowing the analyte to react first with dithiol yields podand with high affinity to Cd^{2+}.[150] This complex then displaces Cd^{2+} from a metal:indicator complex based on 3-methylesculetin, turning on the fluorescence of the freed indicator. A similar concept relying on the displacement of quencher from an indicator complex was developed for detection of copper ion (Cu^{2+}). Use of isothiocyanate functionalized gold nanoparticles coated with FITC produced a FRET-quenched fluorescence. Upon addition of cysteine, the FITC could be displaced leading to recovery of fluorescence intensity. However, in the presence of Cu^{2+}, O_2 oxidation of cysteine occurs and the displacement does not occur, leading to quantitative detection of Cu^{2+} with a detection limit of 0.37 nM.

Other cellular imaging sensors based on near-infrared fluorescent sensor Cy-NO_2 have been developed using a photo-induced electron transfer quencher nitrothiophenol group.[151] This sensor undergoes displacement of nitrothiophenol with thiol to recover the fluorescence intensity. Biological thiols including cysteine, homocysteine, and glutathione play crucial roles in maintaining redox balance of biological systems. These thiols replace the thiolate to form amino-substituted products that afford discrimination of cysteine from homocysteine and other thiols which the authors used for imaging cysteine in living cells. This research group has also advanced a solution to the same problem using a ratiometric fluorescent sensor selective in sensitivity to cysteine over homocysteine and glutathione.[152] This sensor was based on more rapid intramolecular displacement of the sulfur in the monochlorinated boron dipyrromethene (BODIPY) with amino groups of cysteine than with homocysteine and glutathione. Fluorescence imaging of living HeLa cells with various thiols was demonstrated using this system.

■ DATA ANALYSES

The utility of various data analyses and data processing strategies, including multiple linear regression (MLR), partial-least-squares (PLS) regression, unfolded partial-least-squares regression with residual bilinearization (U-PLS/RBL), principal component analysis (PCA), principal component regression (PCR), nonparametric linear-regression (NPLR), successive projections algorithm-linear discriminant analysis (SPA-LDA), and parallel factor analysis (PARAFAC), continue to be of considerable interest. Thus, several practical applications of data analyses and data processing strategies for instrumental calibration, classifications, and pattern recognitions of complex data, and analyses of samples of pharmaceutical, bioanalytical, biomedical, food, agricultural, environmental, energy, and fuel interest have been published during this review period. As an example, the utility of linear regression analysis of fluorescent data for accurate determination of two cephalosporins, cefadroxil (CEFA) and cefuroxime sodium (CEFU), active ingredients in pharmaceutical formulations, has been reported[153] Cephalosporins are a family of bactericidal antibiotics that are structurally related to penicillin. Cephalosporins were also first derived from the fungus, Cephalosporum acremonium. The reported method for CEFA and CEFU analysis was based on the reaction of cephalosporins with 1,2-naphthoquinone-4-sulfonate in an alkaline medium to form fluorescent derivatives that were extracted with chloroform. The fluorescence emissions of CEFA and CEFU were subsequently measured at 610 and 605 nm, respectively, after excitation at 470 nm for CEFA and 460 nm for CEFU. Beer's law was followed over concentration ranges of 20−70 ng/mL for CEFA and 15−40 ng/mL for CEFU. The influence of experimental conditions including pH, temperature, reaction time, 1,2-naphthoquinone-4-sulfonic concentration, and extraction solvent on the accuracy of CEFA and CEFU determination in pharmaceuticals was further examined. At optimum conditions, limits of detection (LOD) of 4.46 ng/mL for CEFA and 3.02 ng/mL for CEFU, and high linear regression square correlation coefficients of R^2 = 0.9984 or better were reported. Excellent recoveries ranging from 97.50 to 109.96% for CEFA and 95.73−98.89% for CEFU were also obtained for the analysis, demonstrating high accuracy for this technique. The reported method has potential practical applications for determination of CEFA and CEFU in pharmaceutical formulations in quality control laboratories.

The potential utility of PCR and PLS regression analysis of synchronous fluorescence data for multicomponent and simultaneous analyses of metoprolol (MET), propranolol (PRO), and amiloride (AMI) in the presence of strong serum albumin signals was demonstrated.[154] Amiloride is a diuretic and is commonly used for treatment of hypertension. Propanol and MET are nonselective β-blockers and are often prescribed for treatment of angina pectoris and cardiac arrest. The measured high R^2 > 0.998, low root-mean-square-error-of-prediction (RMSEP) values (<5%), recoveries (93−108%), and low LOD (7.59 ng/mL for MET, 5.27 ng/mL for PRO, and 13.87 ng/mL for AMI) are quite impressive, demonstrating the high accuracy and sensitivity of the method for MET, PRO, and AMI analysis. A binary mixture, consisting of amlodipine besylate (AML)/candesartan cilexetil (CAN) and telmisartan (TEL), has been analyzed to provide high accuracy and low limit of detection using fluorescence spectroscopy.[155] Amlodipine besylate, CAN, and TEL are drugs commonly used for treatment of hypertension. The fluorescence of AML was recorded at 367 nm excitation and 454 nm emission wavelengths. However, 265 and 392 nm were chosen as excitation and emission wavelengths, respectively, for investigation of the fluorescence of CAN in ethanol, while the fluorescence spectrum of TEL was recorded at a different wavelength in alkaline solution. Regression analysis of the fluorescence data provided excellent correlation between the

DOI: 10.1021/acs.analchem.5b04109
Anal. Chem. 2016, 88, 170−202

fluorescence intensity and the concentration over various ranges for AML, CAN, and TEL. In this regard, the authors reported a low LOD of 0.034 μg/mL for AML, 0.0063 μg/mL for CAN, and 0.0007 μg/mL for TEL.

Multicomponent determination of two antihypertensive drugs, metoprolol (MET) and pindolol (PIN) in synthetic mixtures by use of multivariate curve resolution (MCR), PLSR, and PCR analysis of MET and PIN synchronous fluorescence spectral data was also published.[156] Metoprolol and PIN showed emission maxima at 302 and 310 nm, respectively. The fluorescence spectral profiles of MET and PIN are highly overlapping, preventing the use of a conventional univariate method for MET and PIN quantitative analysis. Consequently, a chemometric multivariate calibration method was used as an alternative strategy for simultaneous quantitative analysis of multicomponent MET and PIN samples. The reported method is capable of determining MET and PIN sample within the concentration range of 0−0.5 mg/L for MET and 0−5 mg/L for PIN. This protocol also allowed successful determination of MET and PIN drugs in blood serum samples. Application of spectrofluorometric methods in conjunction with NPLR analysis (Theil's method) for accurate determination of closely related fluorescent reaction products of fluoxetine and olanzapine drug mixtures was recently published.[157] Fluoxetine is a selective serotonin reuptake inhibitor and antidepressant agent, often used for the treatment of major depressive disorder, panic disorder, and premenstrual dysphoric disorder. Olanzapine is also used for treatment of depression and bipolar disorder. The analytical strategy involved derivatization of fluoxetine and olanzapine drugs using 4-chloro-7- nitrobenzo-2-oxa-1,3-diazole (NBD-Cl) in a borate buffered medium (pH 9.5) to form highly fluorescent products. The first and second derivative ratios of the emission data along with their convolution using 8-point sin x_i or cos x_i polynomials (discrete Fourier functions) were subsequently used for data analysis. This protocol allowed for accurate and simultaneous determination of fluoxetine and olanzapine in the presence of a minor component (olanzapine) and strong overlapping spectra of the two NBD-Cl fluorescent products of fluoxetine and olanzapine. The study is particularly interesting because it combined the advantages of convolution of derivative ratio curves using discrete Fourier functions and the reliability and efficacy of nonparametric analysis of data.

Determination of naproxen (NAP) in serum based on PCR has also been reported.[158] Fluorescence EEMs of NAP in serum with excitation wavelengths from 235 to 293 nm and emission wavelengths in the range 320−420 nm were collected. The resulting excitation emission fluorescence matrix data of NAP were unfolded and subjected to PCA and linear regression data analysis to select the most relevant principal components (PCs): the eigenvalue ranking and the correlation ranking. Results from data analysis showed that the importance of each PC to multivariate calibration was not correctly described by its eigenvalue but by its influence on the prediction of the dependent variable. When compared to a conventional HPLC method, the combined use of simple spectrofluorometry and MRA strategy was found to be faster, easier to use, and of lower cost for quantification of NAP in serum.

The fluorescence-based assay MRA of guest−host spectra data for chiral discrimination and for accurate determination of enantiomeric excess (ee) values of amines, amino, and amino acid ester molecules of pharmaceutical interest with low errors of 1−2% was also demonstrated.[159] This method employed the self-assembly of 2-formylphenylboronic acid with a chiral diol and a chiral amine to produce two diastereomeric iminoboronates that differ in fluorescence intensity and polarization. The use of orthogonal dynamic covalent self-assembly in determination of the enantioselective strategy in this study has great potential application for development of high-throughput procedures for determination of chirality. In a related study, the combined use of fluorescence spectroscopy, guest−host chemistry, and PCR for the determination of enantiomeric composition of tryptophan (Trp) using bovine serum albumin (BSA) as a chiral selector has been reported.[160] Principal component regression was used to correlate changes in the fluorescence spectral data with respect to the enantiomeric composition of Trp. These models were subsequently validated by use of leave-one-out cross validation and external test validation methods. These models were also capable of accurate determination of enantiomeric composition of 2.50 μmol/L Trp in the solution.

Use of multivariate analyses, chemometrics, and data processing has also garnered considerable interest in biomedical, bioanalytical, biomedical, and clinical studies during this review period. For example, Fakayode's research group has reported the first potential utility of fluorescence spectroscopy in conjunction with multivariate PLS regression analysis for accurate determination of Hg(II) concentrations in human serum albumin (HSA) samples.[161] Human serum albumin is a protein responsible for transport and delivery of drug molecules, fatty acids, and metabolites to various targets and removal of waste products from the body. However, binding with heavy metal ions, including Hg(II), can adversely affect the physiological properties of has, with deleterious health consequences. The volatility of Hg at room temperature precludes the use of conventional flame, graphite furnace, or inductively coupled atomic absorption spectroscopy for routine analysis of Hg in most research and medical laboratories. Binding of Hg(II) with HSA results in dramatic quenching of HSA fluorescence emission, with a slight blue shift of the HSA emission λ_{max}, precluding the use of univariate regression analysis of the fluorescent data for Hg(II) determination in HSA samples. This challenge was eliminated by use of multivariate PLS regression analysis. The PLS regression was used to correlate the changes in Hg(II)-HSA fluorescence emission with Hg(II) concentration in HSA samples. Models were able to correctly predict Hg(II) concentrations in HSA sample test solutions, with a RMSEP of 6.59%. The simplicity, low cost, and robustness of this method makes it a promising alternative for rapid determination of Hg(II) concentration in other biological specimens.

Regression analysis of the autofluorescence (AF) of skin has also been examined. This study involving the relationships between past glycemic control and microvascular complications in Japanese patients with type 1 diabetes[162] was implemented for 241 patients and 110 controls. Three monthly HbA1c levels were determined over a 2 decade time period, and the area under the curve (AUC) of the HbA1c was calculated. MRAs were performed to investigate the effect of variables on the severity of diabetic complications. Examination of results showed that skin AF values were directly correlated with the severity of specific diabetic complications. Moreover, during the 3 to 15 year period, the HbA1c AUC values were significantly related to the severity of multiple diabetic complications. Multivariate analyses showed that skin AF was associated with nephropathy when the HbA1c AUC value was removed from

DOI: 10.1021/acs.analchem.5b04109
Anal. Chem. 2016, 88, 170−202

the independent variables. In contrast, other factors such as age at registration, age at onset of diabetes, and skin AF were all directly related to retinopathy. This study concluded that skin AF can replace the HbA1c AUC value for measure of long-term glycemic control and may serve as a biomarker for microvascular complications.

Various biopsy procedures applied toward control of lung disease did not show significant results due to poor recognition of vital tumor tissue. In this regard, two new spectroscopic methods, diffuse reflectance spectroscopy (DRS) and fluorescence spectroscopy (FS)] have been suggested. These spectroscopic methods aid in investigations of tumor tissue composition for accurate classification of tissue types of samples collected during transthoracic lung biopsies.[163] This study involved ex-vivo DRS and fluorescence measurements of lung tissues from 13 patients who were diagnosed with lung cancer or pulmonary metastases. Histological analysis was further used to determine sensitivity and specificity between different types of tissues using this optical method. Examination of data showed great distinction between lung parenchyma and tumor tissue with high selectivity and sensitivity. Data analysis for each patient was further performed to eliminate interpatient variation and resulted in 100% sensitivity and specificity. Additionally, fluorescence measurements allowed discrimination between necrotic and non-necrotic tumor tissues with 91% sensitivity and selectivity. It was concluded that the combined use of DRS and fluorescence measurement and CART with a biopsy device further enhances the quality of diagnosis and transthoracic biopsies.

Adulteration and counterfeiting of food items and agricultural products continues to be problematic in the food industry, with negative impacts on consumer food safety and public heath with severe financial implications for food producers. Consequently, the practical application of multivariate analysis, chemometrics, and data processing for pattern recognition, classifications, and determination of various analytes of interest for quality control and quality assurance in foods items and agricultural products has generated considerable interest during this review period. For instance, fraudulent addition of plant oils during the manufacturing of hard cheeses is problematic and a real issue for the dairy industry, particularly in Brazil. Considering the importance of monitoring adulterations of genuine cheeses, the potential utility of synchronous fluorescence spectroscopy, successive projections algorithm-linear discriminant analysis (SPA-LDA), principal component analysis-linear discriminant analysis (PCA-LDA) and MLR for the detection of cheese adulteration with plant oils in Brazil has been investigated.[164] Synchronous fluorescence spectra were collected within the range of 240−700 nm at different wavelength intervals. The LOD of adulteration, 3.0 and 4.4%, respectively, were observed for application of wavelength intervals of 60 and 80 nm. Multiple linear regression models were used to calculate the level of adulteration, with the lowest RMSEP of 1.5 for the measurement acquired at a wavelength interval of 60 nm. Lower classification errors were obtained for the SPA-LDA rather than for the PCA-LDA method. The lowest classification error rates of 3.8% ($\Delta\lambda$ = 10 and 30 nm) and 0.0% ($\Delta\lambda$ = 60 nm) for the PCA-LDA and SPA-LDA classification methods, respectively. The protocol is envisioned to have practical application and utility for detecting the addition of plant oils to hard cheese.

In another study, use of EEM fluorescence in combination with PARAFAC and PLS regression for accurate determination of the corrupting content of mixed wine spirit in adulterated brandy samples was published.[165] The PARAFAC-PLS regression model was found capable of accurate prediction of mixed wine spirit levels in adulterated brandy with the RMSEP value of 1.9% and a R^2 = 0.995 between reference contents and predicted values. Derivative synchronous fluorescence spectroscopy has been employed for sensitive detection of binary mixtures consisting of 2-naphthoxyacetic acid (BNOA) and indole-3-acetic acid (IAA).[166] Quantitative analysis of BNOA and IAA were performed at 239 and 293 nm using synchronous fluorescence spectra recorded in buffer media. Using a synchronous derivative method, the overlapped fluorescence spectra of BNOA and IAA were effectively resolved and allowed ppm detection limit. Real samples of fruit juice having BNOA and IAA mixture provided reasonable results using this method, showed good recoveries of 83.88−87.43% for BNOA and 80.76−86.68% for IAA, and an RSD of <5.0% without prior separation procedures. The accuracy and precision of the results obtained using a synchronous derivative method for BNOA and IAA analysis was also found to be statistically comparable with the results using HPLC−MS methods.

Applications of multivariate analysis of fluorescence spectral data for determination of analytes in environmental, energy, and fuel related studies were also reported during this review period. Seven polycyclic aromatic hydrocarbons (PAHs) from the EPA priority pollutant list (benzo[*a*]anthracene, benzo[*b*]-fluoranthene, benzo[*k*]fluoranthene, benzo[*a*]pyrene, dibenz-[*a,h*]anthracene, benzo[*g,h,i*]perylene, and indeno[1,2,3-*c,d*]-pyrene) have been analyzed and reported for edible extra virgin olive oil.[167] The PAHs analyses in this study were based on measurement of EEM on nylon membranes and processing data using unfolded partial least-squares regression with residual bilinearization (U-PLS/RBL).The LOD for the method ranged from 0.29 to 1.0 μg kg^{-1}, with recoveries between 64 and 78%. This method was applied to 10 samples of edible oil, two of which presented PAHs ranging from 0.35 to 0.63 μg kg^{-1}. When compared to chromatographic separation methods, this method allowed rapid analysis with a significant reduction in solvent consumption. A selective method for determination of boron in uranium samples by spectrofluorimetry in synchronous derivative mode has also been published.[168] This method is based on complexation of nonfluorescent boron with a fluorescent chromotropic acid to form a fluorescent boron-chromotrope complex. The native fluorescence spectrum of the chromotropic acid was found to overlap with that of the complex. Therefore, a synchronous derivative mode was employed for analysis, eliminating the need for physical separation of excess ligand and complex. Using the optimized experimental and instrumental conditions, LOD of 2 ng/mL, the linear concentration range of 5−100 ng/mL, and an R^2 value of better than 0.997 were obtained. Precisions better than 5% at 10 ng/mL level and 3% at 50 ng/mL level (n = 9) were also reported. The method was further validated using reference materials and was successfully applied to analysis of uranium nuclear fuels, with an accuracy of ±10%. This method is particularly advantageous because it reduces sample size requirement, thus reducing the load of uranium recovery from analytical waste in the case of enriched uranium based samples.

■ ORGANIZED MEDIA

Luminescence studies involving organized media have extended into various aspects of science and technology over the past few years. In addition to use as templates for synthesis of

DOI: 10.1021/acs.analchem.5b04109
Anal. Chem. 2016, 88, 170−202

nanostructured materials and serving as biomimetic systems, organized media can be applied to applications in organic electronics, multimodal nanotheranostics, bio and chemosensing, as well as stimuli responsive drug delivery vehicles. Although there are numerous reports in each of these areas, only a few selected studies are included in this review. Gidron et al. have provided a review on a new class of conjugated oligomers composed of alpha-oligofurans and have discussed use in organic field effect transistors (OFETs) and organic light emitting transistors (OLETs).[169] A hafnium oxide-organic self-assembled nanodielectric (Hf-SAND) material consisting of alternating π-electron layers has been reported by Everaerts et al. with multilayered structure confirmed using X-ray fluorescence and X-ray reflectivity. This represents a significant advance in hybrid organic−inorganic dielectric materials.[170] High radiance of bioluminescent materials hold great promise for photonic application. Gather et al. have presented a study where a dried film of green fluorescent protein (GFP) showed low fluorescence quenching and strong optical amplification that has been exploited in designing vertical cavity surface emitting microlasers.[171] A different study by Masai et al. reports on enhanced solid state phosphorescence from a cyclodextrin based insulated platinum-acetylide with controlled thermal fluctuation. The polymer exhibited identical phosphorescence in both solid state and in solution achieving unimolecular phosphorescence.[172]

Luminescent materials often demonstrate a photophysical phenomenon referred to as aggregation induced emission (AIE). This phenomenon is frequently exploited in high technology applications such as optoelectronics and sensing. In this regard, Mei et al. have presented a critical review of current advancements in this area, wherein mechanistic analysis of the AIE processes have been performed.[173] Restriction of intramolecular motions (RIM) has been demonstrated as the primary reason for AIE and strategies of molecular engineering toward design of new AIE based luminogens are discussed.[173] Luminescence based molecular self-assemblies, complexes, and conjugates are also demonstrated for use as chemical tools in clinical diagnosis. A recent study shows a near-infrared (NIR) squarine dye reported to self-assemble and form nonfluorescent nanoparticles, which selectively respond to human serum albumin (HSA) by turning on green fluorescence with a sensitivity limit of 3 nM.[174] Abo et al. have demonstrated a novel dye−protein conjugate with SNAP-tag protein for detecting H_2O_2 as well as visualization of H_2O_2 endogenously produced in living cells.[175] Label free recognition of biomolecules was achieved using plasmonic nanostructured film derived from Ag nanoparticles-dyes-Au assembly with strongly coupled architecture. Directional surface plasmon coupled emission characteristics of this designed sensor served as the means for biorecognition.[176] Chen et al. have reported live cell imaging using a dual emission fluorescent nanocomplex of gold fabricated through a crown-like assembly of dye encapsulated silica particles decorated with gold nanocrystals. Imaging using this nanocomplex was based on highly sensitive and selective quenching of gold nanocrystals in the presence of reactive oxygen species.[177]

Recently, the use of a hydrogel for tuning the size of NIR nanomaterials has been demonstrated.[178] In this regard, sodium deoxycholate trishydroxymethyl)amino-methane (NaDC/TRIS) hydrogels were prepared at different pH values and at variable concentrations of TRIS. Hydrogels prepared under such conditions were used to tune the size of nanoGUMBOS (nanomaterials derived from GUMBOS). NIR based nanoGUMBOS of altered size suggested the possibility of using these materials for bioimaging. In addition, a detailed rheological study revealed two unusual stable regions of elastic modulus, which suggests potential applications for drug delivery.

Organized media in various forms have also been extensively used in biomedicine as theranostics and controlled release of therapeutic drugs. Bollhorst and co-workers have developed a bifunctional submicrometer colloidosomes coassembled from magnetic iron oxide and fluorescent silica nanoparticles which demonstrates potential applications in drug targeting, bioimaging, and magnetic hyperthermia.[179] Ling et al. have developed a multimodal self-assembled theranostic nanogrenades composed of magnetic iron oxide and pH sensitive ligands. The nanogrenades disassembled into a highly active state in acidic subcellular environment that turns on MR contrast, fluorescence, and photodynamic therapy which enables early detection of cancer.[48] A study by Tian et al. describes the design of multifunctional nanomicelles functionalized with a newly screened cancer specific aptamer for targeting cancer cells. A pH activitable fluorescent probe and NIR photosensitizer encapsulated in these micelles can light up lysosomes for real time imaging and generate reactive oxygen species causing lysosomal destruction, respectively.[180]

A number of reports have surfaced during this time period that describe the design of novel organized media for stimuli responsive, targeted, and controlled drug delivery. For example, a second generation metallodendrimer, peripherallydimethyl isophthalate (DMIP) functionalized poly(benzyl ether) has been found to self-assemble in regular vesicles with hexagonal metallocycle cores. Fluorescent molecules encapsulated in these cores demonstrated halide induced controlled release through vesicle−micelle transition establishing the potential of these vesicles as smart stimuli responsive deliver vehicles.[181] In addition, Deshayes et al.[182] and Duan et al.[183] have reported in two separate studies, pH responsive drug delivery vehicles for release of chemotherapeutic agents. The first study reports a phenylboronic acid (PBA) installed polymeric miceller nanocarrier that was developed to selectively target sialic acid (SA) overexpressed in tumors and thereby aiding target specific release of chemotherapeutic drugs at intratumoral pH conditions.[182] The second study outlines the design of luminescent pH responsive supramolecular vesicles based on water-soluble pillar[6]arene and a ferrocene derivative, which self-assemble via a novel host−guest inclusion complex.[183] Guo and co-workers have developed a protein, enzyme, and light responsive fluorescent supramolecular assembly which undergoes target specific molecular disassembly and drug release with implication for broad biological applications.[184]

There are numerous and very exciting reports on fabrication of novel multifunctional supramolecular assemblies with potential for a multitude of applications. A DNA programmed dynamic assembly of multicolored quantum dots (QD) has been developed by He et al. as a new class of FRET based QD computing systems.[185] Chen et al. have reported a rapidly healing supramolecular polymeric hydrogel based on host guest recognition between poly β-cyclodextrin and polymeric α-bromonaphthalene with photostimulated room temperature phosphorescence for use as artificial soft materials.[186] A supramolecular coordination complex (SCC) with tunable emission has been presented by Pollock and co-workers. This system was designed based on a series of functionalized D 2-h[D(2)A(2)] rhomboids (D = 2,6-bis(4-ethynylpyridine)aniline

DOI: 10.1021/acs.analchem.5b04109
Anal. Chem. 2016, 88, 170−202

based ligands). Tunability of the system was attained by simple functional group modifications para to the aniline amine.[187]

FLUORESCENCE POLARIZATION, MOLECULAR DYNAMICS, AND RELATED PHENOMENA

Fluorescence polarization and anisotropy continue to offer alternative platforms for exploring diverse molecular interactions and enzymatic activities. A representative sampling of notable recent advances and novel applications are provided in the following areas: nanomaterials, DNA analysis, chiral recognition, and protein dynamics. For the purposes of this review, the terms polarization and anisotropy are used interchangeably.

Nanomaterials such as nanoparticle based probes and sensors continue to be of considerable interest to researchers. For example, Zhou et al. have developed novel, simple, and cost-effective sensing graphene oxide (GO) platforms for detection of the activity of protein kinases. This approach eliminates the need for expensive synthesis of specialized reagents, e.g., antibodies specific for phosphopeptide or protein domains.[188] This GO-based platform also offers several benefits including (1) efficient quenching effect to various fluorescence labels, (2) tunable adsorption characteristics of biomacromolecules, and (3) potential future fluorescence anisotropy (FA) kinase assays. The protein kinase activity was investigated by suppressing phosphorylation modification on carboxypeptidase Y (CPY) digestion. Thus, without peptide phosphorylation, free fluorophores originate by cleaving fluorophore-labeled peptide by CPY; however, fluorescence quenching was observed due to GO/peptide nanocomplex formation. The probes validity was proven by using the GO-based method to simultaneously monitor activity of two model kinases with low detection limits (Figure 9).

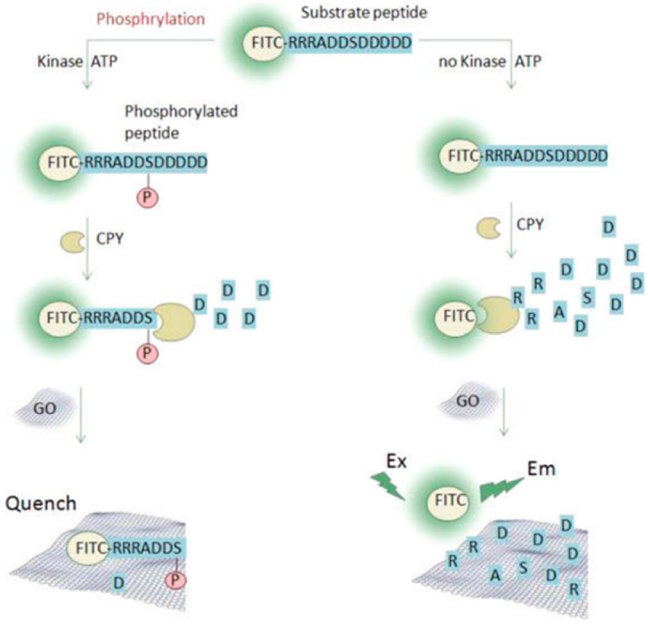

Figure 9. Schematic of the protein kinase activity assay based on GO/peptide nanocomplex and suppression of phosphorylation to carboxypeptidase Y cleavage. Reproduced from Zhou, J.; Xu, X.; Liu, W.; Liu, X.; Nie, Z.; Qing, M.; Nie, L.; Yao, S. *Anal. Chem.* **2013**, *85*, 5746−5754 (ref 188). Copyright 2013 American Chemical Society.

Wang and co-workers have reported a dual opto-electrical sensor for recognition of a single analyte, i.e., vitamin B1, using gold nanorods (Au NR) and gold nanoparticles (Au NP) covalently bound to luminescent terbium complexes.[189] These Au nanosensors were anchored onto the surface of glassy carbon electrodes while both fluorescence and cyclic voltammetry data were collected. Both techniques positively and selectively signaled the presence of vitamin B1 in aqueous samples in comparison with other similar vitamins B2, B3, B4, B5, and B6 present.

Ziegler et al. have designed polarization-sensitive polymer nanoparticles (NPs) for use as fluorescent probes. Preparation of NPs was achieved by use of nanoprecipitation and subsequent bioconjugation, resulting in small NPs (∼7 nm in diameter), easy to functionalize and facilitate binding to protein targets, with a high quantum yield of 0.75.[190] Excitation energy transfer (EET) can occur along the conjugated polymer backbone found in NPs whereby energy from higher-energy local regions of a semiconducting polymer chain efficiently funnel energy to chromophores with localized energy minima where emission is preferred. Practical applications of semiconducting probes were demonstrated by monitoring the rotation of microtubules as they process across a kinesin-coated surface. Future uses for these bright, polarization-sensitive probes include studies of rotational motions of biomolecules.

DNA analyses have garnered a tremendous amount of activity during this review period. Yang and co-workers, strategically used streptavidin, as a molar mass amplifier, coupled with cyclic assembly amplification based on a hybridization chain reaction (HCR) to obtain both large fluorescence polarization assay responses and high sensitivities.[191] In this study, they constructed target-triggered cyclic assembly of DNA−protein hybrid nanowires where one blocking DNA strand is released by target−aptamer recognition. The proposed assay exhibited a turn-on response to the chosen model small molecule-adenosine triphosphate (ATP) with a LOD of 100 nM for ATP. This assay's response range was from 0.5 to 100 μM for ATP in complex biological samples, including cell media, human urine, and human serum, thereby cementing its practicality in real complex biological systems.

Zhang et al. have developed a novel fluorescence anisotropy amplification assay for detection of Pb^{2+}-dependent GR-5 DNAzyme activity.[192] The DNAzyme featured a DNAzyme strand and a hybridized rA-cleavable substrate strand fitted with a tetramethylrhodamine (TMR) fluorophore. They labeled the TMR at the 5′-end of the substrate strand and attached tandem guanine bases (G) at the 3′-end of the enzyme strand to monitor the binding-induced change of the TMR−G interaction. The optimization strategies included investigating the effects of the number of the tandem G base of the DNAzyme strand, incubation time, buffer pH, and ion strength. Under optimum conditions, they reported a large fluorescence anisotropy change, $|\Delta r| = 0.168$, detection limit of Pb^{2+} of 100 pM, and dynamic range from 200 pM to 100 nM.

Huang and co-workers proposed to better understand fluorescence anisotropy modulation by investigating the influence of various dye moieties, molecular volumes, and double stranded DNA (dsDNA) end-structures in order to facilitate facile recognition design strategies suitable for a broad spectrum of analytes.[193] Fluorescence anisotropy of short dsDNA labeled with ROX (6-carboxyl-x-rhodamine) and positively charged centers was systematically investigated in parallel with two-dimensional (2D) 1H−1H nuclear Overhauser enhancement spectroscopy (NOESY) for confirmation.

DOI: 10.1021/acs.analchem.5b04109
Anal. Chem. 2016, 88, 170−202

Fluorescence anisotropy signal for small molecules and ions is inherently weak and therefore typical protocols require signal enhancements procedures including complex covalent labeling of recognition probes to amplify its size/volume and, in turn, its fluorescence anisotropy signal.[194] Zhen et al., eliminated the need for such cumbersome covalent modifications by simply using graphene oxide as a signal enhancer (N9s). The simple label-free and sensitive fluorescence anisotropy approach used a G-rich single stranded DNA (ssDNA) as recognition probe, acridine orange (AO) as a reporting fluorophore, and K^+ as a model target species. ssDNA and AO adsorb onto the GO surface through the electrostatic and $\pi-\pi$ stacking interactions resulting in a large fluorescence anisotropy value resulting from the AO-GO formation. However, in the presence of target species K^+, the ssDNA folds into the G-quadruplex structure thereby allowing primarily AO to interact more closely with the small sized G-qudruplex yielding a much lower anisotropy value.

Chiral recognition continues to be an active area of research during this review period. As an example, Lan et al. report on a novel strategy for creating 3D anisotropic Au nanorod (AuNR) helical superstructures (helices) with designed configurations and properties.[195] The helices were assembled by designing an "X" pattern arrangement of DNA capturing strands (15nt) on both sides of a 2-dimensional origami template whereby AuNRs (functionalized with the complementary DNA sequences) were deliberately placed. The resulting superstructures comprised origami intercalated between neighboring AuNRs with inter-rod distances of 14 nm and an inter-rod angle of 45°. While a full helix was found to contain 9 AuNR with a length of about 220 nm, slight origami/AuNR molar ratio modifications could be used to tailor the number of AuNR from 2 to 9. Fabrications of left handed and right handed helices were also achievable with minor adjustments to the mirrored-symmetric "X" patterns. The macroscopic AuNR assemblies demonstrated maximum anisotropy factor of 0.2 which demonstrates their potential for use in other applications such as chiral fluids or negative index materials.

Amaral et al. have described a sensitive fluorescence polarization chiral sensor platform that rivals conventional chiral detection methods.[196] The technique is based on an enantioselective *L*-histidine-dependent DNAzyme, which is composed of an enzyme strand (E) and a fluorescently labeled substrate domain (S*) joined via complementary regions at their extremities. While the assembled enzyme−substrate probe alone displayed high fluorescence anisotropy due to its large volume, upon *L*-histidine induced cleavage of RNA phosphoester bonds of labeled substrate domains (S*) and subsequent formation of single strand small size fragments, a significant loss of fluorescence anisotropy response was observed. However, no significant change in probe anisotropy was observed upon addition of its antipode, *D*-histidine. Both uni- and bimolecular formats of this sensor were evaluated as well as optimization of the sensor via enzyme and substrate sequence modifications were conducted and resulted in detectable trace levels of *L*-histidine as low as 0.05%.

Great strides have been made in understanding protein dynamics and function during this review period. Flavenols, a class of bioactive naturally occurring phenolic compounds and related derivatives, such as robinetin, have recently been demonstrated as alternatives to conventional therapeutics; thus, the details of their interactions with biorelevant targets, are of great interest.[197] Robinetin is also of interest to the fluorescence sensing community, because it undergoes a photoinduced excited state intramolecular proton transfer (ESIPT) reaction resulting in "two color" intrinsic fluorescence emission which allows for multiparametric sensing. Pahari et al. have explored the binding characteristics of robinetin with the carrier protein human serum albumin (HSA) using both spectroscopic and molecular modeling studies. In agreement with molecular docking studies, time-resolved anisotropy studies showed a marked (~170 times) increase in the rotational correlation time (τ_{rot}) due to substantially restricted motion of robinetin within the hydrophobic subdomain IIA site of HSA protein matrix.

McCarroll and co-workers have recognized the need for a more purposeful approach at understanding molecular interactions based on a systematic approach to isolate compatible target−ligand pairs, rather than the current method of mostly trial and error.[198] In this regard, they describe a novel comprehensive approach used to rationally identify suitable protein targets for a given ligand molecule based on a dynamic isoelectric anisotropy binding ligand assay or DIABLA. This technique is derived from a melding of dynamic isoelectric focusing (DIEF) and fluorescence anisotropy. Optimization parameters weighed heavily on evaluating the use of fluorescence anisotropy as a detection mechanism but also explored protein focusing pH, effect of ligand concentration, and nonspecific binding effects. Future studies will examine mixtures of proteins, such as cell lysates, where fluorescence anisotropy is performed on separated protein bands obtained after DIEF in order to detect a target protein of interest.

Development of a one-step highly rapid assay for detection of bacterial protective antigen (PA) protein based on a combinatorial approach of Förster resonance energy transfer (FRET) and homogeneous time-resolved fluorescence (HTRF) of a lanthanide complex has been reported.[199] This immunoassay was designed as follows: two distinct antibodies (Abs) labeled with donor and acceptor fluorophores (europium cryptate (EuK) and Alexafluor647, respectively) were bound to PA in close proximity to one another, thereby inducing the energy transfer between them and giving rise to two emitted wavelengths over time. The sensitive detection method was able to detect 2 ng/mL PA in serum of *B. anthracsis*-infected rabbits in as little as 15 min. With appropriate modifications, a similar immunoassay was also developed for detection of bacterial spores with similar success (LOD 2×10^6 spores/mL) employing an incubation time of 30 min.

CHEMILUMINESCENCE

Chemiluminescence (CL) is a well-established technique with a wide range of applications, including but not limited to biological and environmental chemical analysis. Recently, CL has been widely explored for examination of bioanalytical systems due to the powerful detection and rapid response of this method. Significant growth in the number of publications around the globe emphasizes the importance of this technique. In this review, we focus on the progress of chemiluminescence during the last 2 years. In this period, thousands of peer reviewed manuscripts and review articles have concentrated on improvement of the CL technique in terms of sensitivity, selectivity, accuracy, and quantum efficiency. In this regard, new strategies were considered, which mostly implicate synthesis of new chemical compounds,[200,201] utilization of nanoparticles,[202−206] technologies for fabrication of electroluminescent sensors, and development of new methodologies,[207] etc.

DOI: 10.1021/acs.analchem.5b04109
Anal. Chem. 2016, 88, 170−202

A new system based on carbon nitride quantum dots (g-CNQD) has been introduced for chemiluminescence measurement. These g-CNQD are known for their fluorescent properties, but chemiluminescent behavior has never previously been detected in this system. Yurong Tang and co-workers[203] have investigated remarkable CL properties of carbon nitride quantum dots (g-CNQD) which exhibited extraordinary sensitivity and selectivity for free chlorine in real water samples. A very simple microwave-assisted synthetic approach was introduced to obtain monodispersed g-CNQD. The g-CNQD displayed strong CL emission in the presence of sodium hypochlorite (NaClO) at pH values greater than 9 due to the presence of hypochlorite anion. In addition, no interference in CL intensity was observed in the presence of other commonly present ions in a real sample of water. This CL behavior of g-CNQD was attributed to the exciton formation. Moreover, singlet oxygen could transfer energy to g-CNQD which aids to amplify CL signal.

Recently, carbon nanoparticles (carbon dots, green nanomaterial for next generation) have been presented for dual peak electrogenerated chemiluminescence (ECL) in order to detect iron ion with high accuracy and sensitivity.[206] In these spectra, the first ECL peak appeared to be sensitive to iron ion concentration, while the second peak served as an internal reference. This two peak ECL system provided great advantages for detection of metal ions by displaying high accuracy and sensitivity in comparison to single peak ECL. In another development, a highly selective, sensitive, and label free ECL system has been introduced for cancer cell detection which is based on carbon nanodots (C-dots) and graphene nanosheets. In this study, carbon nanodots served as an ECL probe and graphene nanosheets were used to amplify the signal. Evaluation of data displayed remarkable cell capture ability of this newly designed cytosensor with excellent sensitivity for cancer cells.[208]

Different electrogenerated chemiluminescence (ECL) emission colors in spectra can easily be achieved by simply changing the solvent and surface attachment.[209] To tune the emission color from electrogenerated chemiluminescence, five new heteroleptic iridium(III) complexes have been synthesized by Yuyang Zhou et al.[201] Furthermore, the role of ancillary ligand on quantum efficiencies has also been demonstrated. Multicolor emission including green, orange, and red was attained, which is important for expending multichannel analytical techniques. Interestingly, these complexes showed high ECL efficiency in the presence of tripropylamine. Moreover, 2, 11, and 214 times higher ECL efficiencies were achieved in these newly synthesized complexes compared to well established electroluminescent chromophore, i.e., tri-2,2′-bipyridylruthenium(II) ($Ru(bpy)_3^{2+}$), under similar experimental conditions. Another exciting study regarding multicolor ECL is presented by Paul S. Francis et al. In this work, an ECL system exhibiting the three primary colors (red, green, and blue) was established for inexpensive, portable devices. To achieve all primary colors of emission with minimum or no spectral overlap, new iridium and ruthenium complexes were synthesized. An ECL spectrum of the three dye mixture was efficiently resolved with good intensity in three-dimensional space. Furthermore, simply by tuning the applied potential, specific molecules could be excited in the mixture with the emission detected by use of a digital camera.[200]

Recently, a new concept of chemiluminescence (cyclic chemiluminescence (CCL)) has been presented by Gongke Li et al.[207] CCL has many advantages over existing electroluminescence methods, including flow injection CL. Using CCL, one can obtain more information on the reaction by recording the signal at multiple stages after a single time injection of a sample. An exponential decay curve was recorded which was typical for a given reaction. Additionally, this technique has been shown to discriminate closely related compounds, including structural isomers because of variations in the decay curve.

Significant developments in chemiluminescence resonance energy transfer (CRET) methodology have been demonstrated by the Chao Lu group.[204,210,211] CRET has been demonstrated to be a promising approach for selective detection of analytes,[210] providing high sensitivity[204] as well as for cathodic ECL.[211] In this regard, a novel fluorescent dye was chosen as an analyte to accomplish high energy transfer by matching energy levels of donor and acceptor for CRET. Dye aggregation usually produces quenching, resulting in lowered CRET efficiency. To overcome this issue, an orderly arranged structure was fabricated that provides improvement in the CRET efficiency. This CRET strategy was applied to selective determination of peroxynitrile (a reactive oxygen specie) among various other reactive oxygen species in vitro, as depicted in Figure 10.[210]

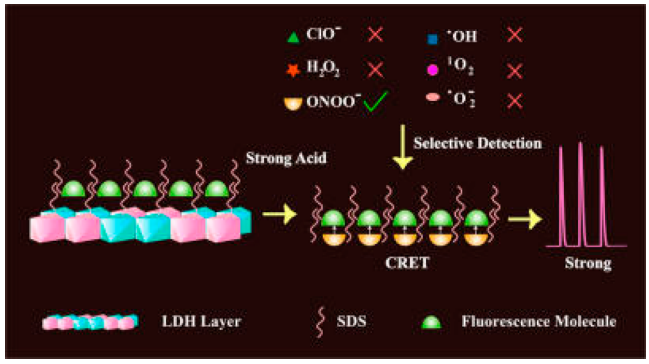

Figure 10. Chemiluminescence features of the calcein@SDS solution in the presence of different ROS. Reproduced from Wang, Z.; Teng, X.; Lu, C. *Anal. Chem.* **2015**, *87*, 3412−3418 (ref 210). Copyright 2015 American Chemical Society.

In another study, this same research group demonstrated CRET in aggregation induced emission of gold nanoclusters.[212] A confinement effect has also been introduced in CL field by this group.[213] A confined bilayer of cetyltrimethylammonium bromide (CTAB) in carbon dots assist in bringing the reactive intermediate to the central carbon dot, which produces an amplification of the CL signal.

Use of ionic liquids in chemical measurements has offered new opportunities for fabrication of new electroluminescence systems. During the last 2 decades, ionic liquids have received tremendous attention due to their characteristics of great tunability.[202] On the basis of the tunable hydrophobic characteristics of ionic liquids, Junho Jang and Won-yong have designed a new ECL system to control selectivity of the well-known electroluminophore ($Ru(bpy)_3^{2+}$) toward analytes of variable hydrophobicity. This system provided high sensitivity and does not require coupling of the ECL system with a separation technique (e.g., HPLC or CE) or enzymatic reaction. In this regard, ionic liquids of appropriate hydrophobicity were introduced into a sol−gel titania/Nafion composite film. Since ionic liquids are known to increase the conductivity of composite films, as well as oxidation rate of

DOI: 10.1021/acs.analchem.5b04109
Anal. Chem. 2016, 88, 170−202

tripropylamine (a hydrophobic ECL co reactant), such addition improves the sensitivity of the ECL sensor. A clear trend of increasing electroluminescence signal intensity was observed for the hydrophobic analyte as the hydrophobicity of ionic liquids used in the composite film increased.[214] In a similar manner, hydrophilic analytes exhibit high ECL signal in the presence of hydrophilic ionic liquids.

Numerous highly sensitive chemiluminescence immunoassays have been developed and significant strides have been made in this field during the last 2 years for selective and sensitive analyses of biomolecules.[205] Lei Ma and co-workers[205] have used chemiluminescence immunoassay based on nanobodies immobilized on magnetic beads for sensitive detection of human prealbumin in serum sample. In another study, Fei et al.[215] have developed a very simple, reliable, and inexpensive chemiluminescence immunoassay. In this work, three different technologies, chemiluminescence, immunoassay, and microfluidic system, were synchronized. This microfluidic chips based immunoassay was employed for detection of alpha fetoprotein in serum with a detection limit of 1.5 ng/mL. They also tested this system for use in clinical samples and results are in agreement with the Roche's ECL kit.

A very interesting report regarding mechanically induced emission has been presented by the Sijbesma group.[216] In this study, a mechanoluminophore was designed by incorporating a very well-known, highly stable, and sensitive 1,2-dioxetane into a polymer chain. Mechanically induced chemiluminescence produced blue light in the molecule, which was recorded upon stress using a digital camera. Emission spectra were also tuned from blue to green to red by varying the acceptor groups.

NEAR-INFRARED FLUORESCENCE

Similar to previous reviews, a significant number of published manuscripts report on the use of NIR fluorescence for in vivo imaging. Lower interference from biological matrixes and high penetration depths of NIR light are powerful combinations for such applications. Other nonimaging applications are also exploring the utility of this phenomenon. The number of publications using NIR fluorescence seems to be reaching a level of maturity as new innovative chemistries are introduced into this area. The most interesting aspects over the last 2 years of NIR fluorescence in analytical applications are in development of unique chemistries for detecting specific analytes, either as probes or sensors.

A novel copper sensor has been described[217] for rapid and ultrasensitive detection of copper ions using the specificity of click ligation chemistry and a dark-quenching mechanism. This sensor was prepared using azide-functionalized polyethylene glycol-cyanine 5.5 (azido-PEG-Cy5.5) and alkyne-functionalized blackhole quencher-3 (alkyne-BHQ3). The detection mechanism is based on click chemistry and FRET. Selectivity was evaluated using other metal ions ~10 000 times higher in concentration than that of Cu^{2+}. However, no quenching was observed, suggesting that this specific chemosensor can be used for detection of intracellular and serum levels of copper ions.

Another metal ion detection technique using NIR fluorescence has been described by Wang,[218] based on NIR fluorescence changes caused by Hg^{2+}-induced dissolution and aggregation of label free single strand DNA (ssDNA) wrapped in single-walled carbon nanotubes (SWNTs). Long wavelength NIR fluorescence signal (>1000 nm) was linear up to 200 nM concentrations. This microfluidic chip detection was successfully evaluated with real environmental water samples.

An interesting glucose monitoring device has been described by Khan et al.[219] Mutants of glucose/galactose-binding protein (GBP) used as the glucose receptor were site specific and covalently labeled with Blue Oxazine using click chemistry. This system exhibited fluorescence increases of 15% and 21% upon addition of saturating glucose concentrations. Fluorescence responses to glucose were also observed when GBP Blue Oxazine was immobilized to agarose beads. The solvatochromic behavior of Blue Oxazine was utilized as a detection method.

NIR fluorescence detection of DNA methylation and transcription has been described by Chen et al.[220] The assay consisted of two connected systems, transcription and methylation. The gene transcription used biotinylated cDNA and DNA methylation used anti-5-methylcytidine antibody (5MC-Ab) reported by near-infrared fluorescence labeled streptavidin and a secondary antibody using IRDye800 as the signal generating fluorophore. This method was fully validated and optimized for simultaneous detection of DNA methylation and transcription processes.

Protein−peptide interactions have been visualized by use of NIR fluorescence.[136] An understanding of these interactions is important for gaining insight into development of therapeutics for many ailments. The authors report synthesis of a far red-NIR fluorescence light-up probe for selective detection of protein−polyprotein peptide interactions without employing a quenching mechanism. The probe synthesized for these studies is very soluble and virtually nonfluorescent in an aqueous environment. By utilizing self-assembly of the protein and the probe, its far red-NIR fluorescence turns on and hence allows detection of specific protein−polyprotein peptide interactions, which was demonstrated in both solution and live bacteria. The use of long wavelength fluorescence makes this a promising technique for bioimaging and biosensing applications.

NIR fluorescent organic dye nanoparticles have been described in another manuscript by Yu et al.[221] The authors use small-molecule organic dye nanoparticles (ONPs) to achieve encapsulation of NIR dyes. Fluorescence resonance energy transfer is utilized to achieve large Stokes shifts for fluorescent nanoparticles. The host nanoparticles have a double role which is not only entrapping and protecting the NIR fluorophores but also serve as an acceptor for FRET. When compared to the entrapped pure NIR dyes, the nanoparticles have almost 50-fold brightness and large Stokes shifts in combination with dramatically enhanced photostability. These studies utilized a commercially available phthalocyanine dye, NIR712. NIR712-doped NPs were prepared by use of a simple solvent exchange method making the preparations very attractive even for nonchemists, achieving single mode distribution of nanoparticles of about 100 nm size with spherical structures. NIR712-doped NPs have proven to be nontoxic to mice, indicating a safe fluorescence probe for bioimaging and other applications.

Kraft et al.[222] have reported an enhanced approach to using ICG in medical tests. Since ICG is the only NIR fluorescent dye approved by the U.S. FDA, improvement in its utility for human applications is very important. ICG's protein binding properties create significant difficulties in most bioanalytical assays. In this manuscript, Kraft et al. describe a study to determine lipid−ICG interactions on ICG fluorescence intensity and ICG−lipid complex stability. They found that ICG−lipid binding stabilizes and enhances fluorescence and that the liposomal ICG nanoparticles that form during these steps had excellent light and storage stability. Liposomal ICG

DOI: 10.1021/acs.analchem.5b04109
Anal. Chem. 2016, 88, 170−202

could also have surface ligands or antibodies in order to target specific tissues in the lymphatic system and for delivering therapeutics.

Cui et al. have reported a donor−acceptor based system for detecting β-amyloid deposits.[223] Imaging agents specifically targeting Aβ plaques in the brain are useful for early diagnosis of Alzheimer disease. The authors report synthesis and characterization of NIR fluorescence imaging probes utilizing donor−acceptor architecture for binding to Aβ plaques. An ideal probe for this purpose should have significant fluorescence intensity change upon binding to Aβ aggregates but weak interactions with serum albumin. The authors achieved these goals with very simple molecular design. Results were confirmed by use of both in vivo and in vitro fluorescence imaging and histological data.

Zhao et al.[224] have developed a fluorescence sensor for detection of Hg(II) using the turn-on mechanism of BODIPY-SAN. The authors report a 0.5 μM detection limit using this technique. The fluorescence emission of the probe at 637 nm significantly increased in the presence of Hg(II) due to the NIR fluorescence turn-on response of BODIPY-SAN upon Hg(II) binding to the receptor. The phenol moiety is deprotonated and inhibits the PET quenching in the same time. The probe has high selectivity as compared to other cations.

An interesting and potentially significant probe has recently been reported by Liu[225] for detection of dicyanamide (DCD), using functionalized quantum dots' fluorescence quenching. DCD is known to be a significant health risk. Detection chemistry utilizes cyclization of the guanidine moiety of DCD with 2,3-butanedione and 3-aminophenylboronic acid, resulting in diminished fluorescence of the QD. This chemistry has proved to be selective for DCD in the presence of other amino acids, many cations, and also nitrogen containing compounds. The published detection method, which has 0.6 μm detection limit, should have significant utility in light of recent milk adulteration cases of melamine contamination in milk.

Ling[226] has described a detailed study for development of a novel near-infrared fluorescence imaging probe that preferentially binds to cannabinoid receptors. Several other detection schemes can also be noted for different sensor developments. Pennacchio[227] describes an interesting approach to detection of patulin in food. Patulin is detected by utilizing NIR fluorescent labeled anti-PAT antibodies which makes possible the detection of PAT directly in apple juice without any sample pretreatment. This approach employs an increase in fluorescence upon antigen−antibody binding using commercially produced antibodies. Excellent detection limits of 60 ng/L were achieved, much lower than required by regulators in OECD countries. The immunochemical reaction was simply detected using fluorescence polarization measured directly in 1:10 diluted apple juice sample.

Hou et al.[228] have described a new application of polarity sensitive cyanine dyes. Modified Cy5 fluorophores prepared during these studies self-assemble to form fluorescence-quenched J-type aggregate. In the presence of specific analytes, as determined by the modification moieties on Cy5 significant fluorescence, increased fluorescence is observed. This increased fluorescence is due to a substitution moiety induced dissociation of the probe aggregate. This study reports a generalized strategy to design an analyte selective response resulting in increase NIR fluorescence for selective detection of proteins.

In a study by Pan et al.[229] a novel NIR fluorescent probe has been reported for detection of ascorbic acid metabolites. The probe that has Arg-Cy composition employs the reaction of the guanidine group in Arg-Cy with the adjacent diketone present in the ascorbic acid metabolites. In addition to the above-mentioned NIR fluorescence probe developments, a significant number of publications were devoted to NIR fluorescence imaging, including some dual modality imaging.[97,230−236] Since imaging applications are somewhat similar, we do not provide details on any individual publications.

FLUORESCENT NANOPARTICLES

Developments in luminescent nanoparticles have surged unabatedly and have had an enormous impact in critical areas ranging from food security and environmental monitoring to cellular imaging and biomedical theranostics. Given the vast literature from which to choose, accounting for literally tens of thousands of peer-reviewed contributions within the previous 2 years alone, we have made the arbitrary choice to cover a few of the more innovative advances in this budding area of fluorescent nanoparticles prepared using environmentally responsible chemistry: (i) fluorescent copper nanoclusters and (ii) metal nanocluster nanothermometers. In aggregate, these examples offer a representative snapshot of the current sophistication accessible for preparation of fluorescent nanoparticles in water using sustainable methods coupled with their clever application in analytical problem-solving.

GUMBOS based fluorescent nanomaterials have also been recently synthesized. In this regard, iron(III)phthalocyanine-based nanomaterials were prepared in order to acquire fluorescent, magnetic, as well as pH responsive characteristics in a single compound.[237] A simple procedure for synthesis of this compound has been demonstrated and used for biomedical imaging. It was observed that this material showed no cytotoxicity toward cancerous or normal breast cells. In addition, paramagnetic characteristics of these biocompatible nanoparticles suggest possible use of these materials for targeted drug delivery using an external magnetic field and magnetic hyperthermia.

Using bovine serum albumin (BSA) as a template and hydrazine hydrate as reducing agent under alkaline conditions at room temperature, Wang et al.[238] have prepared stable, red-emitting copper nanoclusters (CuNCs) with peak emission near 620 nm and a quantum yield (QY) of 4.1%. The PL from these CuNCs showed a pH dependence in the 6−10 range which was ascribed to conformational changes of the host protein. An MTT assay using CAL-27 human epithelial cells revealed only slight cytotoxicity for concentrations up to 80 μg mL^{-1}. Because of their ultrafine sizes, CuNCs might be anticipated to exhibit catalytic potential. In pilot studies, the CuNCs were found to catalyze oxidation of styrene, with benzaldehyde as the major product (~70%).

In addition to BSA, other proteins have also been employed as biomineralization scaffolds to direct the preparation of CuNCs. For example, the Li group has prepared transferrin (Trf)-stabilized CuNCs emitting at 670 nm (QY ≈ 6.2%) using ascorbic acid at room temperature in 3.5 h.[239] The fluorescence intensity from the resulting CuNCs was found to be insensitive to pH from 4−10. Most notably, Trf allowed for site-specific targeting of overexpressed receptors on HeLa (human cervical cancer) cell surfaces. A control experiment using a Trf receptor negative mouse fibroblast cell line (3T3) validated that targeted bioimaging was only accomplished for cell lines that were Trf receptor positive.

The Wang group has developed a straightforward one-pot method to prepare very bright CuNCs with a QY as high as

DOI: 10.1021/acs.analchem.5b04109
Anal. Chem. 2016, 88, 170−202

14.1% in water using D-penicillamine.[240] Intriguingly, the CuNCs exhibited aggregation-induced emission (AIE), allowing them to serve as pH stimuli-responsive reporters (i.e., at pH 6 and above, they are essentially nonluminescent). These researchers showed that the PL (640 nm) from these CuNCs was efficiently quenched by H_2O_2, allowing for the indirect detection of analytes (e.g., glucose) using the corresponding O_2-dependent oxidase. Additionally, they demonstrated the rapid (~1 min) reduction of methylene blue to its colorless "leuco" form by hydrazine using the CuNCs as catalysts ($k_0 \approx 10^4$ M^{-2} s^{-1}).

Chen and co-workers have reported a one-pot synthesis of CuNCs capped with glutathione (GSH) using a chemical reduction route (hydrazine under alkaline conditions in water).[241] Matrix-assisted laser desorption ionization-time-of-flight mass spectroscopy (MALDI-TOF MS) and electrospray ionization-mass spectrometry (ESI-MS) measurements performed for compositional analysis suggested a $Cu_6(GS)_3$ composition for the original CuNCs. The authors further proposed $Cu_3(GS)_2$ as a "staple" motif in analogy with gold thiolate $Au_x(SR)_y$ clusters. Highly reminiscent of previous results from the Wang group,[240] the as-synthesized clusters were found to be weakly fluorescent in water but show a strong AIE enhancement, displaying intense 617 nm emission in 80 vol % ethanol (a QY value was not reported). Also, similar to the earlier work, these CuNCs catalyzed reduction of methylene blue in the presence of hydrazine.

In another development, the Zhang group has established a one-pot sonochemical route to GSH-stabilized CuNCs which fluoresce at 608 nm with a QY of 5.6%.[242] The multifunctional character of the GSH ligand allowed for conjugation with the cell targeting agent folic acid. In laser scanning confocal fluorescence imaging studies, folic acid-modified GSH-CuNCs were shown to be highly selective for HeLa cells known to express a high level of folate receptors on their surfaces. In contrast, in normal 293T (human embryonic kidney) cells where folate receptors are expressed at very low levels, the cells displayed almost no fluorescence signal. An MTT assay using HeLa cells demonstrated an 80% viability after 24 h incubation at a CuNC concentrations of 80 μg mL^{-1}. Finally, the GSH-CuNCs showed paramagnetic properties, showing potential as transverse relaxation time (T_1) contrast agents for magnetic resonance imaging (MRI).

On the basis of the ability of single-stranded poly(thymine) (poly T) of sufficient length (i.e., 15 or more bases) to template the formation of fluorescent CuNCs (615 nm) using ascorbate, Qing et al.[243] have developed a simple, label-free, sensitive, and rapid nuclease assay using a 30-mer of poly T as a reporter. In the presence of S1 nuclease as a model system, T-30 was digested to mono- or oligo-nucleotide fragments which failed to template fluorescent CuNCs. The fluorescence assay required no complex labeling nor sophisticated synthesis or instrumentation and showed an SI nuclease detection limit of only 5×10^{-7} U μL^{-1}, significantly lower than many recently developed analytical approaches.

Similarly, Chen et al. used the in situ formation of fluorescent CuNCs as a diagnostic to distinguish deletion or duplication genotypes of Duchenne muscular dystrophy (DMD).[244] Following the polymerase chain reaction (PCR), appropriately designed duplex DNA (DMD amplicons containing the target exon) was reacted with copper ions using ascorbate reduction. The resulting fluorescence (565 nm) provided a rapid, simple, and cost-effective method to examine the exons of DMD diagnosis. For example, the deletion genotype gave non-fluorescent products, whereas the duplication genotype emits stronger fluorescence than the normal type. In fact, the genotyping assay gave results consistent with those from the multiplex ligation-dependent probe amplification method for real clinical DNA samples obtained from DMD patients. As a final note on the subject, although the analytical utility is beyond question, the origin of the photoluminescence from CuNCs, thought to arise from surface states involving Cu^+, remains poorly understood and requires deeper elucidation.

Temperature represents one of the most fundamental parame`ters measured in science and engineering. Indeed, sensors for monitoring temperature dominate the global sensor market, accounting for some 80% of sales. Optical sensors offer attractive advantages for stand-off deployment in harsh, dangerous, and remote environments. Nanoscale thermometry based on PL is gaining particular momentum as this approach provides an avenue for mapping temperature fluctuations with high spatial resolution, making this approach appropriate for cellular imaging, microfluidics, monitoring of laser-induced hyperthermia, and many others. An exciting development in this regard, which has occurred during the course of this review period, is the emergence of high-performance nanothermometry based on fluorescent metal nanoclusters. In the first example, Nienhaus and colleagues have reported on lipoic acid-protected red-emitting (710 nm) AuNCs as sensitive probes of local temperature over the physiological temperature range.[245] By using time-correlated single-photon counting (TCSPC)-based fluorescence lifetime imaging microscopy (FLIM), these authors have demonstrated the potential of AuNCs for spatially resolving temperature measurements within living HeLa cells, reporting a temperature resolution of 0.3−0.5 °C in the 14−43 °C range.

Baker and co-workers have explored the analytical performance of BSA-protected AuNCs as nanoscale fluorescent thermometers.[246] For conventionally prepared BSA-AuNCs, a clear thermal hysteresis was evident in the emission intensity (peaked at 645 nm, QY as high as 13%) during repeated heating and cooling cycles. This detrimental behavior was eliminated completely by a number of strategies, including sol−gel coating of the protein, halide treatment, and thermal denaturation of the protein prior to BSA-AuNC synthesis, making rigorous temperature tracking possible. These simple strategies gave a temperature resolution of 0.2 °C in the 10−45 °C range. An activation energy for thermal quenching (E_a) of 206 meV was calculated for these BSA-AuNCs, making this nanothermometer inherently more sensitive to temperature than most reported nanoscale thermometers, including thiolate-capped AuNCs.

Finally, Ghosh et al.[247] have reported CuNCs stabilized by human serum albumin (HSA) that emit blue PL centered at 414 nm (QY ≈ 4%). By noncovalently hosting the fluorophore coumarin 153 (C153) within HSA-CuNC, a temperature-dependent luminescence was established based on variable Förster resonance energy transfer (FRET) from the CuNC donor to C153 as a suitable acceptor. Changes in FRET efficiency were believed to be associated with the temperature-induced conformational changes of the HSA host and were reported to be fully reversible. Although no attempt was made to estimate the temperature resolution possible with the HSA-CuNC/C153 system, it appears to be useful in the 10−45 °C range and should have a resolution somewhere in the 0.5−2.0 °C range.

DOI: 10.1021/acs.analchem.5b04109
Anal. Chem. 2016, 88, 170−202

Fluorescence-Based Plasmonics. Fluorescence-based plasmonics, also called metal-enhanced fluorescence (MEF) and surface enhanced fluorescence (SEF) has grown significantly over the past few years. Today, the concept is significantly better understood, and indeed one can readily find several thousand papers on this subject. In addition, there are several commercial suppliers of both plasmonic substrates and particles. During the past couple of years, several review articles[248−250] and one journal special issue have been dedicated to the topic.[251]

Development of surfaces for enhanced fluorescence continues to be a major area of research both academically and commercially. Historically, a great many types of surfaces featuring different sized and shaped nanoparticles as well as different and combined metals have been constructed. Recently, a resurgence in the use of aluminum for enhanced fluorescence has been observed.[252−254] This is primarily due to aluminum having plasmon bands in the UV and therefore its ability to enhance fluorescence in the UV spectral region as well as to pump high-energy photophysics. A recent review by Gray et al. outlines aluminum as a UV plasmonic metal,[254] while Watson et al. similarly describes the use of rhodium-based nanoparticles.[255] Other notable surfaces include hybrid nanotubes,[256] 2D silver gratings,[257] high aspect ratio silver nanowires,[258] silver wires deposited on gold mirrors[259] and the development of nanoraspberry substrates,[260] and a high electric field enhancing substrate composed of gold nanoparticles and aniline oligomers.[260]

Virtually all reports of metal-enhanced fluorescence to date involve reports of enhanced emission spectra, whether fluorescence, phosphorescence, or indeed α-fluorescence, which appear almost identical to control samples, i.e., similar to visualizing the emission in the far-field condition. However, Geddes and colleagues have shown[261] that depending on the metal−fluorophore combination and the respective overlap of the metals scattering spectrum (a component of its extinction spectrum which is dominant for larger particle sizes), enhanced emission spectra can also be spectrally distorted. These spectral shifts were first reported for copper nanoparticulate thin films in 2014, where a 2 nm red shift was reported for Rhodamine 800 accompanied by a 1 nm reduction in the spectra full-width at half-maximum (fwhm). Similarly, Hamo et al.[262] have shown dramatic distortions at the red edge of the spectra of Basic Fuchsin on zinc nanoparticulate films, accompanied by an increase in the fwhm.

It has also been recently shown that the synchronous scattering spectrum of Nobel metal surfaces is a good predictor of wavelength-dependence of metal-enhanced fluorescence.[263] The significance of this technique is that shape and magnitude of fluorescence enhancement can be determined rapidly for a particular plasmonic substrate.[263]

There has been continued use of plasmonic substrates for enhancing the photophysical properties of luminescent particles.[264,265] To this list, quantum dots have been extensively studied, not only to enhance their luminescence but to additionally improve quantum dot photostability.[265] In addition, a recent report has appeared on the use of plasmonic substrates to enhance the intrinsic emission of carbon nanodots,[266] small amorphous carbon nanoparticles formed from burning hydrocarbons. Interestingly, the apparent quantum yield of these particles can be dramatically enhanced near to silver, but remains low distal from the substrate, making these particles ideal as a luminescent label for immunoassays.[266]

It is well recognized that formation of fluorophore aggregates typically leads to quenching. Sorokin and co-workers have subsequently shown in several manuscripts that the fluorescence of pseudoisocyanine dye *J*-aggregates in a polyelectrolyte film can be enhanced as much as 8-fold, when gold nanoparticles were added and spaced at approximately 16 nm,[267,268] suggesting a plasmon-unquenching effect, not unlike what has previously been observed for both over labeled DNA and proteins.

The use of localized surface plasmons to enhance triplet yields and then subsequently in turn enhance triplet-based photophysical phenomena has also been an active area of research. These can be categorized into three primary areas (i) enhanced phosphorescence (and α-fluorescence),[269] (ii) enhanced singlet oxygen generation,[270,271] and (iii) enhanced upconversion via enhanced triplet−triplet annihilation.[272] Most notably, Mishra et al.[269] have shown for the first time using the acriflavin fluorophore that the distance dependence of enhancement has the same profile for S_1, T_1, and α-S_1 emission, all within the same fluorophore.

Finally, as plasmon-based fluorescence matures into a fluorescence discipline in its own right, it is being used in clinical testing. For example, Wang et al. have recently summarized the applications of MEF in the biomedical field.[273] Chang et al.[274] have recently used a MEF-based high-throughput biosensor to diagnose human metapneumovirus (common respiratory tract infection), using 91 clinical samples. They report a 77.4% sensitivity and a specificity of 91.7% as compared to a standard immunofluorescent-antibody test.[274] Similarly, the Geddes group has continued to develop several clinical platforms based on the microwave-accelerated metal-enhanced fluorescence (MAMEF) technique.[275,276] The MAMEF technique combines the benefits of MEF for enhancing assay sensitivity (enhanced signal) but additionally utilizes low power microwaves to rapidly accelerate assay kinetics to completion within 1 min. This technology has been shown to have sensitivity levels similar to PCR but only much more rapid.[275,276] In a recent *blinded clinical study*, an MAMEF assay for detection of *Chlamydia trachomatis* from 257 vaginal swabs showed 89.5% sensitivity and 91.0% specificity agreement with a gold-standard nucleic acid amplification test. This new technology provided a result in less than 9 min (which included sample preparation) and cost about $1, significantly cheaper than other commercially available nucleic acid amplification tests.

AUTHOR INFORMATION

Corresponding Author

*E-mail: iwarner@lsu.edu.

Notes

The authors declare no competing financial interest.

Biographies

Noureen Siraj is a research associate in the Warner research group at Louisiana State University. She received her M.Sc. in physical chemistry from the University of Karachi, Pakistan, and received four gold medals for securing first position. She earned her Ph.D. in the field of electrochemistry using ionic liquids from the Graz University of Technology, Austria, in 2011, under the supervision of Professor Gunter Grampp. After completion of her Ph.D., she joined the Warner Research group as a postdoctoral research scholar. Her current research interests include development of multifunctional ionic liquids, GUMBOS, and their nanomaterials for different applications

DOI: 10.1021/acs.analchem.5b04109
Anal. Chem. 2016, 88, 170−202

such as optoelectronics (solar cells, OLEDs), cancer therapy, and sensors. She is interested in investigations of photodynamics and electrochemical characteristics of novel materials at the molecular, as well as at the nanoscale level.

Bilal El-Zahab is Assistant Professor of Mechanical and Materials Engineering at Florida International University since 2012. He previously was a Postdoctoral Associate in P.T. Hammond's laboratory in the Chemical Engineering Department at Massachusetts Institute of Technology, Cambridge, Massachusetts, and before that in I. M. Warner's laboratory in the Department of Chemistry at Louisiana State University. He received his B.S. degree in Chemical Engineering from Middle East Technical University, Turkey, and Ph.D. in Chemical and Biomolecular Engineering from the University of Akron, Ohio. His current research interests are in the fields of microfabrications, nanomaterials, ionic liquids, and their applications in biomedical, environmental, and energy research.

Suzana Hamdan is currently a postdoctoral researcher in the Warner Research Group at Department of Chemistry, Louisiana State University. Suzana pursued her undergraduate studies in general chemistry at Lebanese University and graduated in 2006. She then joined East Tennessee State University where she completed her master's degree in analytical chemistry under the supervision of Dr. Chu-Ngi Ho. After her graduation in 2009, she started working on her Ph.D. degree in the Warner Research Group, and her research interests include nanotechnology and analytical chemistry. Suzana received her doctorate on May 2015 with a dissertation topic related to the synthesis and studies of nanoparticles made from organic salts. She developed novel techniques for size-control of nanoGUMBOS and designed molecularly imprinted polymeric nanoGUMBOS for chiral recognition of biological targets. She has also been investigating size-dependent optical properties of nanoGUMBOS and possible application of these nanomaterials in optoelectronic devices including organic light emitting diodes.

Tony E. Karam studied chemistry at Saint-Joseph University in Lebanon, where he received his B.Sc. in chemistry in 2008. In 2011, he received a M.Sc. degree in chemistry from the American University of Beirut, where he studied nonlinear dynamics and periodic precipitation focusing on chemical reactions coupled to transport properties. He is currently a Ph.D. candidate in the Haber group at Louisiana State University. His research interests focus on the use of ultrafast and nonlinear spectroscopy for the study of processes such as molecular adsorption, molecular structure and orientation, and energy and electron transfer at nanoparticle surfaces.

Louis H. Haber studied chemistry at the University of California, Berkeley, where he received his B.S and Ph.D. degrees in 2002 and 2009, respectively. He worked for 3 years as a postdoctoral researcher in the Department of Chemistry at Columbia University from 2009–2012. In 2012, he accepted a position as Assistant Professor in the Department of Chemistry at Louisiana State University. His current research interests include fundamental investigations of nanoparticles and nanomaterials and their interactions with molecules and light using ultrafast spectroscopy and nonlinear spectroscopy. Additionally, his research focuses on potential advances in applications of molecular sensing, nanomedicine, catalysis, nanoengineering, solar energy, and optoelectronics.

Min Li is currently a Senior R&D Specialist at Albemarle Corporation. He was a postdoctoral researcher under the direction of Professor Isiah M. Warner at Louisiana State University. Min received his B.A. in chemistry from Hubei Normal University in 1999 and his Ph.D. in organic chemistry under the guidance of Professor Xianjun Li at Sichuan University in China, 2004. He was a postdoctoral researcher working for Dr. Tingyu Li at Mississippi State University at Starkville, MS, from 2005 to 2008. His research interests include synthesis of novel functionalized ionic liquids and their applications in separation, luminescent materials, bioimaging, and cancer therapy fields. Dr. Li is also interested in organometallic compound synthesis and their applications in various catalysis reactions.

Sayo O. Fakayode is an Associate Professor in the Department of Chemistry at North Carolina A&T State University, Greensboro, North Carolina. He received his B.Sc. degree in chemistry from the University of Ibadan, Nigeria, in 1994 and received his M.Sc. degree in analytical chemistry from the University of Ibadan, in 1997. He obtained his Ph.D. in analytical chemistry from Baylor University, Waco, Texas, in 2004 under the supervision of Dr. Marianna A. Busch and Dr. Kenneth W. Busch. He was a postdoctoral researcher in Dr. Isiah Warner's research group at Louisiana State University between 2004 and 2007. His research interests include chiral analysis, guest–host inclusion complexation, analytical spectroscopy, fluorescence detection of molecules of pharmaceutical, clinical, biomedical, forensic, and environmental interest as well as the use of chemometrics, multivariate analysis, and experimental design for instrumental calibration, process optimization, and process control.

Susmita Das is presently working as Associate Professor in the Civil Engineering Department of Adamas Institute of Technology, Barasat, WB, India, since August 2015. Prior to this she had worked as a CSIR Senior Research Associate (Scientist Pool Scheme) at Indian Institute for the Cultivation of Science, Kolkata, WB, India. Susmita had worked as a postdoctoral associate with Prof. Isiah M. Warner, Louisiana State University, Baton Rouge, LA, during 2009–2013 when she had primary investigated biomedical applications of fluorescent and multifunctional nanoGUMBOS. She had obtained her Ph.D in the year 2009 from University of Kalyani, WB, India, under the supervision of Prof. Swati De. Her Ph.D research was mainly based on fluorescence based study of organized media using fluorescent dyes.

Bertha Valle is currently on family leave from Texas Southern University. She received a B.S. degree in Chemistry from Texas Tech University, Lubbock, TX, in 1998. She went on to pursue a Ph.D, investigating chiral recognition with spectroscopy and chromatography, under the direction of Dr. Isiah M. Warner at Louisiana State University where she received her Ph.D. degree in 2005. She completed postdoctoral training, from 2005 and 2007, in optical imaging in the research group of Dr. Richards-Kortum at Rice University, Houston, TX. In 2008, she joined the faculty at Texas Southern University in Houston, TX, in the Department of Chemistry. Her current research interest includes fluorescence spectroscopy and associated applications.

Robert M. Strongin is Professor of Chemistry, Portland State University (PSU). He received his B.A. degree in chemistry from Temple University in Philadelphia, PA. He worked at FMC Corporation and SmithKline Beecham Corporation before pursuing his doctoral studies. He received his Ph.D. in Organic Chemistry from the University of Pennsylvania in the laboratory of Amos B. Smith, III. He served on the faculty of Louisiana State University for 12 years before joining the faculty of PSU in 2007. His research interests include synthetic, physical organic, materials, and bioorganic chemistry, with a focus on creating new sensing reagents, probes, and pharmaceuticals.

Gabor Patonay obtained his M.S. (1973) and Ph.D. (1979) degrees from the Faculty of Chemistry of the Technical University of Budapest, Hungary. In 1982, he became a postdoctoral fellow in Professor Isiah M. Warner's group at Emory University. He joined the faculty of Georgia State University (GSU) in 1987 where he is

DOI: 10.1021/acs.analchem.5b04109
Anal. Chem. 2016, 88, 170–202

currently Professor. During the last several years, Dr. Patonay and his research group have developed new bioanalytical and biomedical applications using NIR dyes as probes and labels, forensic analytical tools for presumptive trace evidence detection and for medical imaging. Recently, his research group has developed new silica nanoparticle probes using covalently incorporated NIR dyes for forensic analyses and bioanalytical applications.

Herman O. Sintim obtained his B.S. in medicinal chemistry from University College London (UCL), U.K., in 1999. After graduate studies in synthetic organic chemistry under the direction of David M. Hodgson at Oxford University, he did postdoctoral research with Timothy J. Donohoe, also at Oxford. He then joined the laboratory of Eric T. Kool at Stanford University. At Stanford, he investigated DNA polymerization using non-natural nucleobases. He started his independent career as assistant professor at the University of Maryland, College Park, in 2006 and was promoted to associate professor in 2012 and then to a full professor in 2015. From January 2016, Herman will become a professor at Purdue University. His research interests include bacterial biofilm formation and virulence factors production, new cancer therapeutics, and development of new fluorogenic or chromogenic paradigms to detect bioanalytes.

Gary A. Baker studied chemistry at the State University of New York at Oswego and earned his doctoral degree in Analytical Chemistry under the supervision of Prof. Frank V. Bright at the University at Buffalo. Following graduate studies, he was a Frederick Reines postdoctoral fellow at Los Alamos National Laboratory. He then joined Oak Ridge National Laboratory as a Eugene P. Wigner fellow and staff scientist remaining there until the end of 2010, at which time he accepted a position as Assistant Professor in the Chemistry Department at the University of Missouri-Columbia. He has authored more than 225 peer-reviewed journal articles and has won several awards for his research, most notably a Presidential Early Career Award for Scientists and Engineers (PECASE) from the U.S. Department of Energy (2008), as well as becoming a Cottrell Scholar (2015). His research interests include energy applications of ionic liquids, microfluidic platforms for nanomaterials synthesis, two-dimensional materials, deep eutectic solvents, and all things luminescent.

Aleeta M. Powe received her B.S. in chemistry from the University of South Alabama, Mobile, AL, in 1990. She worked as a Special Volunteer at the Gerontology Research Center of the National Institute on Aging, National Institutes of Health, Baltimore, MD, as a researcher at Georgetown University Medical Center and as a Chemical Information Specialist for the Food and Drug Administration before receiving her Ph.D. in Analytical Chemistry from American University, Washington, DC, in 2002. For 2 years, she served as a postdoctoral researcher under the supervision of Professor Isiah Warner before joining the faculty at the University of Louisville in 2005. At the University of Louisville, she studied carbohydrate polymers using mass spectrometry and was the PI of the first departmental Research Experiences for the Undergraduates (REU) Program.

Mark Lowry received his Ph.D. in Analytical Chemistry using fluorescence techniques to investigate chemical separations with Professor Maxwell Lei Geng at The University of Iowa. He was subsequently involved with wide-ranging projects as a Research Associate in the laboratory of Professor Isiah M. Warner at Louisiana State University. He is currently working on the development and application of novel fluorescent probes in Professor Robert M. Strongin's laboratory at Portland State University. His interests include fluorescence techniques, instrumentation and reagents, separations, and sensing.

Jan O. Karolin undertook his Ph.D. studies in fluorescence spectroscopy in the Biophysical Department at the University of Umea, Sweden, under the guidance of Professor Lennart B.-A. Johansson. He then worked as a postdoctoral research fellow in the Physics Department, University of Strathclyde, Scotland, from 1999 until 2004, after that he worked as a lecturer until 2012. In 2012, Dr. Karolin took a position at the world renowned Institute of Fluorescence in Maryland, USA, where he is currently working as an Assistant Professor. Dr. Karolin has significant experience in fluorescence spectroscopy and plasmonic fluorescence and has published over 30 peer reviewed papers. Dr. Karolin's particular fluorescence expertise lies in the deconvolution of complex time-resolved fluorescence decays as well as the photophysics of fluorophores in plasmonic near-fields.

Chris D. Geddes, Ph.D., FRSC, Professor, and director of UMBC's Institute of Fluorescence, has extensive experience in fluorescence spectroscopy, particularly in fluorescence sensing and metal-fluorophore interactions, publishing over 250 peer-reviewed papers (h-index, 42) and 30 books. Dr. Geddes is internationally known in fluorescence and plasmonics and his laboratory is widely attributed to the development of the metal-enhanced fluorescence (MEF) and related plasmon-fluorescence technologies, securing in excess of $25 million in recent years to pursue his research aspirations. He is the editor-in-chief of the *Journal of Fluorescence* and founding editor-in-chief of the *Who's Who in Fluorescence*, *Annual Reviews in Fluorescence*, *Annual Reviews in Plasmonics*, and the *Plasmonics Journal*. Dr. Geddes is a fellow of both the Royal Society of Chemistry (FRSC) and the Institute of Physics. Dr. Geddes holds 100 patents in the fields of fluorescence and plasmonics.

Isiah M. Warner is a Boyd Professor of the LSU System, Philip W. West Professor of Analytical and Environmental Chemistry, and Howard Hughes Medical Institute Professor in the Department of Chemistry at Louisiana State University (LSU). He received his B.S. degree in chemistry from Southern University in Baton Rouge, LA, in 1968. He worked at Battelle Northwest in Richland, Washington, for 5 years before pursuing his Ph.D. in Analytical Chemistry from the University of Washington in 1973. He received his Ph.D. in Analytical Chemistry from the University of Washington in 1977. He served on the faculty of Texas A&M University for 5 years and on the faculty of Emory University for 10 years before joining the faculty of LSU in 1992. His research interests include fluorescence spectroscopy, ionic liquids, ionic liquid chemistry in the solid phase, studies in organized media, separation science, and nanomaterials, with a focus on solving biomedical, forensic, and environmental analytical problems.

■ ACKNOWLEDGMENTS

I.M.W. acknowledges support from the National Science Foundation under Grant Nos. CHE-1307611 and CHE-1508726 and the Philip W. West Endowment during preparation of this review manuscript.

■ REFERENCES

(1) Das, S.; Powe, A. M.; Baker, G. A.; Valle, B.; El-Zahab, B.; Sintim, H. O.; Lowry, M.; Fakayode, S. O.; McCarroll, M. E.; Patonay, G. *Anal. Chem.* **2012**, *84*, 597−625.

(2) Jameson, D. M. *Introduction to Fluorescence*; Taylor & Francis: Boca Raton, FL, 2014.

(3) Engelborghs, Y., Visser, A., Eds. *Fluorescence Spectroscopy and Microscopy: Methods and Protocols*; Springer: New York, 2014.

DOI: 10.1021/acs.analchem.5b04109
Anal. Chem. 2016, 88, 170−202

(4) Kubitscheck, U. *Fluorescence Microscopy: From Principles to Biological Applications*; John Wiley & Sons: Weinheim, Germany, 2013.
(5) Marcu, L.; French, P. M.; Elson, D. S. *Fluorescence Lifetime Spectroscopy and Imaging: Principles and Applications in Biomedical Diagnostics*; CRC Press: Boca Raton, FL, 2014.
(6) Gell, C.; Brockwell, D.; Smith, A. *Handbook of Single Molecule Fluorescence Spectroscopy*; Oxford University Press: Oxford, U.K., 2006.
(7) Mondal, P. P.; Diaspro, A. *Fundamentals of Fluorescence Microscopy: Exploring Life with Light*; Springer Science & Business Media: Dordrecht, The Netherlands, 2014.
(8) Gilmore, A. M. *Luminescence: The Instrumental Key to the Future of Nanotechnology*; Pan Stanford: Singapore, 2013.
(9) Sabnis, R. W. *Handbook of Fluorescent Dyes and Probes*; John Wiley & Sons: Hoboken, NJ, 2015.
(10) Tsukanov, R.; Tomov, T. E.; Liber, M.; Berger, Y.; Nir, E. *Acc. Chem. Res.* **2014**, *47*, 1789−1798.
(11) Pushie, M. J.; Pickering, I. J.; Korbas, M.; Hackett, M. J.; George, G. N. *Chem. Rev.* **2014**, *114*, 8499−8541.
(12) Cordes, T.; Blum, S. A. *Nat. Chem.* **2013**, *5*, 993−999.
(13) Haas, B. L.; Matson, J. S.; DiRita, V. J.; Biteen, J. S. *Molecules* **2014**, *19*, 12116−12149.
(14) Shivanandan, A.; Deschout, H.; Scarselli, M.; Radenovic, A. *FEBS Lett.* **2014**, *588*, 3595−3602.
(15) Endesfelder, U.; Heilemann, M. *Nat. Methods* **2014**, *11*, 235−238.
(16) Burgert, A.; Letschert, S.; Doose, S.; Sauer, M. *Histochem. Cell Biol.* **2015**, *144*, 123−131.
(17) Coltharp, C.; Yang, X.; Xiao, J. *Curr. Opin. Struct. Biol.* **2014**, *28*, 112−121.
(18) Sage, D.; Kirshner, H.; Pengo, T.; Stuurman, N.; Min, J.; Manley, S.; Unser, M. *Nat. Methods* **2015**, *12*, 717−724.
(19) Lin, Y.; Long, J. J.; Huang, F.; Duim, W. C.; Kirschbaum, S.; Zhang, Y.; Schroeder, L. K.; Rebane, A. A.; Velasco, M.; Virrueta, A. *PLoS One* **2015**, *10*, e0128135−e0128135.
(20) Lew, M. D.; Backlund, M. P.; Moerner, W. *Nano Lett.* **2013**, *13*, 3967−3972.
(21) Long, F.; Zeng, S.; Huang, Z. *Phys. Chem. Chem. Phys.* **2014**, *16*, 21586−21594.
(22) Kim, D.; Curthoys, N. M.; Parent, M. T.; Hess, S. T. *J. Opt.* **2013**, *15*, 094011.
(23) McGorty, R.; Schnitzbauer, J.; Zhang, W.; Huang, B. *Opt. Lett.* **2014**, *39*, 275−278.
(24) Allen, J. R.; Ross, S. T.; Davidson, M. W. *Phys. Chem. Chem. Phys.* **2013**, *15*, 18771−18783.
(25) Whelan, D. R.; Bell, T. D. M. *Sci. Rep.* **2015**, *5*, 7924.
(26) Enderlein, J. *Pure Appl. Chem.* **2013**, *85*, 999−1016.
(27) Sanguigno, L.; Cosenza, C.; Causa, F.; Netti, P. A. *Analyst* **2013**, *138*, 1674−1681.
(28) Sankaran, J.; Bag, N.; Kraut, R. S.; Wohland, T. *Anal. Chem.* **2013**, *85*, 3948−3954.
(29) Sun, G.; Guo, S.-M.; Teh, C.; Korzh, V.; Bathe, M.; Wohland, T. *Anal. Chem.* **2015**, *87*, 4326−4333.
(30) Müller, P.; Schwille, P.; Weidemann, T. *Bioinformatics* **2014**, *30*, 2532−2533.
(31) Laurence, T. A.; Ly, S.; Bourguet, F.; Fischer, N. O.; Coleman, M. A. J. *J. Phys. Chem. B* **2014**, *118*, 9662−9667.
(32) Ma, L.; Yang, F.; Zheng, J. *J. Mol. Struct.* **2014**, *1077*, 87−100.
(33) Saremi, B.; Wei, M.-Y.; Liu, Y.; Cheng, B.; Yuan, B. *J. Biomed. Opt.* **2014**, *19*, 085008−085008.
(34) Jordan, A. N.; Siraj, N.; Das, S.; Warner, I. M. *RSC Adv.* **2014**, *4*, 28471−28480.
(35) Siraj, N.; Das, S.; Hasan, F.; Lu, C.; Kiruri, L. W.; Gall, K. E. S.; Warner, I. M. *RSC Adv.* **2015**, *5*, 9939−9945.
(36) Kelliher, M. T.; Piraino, M. S.; Gemoules, M. E.; Southern, C. A. *Anal. Biochem.* **2013**, *441*, 44−50.
(37) Krüger, A. C.; Birkedal, V. *Methods* **2013**, *64*, 36−42.
(38) Hohlbein, J.; Craggs, T. D.; Cordes, T. *Chem. Soc. Rev.* **2014**, *43*, 1156−1171.
(39) Cho, S.; Jang, J.; Song, C.; Lee, H.; Ganesan, P.; Yoon, T.-Y.; Kim, M. W.; Choi, M. C.; Ihee, H.; Do Heo, W. *Sci. Rep.* **2013**, *3*, 1208.
(40) Kim, D.; Moon, H.; Baik, S. H.; Singha, S.; Jun, Y. W.; Wang, T.; Kim, K. H.; Park, B. S.; Jung, J.; Mook-Jung, I. *J. Am. Chem. Soc.* **2015**, *137*, 6781−6789.
(41) Zhang, X.; Tian, Y.; Zhang, C.; Tian, X.; Ross, A. W.; Moir, R. D.; Sun, H.; Tanzi, R. E.; Moore, A.; Ran, C. P. *Proc. Natl. Acad. Sci. U. S. A.* **2015**, *112*, 9734−9739.
(42) Zhou, L.; Zhang, X.; Wang, Q.; Lv, Y.; Mao, G.; Luo, A.; Wu, Y.; Wu, Y.; Zhang, J.; Tan, W. *J. Am. Chem. Soc.* **2014**, *136*, 9838−9841.
(43) Agrawalla, B. K.; Chandran, Y.; Phue, W.-H.; Lee, S.-C.; Jeong, Y.-M.; Wan, S. Y. D.; Kang, N.-Y.; Chang, Y.-T. *J. Am. Chem. Soc.* **2015**, *137*, 5355−5362.
(44) Zhang, H.; Fan, J.; Wang, J.; Zhang, S.; Dou, B.; Peng, X. *J. Am. Chem. Soc.* **2013**, *135*, 11663−11669.
(45) Ghosh, D.; Bagley, A. F.; Na, Y. J.; Birrer, M. J.; Bhatia, S. N.; Belcher, A. M. P. *Proc. Natl. Acad. Sci. U. S. A.* **2014**, *111*, 13948−13953.
(46) Hettiarachchi, S. U.; Prasai, B.; McCarley, R. L. *J. Am. Chem. Soc.* **2014**, *136*, 7575−7578.
(47) Nawimanage, R. R.; Prasai, B.; Hettiarachchi, S. U.; McCarley, R. L. *Anal. Chem.* **2014**, *86*, 12266−12271.
(48) Ling, D.; Park, W.; Park, S.-j.; Lu, Y.; Kim, K. S.; Hackett, M. J.; Kim, B. H.; Yim, H.; Jeon, Y. S.; Na, K. *J. Am. Chem. Soc.* **2014**, *136*, 5647−5655.
(49) Harrison, V. S.; Carney, C. E.; MacRenaris, K. W.; Waters, E. A.; Meade, T. J. *J. Am. Chem. Soc.* **2015**, *137*, 9108−9116.
(50) Kim, E.-J.; Bhuniya, S.; Lee, H.; Kim, H. M.; Cheong, C.; Maiti, S.; Hong, K. S.; Kim, J. S. *J. Am. Chem. Soc.* **2014**, *136*, 13888−13894.
(51) Hembury, M.; Chiappini, C.; Bertazzo, S.; Kalber, T. L.; Drisko, G. L.; Ogunlade, O.; Walker-Samuel, S.; Krishna, K. S.; Jumeaux, C.; Beard, P. P. *Proc. Natl. Acad. Sci. U. S. A.* **2015**, *112*, 1959−1964.
(52) Nan, X.; Collisson, E. A.; Lewis, S.; Huang, J.; Tamgüney, T. M.; Liphardt, J. T.; McCormick, F.; Gray, J. W.; Chu, S. P. *Proc. Natl. Acad. Sci. U. S. A.* **2013**, *110*, 18519−18524.
(53) Rollins, G. C.; Shin, J. Y.; Bustamante, C.; Pressé, S. P. *Proc. Natl. Acad. Sci. U. S. A.* **2015**, *112*, E110−E118.
(54) Liu, D. S.; Nivón, L. G.; Richter, F.; Goldman, P. J.; Deerinck, T. J.; Yao, J. Z.; Richardson, D.; Phipps, W. S.; Anne, Z. Y.; Ellisman, M. H. P. *Proc. Natl. Acad. Sci. U. S. A.* **2014**, *111*, E4551−E4559.
(55) Hajj, B.; Wisniewski, J.; El Beheiry, M.; Chen, J.; Revyakin, A.; Wu, C.; Dahan, M. P. *Proc. Natl. Acad. Sci. U. S. A.* **2014**, *111*, 17480−17485.
(56) Zhao, Z. W.; Roy, R.; Gebhardt, J. C. M.; Suter, D. M.; Chapman, A. R.; Xie, X. S. P. *Proc. Natl. Acad. Sci. U. S. A.* **2014**, *111*, 681−686.
(57) Zhang, Y.; Lucas, J. M.; Song, P.; Beberwyck, B.; Fu, Q.; Xu, W.; Alivisatos, A. P. P. *Proc. Natl. Acad. Sci. U. S. A.* **2015**, *112*, 8959−8964.
(58) Liu, H.-Y.; Wu, P.-J.; Kuo, S.-Y.; Chen, C.-P.; Chang, E.-H.; Wu, C.-Y.; Chan, Y.-H. *J. Am. Chem. Soc.* **2015**, *137*, 10420−10429.
(59) Wu, I.-C.; Yu, J.; Ye, F.; Rong, Y.; Gallina, M. E.; Fujimoto, B. S.; Zhang, Y.; Chan, Y.-H.; Sun, W.; Zhou, X.-H. *J. Am. Chem. Soc.* **2015**, *137*, 173−178.
(60) Takai, A.; Nakano, M.; Saito, K.; Haruno, R.; Watanabe, T. M.; Ohyanagi, T.; Jin, T.; Okada, Y.; Nagai, T. P. *Proc. Natl. Acad. Sci. U. S. A.* **2015**, *112*, 4352−4356.
(61) Arena, E. T.; Campbell-Valois, F.-X.; Tinevez, J.-Y.; Nigro, G.; Sachse, M.; Moya-Nilges, M.; Nothelfer, K.; Marteyn, B.; Shorte, S. L.; Sansonetti, P. J. P. *Proc. Natl. Acad. Sci. U. S. A.* **2015**, *112*, E3282−E3290.
(62) Hettie, K. S.; Klockow, J. L.; Glass, T. E. *J. Am. Chem. Soc.* **2014**, *136*, 4877−4880.
(63) Au-Yeung, H. Y.; Chan, J.; Chantarojsiri, T.; Chang, C. J. *J. Am. Chem. Soc.* **2013**, *135*, 15165−15173.
(64) Xia, T.; Li, N.; Fang, X. *Annu. Rev. Phys. Chem.* **2013**, *64*, 459−480.
(65) Horton, N. G.; Wang, K.; Kobat, D.; Clark, C. G.; Wise, F. W.; Schaffer, C. B.; Xu, C. *Nat. Photonics* **2013**, *7*, 205−209.

DOI: 10.1021/acs.analchem.5b04109
Anal. Chem. 2016, 88, 170−202

(66) Karam, T. E.; Haber, L. H. *J. Phys. Chem. C* **2014**, *118*, 642−649.
(67) Kumal, R. R.; Karam, T. E.; Haber, L. H. *J. Phys. Chem. C* **2015**, *119*, 16200−16207.
(68) Xing, G.; Liao, Y.; Wu, X.; Chakrabortty, S.; Liu, X.; Yeow, E. K.; Chan, Y.; Sum, T. C. *ACS Nano* **2012**, *6*, 10835−10844.
(69) Kierdaszuk, B. *J. Fluoresc.* **2013**, *23*, 339−347.
(70) Rich, R. M.; Mummert, M.; Gryczynski, Z.; Borejdo, J.; Sørensen, T. J.; Laursen, B. W.; Foldes-Papp, Z.; Gryczynski, I.; Fudala, R. *Anal. Bioanal. Chem.* **2013**, *405*, 4887−4894.
(71) Shibata, Y.; Nishi, S.; Kawakami, K.; Shen, J.-R.; Renger, T. *J. Am. Chem. Soc.* **2013**, *135*, 6903−6914.
(72) Chen, K.; Gallaher, J. K.; Barker, A. J.; Hodgkiss, J. M. *J. Phys. Chem. Lett.* **2014**, *5*, 1732−1737.
(73) Cordones, A. A.; Leone, S. R. *Chem. Soc. Rev.* **2013**, *42*, 3209−3221.
(74) Jiang, C.; Zhao, T.; Yuan, P.; Gao, N.; Pan, Y.; Guan, Z.; Zhou, N.; Xu, Q.-H. *ACS Appl. Mater. Interfaces* **2013**, *5*, 4972−4977.
(75) Hao, F.; Li, D.; Zhang, Q.; Li, S.; Zhang, S.; Zhou, H.; Wu, J.; Tian, Y. *Spectrochim. Acta, Part A* **2015**, *150*, 867−878.
(76) Zhao, T.; Jiang, X.-F.; Gao, N.; Li, S.; Zhou, N.; Ma, R.; Xu, Q.-H. *J. Phys. Chem. B* **2013**, *117*, 15576−15583.
(77) Chan, E. M.; Han, G.; Goldberg, J. D.; Gargas, D. J.; Ostrowski, A. D.; Schuck, P. J.; Cohen, B. E.; Milliron, D. *Nano Lett.* **2012**, *12*, 3839−3845.
(78) Gong, S.; Li, M.; Ren, Z.; Yang, X.; Li, X.; Shen, G.; Han, G. *J. Phys. Chem. C* **2015**, *119*, 17326−17333.
(79) Guarin, C. A.; Villabona-Monsalve, J. P.; López-Arteaga, R.; Peon, J. *J. Phys. Chem. B* **2013**, *117*, 7352−7362.
(80) Keene, J. D.; McBride, J. R.; Orfield, N. J.; Rosenthal, S. *ACS Nano* **2014**, *8*, 10665−10673.
(81) Guan, Z.; Gao, N.; Jiang, X.-F.; Yuan, P.; Han, F.; Xu, Q.-H. *J. Am. Chem. Soc.* **2013**, *135*, 7272−7277.
(82) Jiang, X.-F.; Pan, Y.; Jiang, C.; Zhao, T.; Yuan, P.; Venkatesan, T.; Xu, Q.-H. *J. Phys. Chem. Lett.* **2013**, *4*, 1634−1638.
(83) Zieschang, F.; Schmiedel, A.; Holzapfel, M.; Ansorg, K.; Engels, B.; Lambert, C. *J. Phys. Chem. C* **2013**, *117*, 19816−19831.
(84) Pavitra, E.; Raju, G. S. R.; Park, W.; Yu, J. S. *New J. Chem.* **2014**, *38*, 163−169.
(85) Lu, D.; Lei, J.; Wang, L.; Zhang, J. *J. Am. Chem. Soc.* **2012**, *134*, 8746−8749.
(86) Dramićanin, T.; Lenhardt, L.; Zeković, I.; Dramićanin, M. D. *J. Fluoresc.* **2012**, *22*, 1281−1289.
(87) Zeković, I.; Dramićanin, T.; Lenhardt, L.; Bandić, J.; Dramićanin, M. D. *Appl. Spectrosc.* **2014**, *68*, 823−830.
(88) Rajasekaran, R.; Aruna, P.; Koteeswaran, D.; Baludavid, M.; Ganesan, S. *J. Fluoresc.* **2014**, *24*, 1199−1205.
(89) Abdel-Aziz, O.; El Kosasy, A.; Okeil, S. E.-S. *J. Fluoresc.* **2014**, *24*, 549−556.
(90) Chang, H.-Y.; Chang, H.-T.; Hung, Y.-L.; Hsiung, T.-M.; Lin, Y.-W.; Huang, C.-C. *RSC Adv.* **2013**, *3*, 4588−4597.
(91) Wang, D.; Li, L.; Yang, W.; Zuo, Y.; Feng, S.; Liu, H. *RSC Adv.* **2014**, *4*, 59877−59884.
(92) Zeng, Y.-p.; Hu, J.; Long, Y.; Zhang, C.-y. *Anal. Chem.* **2013**, *85*, 6143−6150.
(93) Zong, C.; Wu, J.; Liu, M.; Yang, L.; Yan, F.; Ju, H. *Anal. Chem.* **2014**, *86*, 9939−9944.
(94) Gao, Y.; Li, B. *Anal. Chem.* **2013**, *85*, 11494−11500.
(95) Al-Ogaidi, I.; Gou, H.; Aguilar, Z. P.; Guo, S.; Melconian, A. K.; Al-kazaz, A. K. A.; Meng, F.; Wu, N. *Chem. Commun.* **2014**, *50*, 1344−1346.
(96) Bi, S.; Zhang, Z.; Dong, Y.; Wang, Z. *Biosens. Bioelectron.* **2015**, *65*, 139−144.
(97) Li, Z.; He, X.; Wang, Z.; Yang, R.; Shi, W.; Ma, H. *Biosens. Bioelectron.* **2015**, *63*, 112−116.
(98) Chyan, W.; Zhang, D. Y.; Lippard, S. J.; Radford, R. J. P. *Proc. Natl. Acad. Sci. U. S. A.* **2014**, *111*, 143−148.
(99) Peng, J.; Xu, W.; Teoh, C. L.; Han, S.; Kim, B.; Samanta, A.; Er, J. C.; Wang, L.; Yuan, L.; Liu, X. *J. Am. Chem. Soc.* **2015**, *137*, 2336−2342.
(100) Vali, R.; Loidl, W.; Pirich, C.; Langesteger, W.; Beheshti, M. *Am. J. Nucl. Med. Mol. Imaging* **2015**, *5*, 96.
(101) Pires, A. O.; Borges, U. S.; Lopes-Costa, P. V.; Gebrim, L. H.; da Silva, B. B. *Eur. J. Obstet. Gynecol. Reprod. Biol.* **2014**, *180*, 138−141.
(102) Tummers, Q.; Verbeek, F.; Schaafsma, B.; Boonstra, M.; van der Vorst, J.; Liefers, G.-J.; van de Velde, C.; Frangioni, J.; Vahrmeijer, A. *Eur. J. Surg. Oncol.* **2014**, *40*, 850−858.
(103) Yuen, K.; Miura, T.; Sakai, I.; Kiyosue, A.; Yamashita, M. *J. Urol.* **2015**, *194*, 371−377.
(104) Metildi, C. A.; Kaushal, S.; Felsen, C. N.; Nguyen, Q. T.; Hoffman, R. M.; Tsien, R. Y.; Bouvet, M. *Cancer Res.* **2014**, *74*, 4311−4311.
(105) Yano, S.; Hiroshima, Y.; Maawy, A.; Katz, M. H.; Fleming, J. B.; Kishimoto, H.; Suetsugu, A.; Uehara, F.; Miwa, S.; Tazawa, H. *Cancer Res.* **2014**, *74*, 1218−1218.
(106) Gordo, V. O.; Arslanli, Y. T.; Canimoglu, A.; Ayvacikli, M.; Gobato, Y. G.; Henini, M.; Can, N. *Appl. Radiat. Isot.* **2015**, *99*, 69−76.
(107) Baran, A.; Mahlik, S.; Grinberg, M.; Cai, P.; Kim, S. I.; Seo, H. *J. Phys.: Condens. Matter* **2014**, *26*, 385401.
(108) Lu, C.; Das, S.; Siraj, N.; Magut, P. K. S.; Li, M.; Warner, I. M. *J. Phys. Chem. A* **2015**, *119*, 4780−4786.
(109) Li, L.; Peng, M.; Viana, B.; Wang, J.; Lei, B.; Liu, Y.; Zhang, Q.; Qiu, J. *Inorg. Chem.* **2015**, *54*, 6028−6034.
(110) Wang, T.; Li, P.; Li, H. *ACS Appl. Mater. Interfaces* **2014**, *6*, 12915−12921.
(111) Cano, N. F.; dos Santos, L. H.; Chubaci, J. F.; Watanabe, S. *Spectrochim. Acta, Part A* **2015**, *137*, 471−476.
(112) Karaliunas, M.; Kuokstis, E.; Ting, S.-Y.; Huang, J.-J.; Yang, C. *J. Appl. Phys.* **2014**, *116*, 123501.
(113) Liu, L.; Wang, Q.; Gao, C.; Chen, H.; Liu, W.; Tang, Y. *J. Phys. Chem. C* **2014**, *118*, 14511−14520.
(114) Jiang, H.; Rooh, G.; Kim, H.; Lee, J.; Lee, Y.; Zhang, W.; Kim, S. *J. Cryst. Growth* **2015**, *418*, 163−166.
(115) Spassky, D. A.; Nagirnyi, V.; Savon, A. E.; Kamenskikh, I. A.; Barinova, O. P.; Kirsanova, S. V.; Grigorieva, V. D.; Ivannikova, N. V.; Shlegel, V. N.; Aleksanyan, E.; Yelisseyev, A. P.; Belsky, A. *J. Lumin.* **2015**, *166*, 195−202.
(116) Sokolov, V.; Pustovarov, V.; Gruzdev, N.; Sokolov, P.; Baranov, A. *Opt. Spectrosc.* **2014**, *116*, 790−792.
(117) Kostka, P.; Zavadil, J.; Iovu, M. S.; Ivanova, Z. G.; Furniss, D.; Seddon, A. B. *J. Alloys Compd.* **2015**, *648*, 237−243.
(118) Green, T. D.; Yi, C.; Zeng, C.; Jin, R.; McGill, S.; Knappenberger, K. L., Jr *J. Phys. Chem. A* **2014**, *118*, 10611−10621.
(119) Vialla, F.; Chassagneux, Y.; Ferreira, R.; Roquelet, C.; Diederichs, C.; Cassabois, G.; Roussignol, P.; Lauret, J.-S.; Voisin, C. *Phys. Rev. Lett.* **2014**, *113*, 057402.
(120) Reshchikov, M.; Usikov, A.; Helava, H.; Makarov, Y. *J. Electron. Mater.* **2015**, *44*, 1281−1286.
(121) Zhang, F.; Zhong, H.; Chen, C.; Wu, X.-g.; Hu, X.; Huang, H.; Han, J.; Zou, B.; Dong, Y. *ACS Nano* **2015**, *9*, 4533−4542.
(122) Manohara, B.; Nagabhushana, H.; Thyagarajan, K.; Prasad, B. D.; Prashantha, S.; Sharma, S.; Nagabhushana, B. *J. Lumin.* **2015**, *161*, 247−256.
(123) Singh, A. K.; Thool, G. S.; Bangal, P. R.; Madhavendra, S. S.; Singh, S. P. *Ind. Eng. Chem. Res.* **2014**, *53*, 9383−9390.
(124) Shi, T.; Jackson, H. E.; Smith, L. M.; Jiang, N.; Gao, Q.; Tan, H. H.; Jagadish, C.; Zheng, C.; Etheridge, J. *Nano Lett.* **2015**, *15*, 1876−1882.
(125) Wang, W.; Xu, J. *ACS Appl. Mater. Interfaces* **2015**, *7*, 415−421.
(126) Tregnago, G.; Wykes, M.; Paternò, G. M.; Beljonne, D.; Cacialli, F. *J. Phys. Chem. C* **2015**, *119*, 11846.
(127) Prokhorov, A. M.; Hofbeck, T.; Czerwieniec, R.; Suleymanova, A. F.; Kozhevnikov, D. N.; Yersin, H. *J. Am. Chem. Soc.* **2014**, *136*, 9637−9642.
(128) Abdukayum, A.; Chen, J.-T.; Zhao, Q.; Yan, X.-P. *J. Am. Chem. Soc.* **2013**, *135*, 14125−14133.
(129) Wang, Y.-F.; Liu, G.-Y.; Sun, L.-D.; Xiao, J.-W.; Zhou, J.-C.; Yan, C.-H. *ACS Nano* **2013**, *7*, 7200−7206.

DOI: 10.1021/acs.analchem.5b04109
Anal. Chem. 2016, 88, 170−202

(130) Xie, X.; Gao, N.; Deng, R.; Sun, Q.; Xu, Q.-H.; Liu, X. *J. Am. Chem. Soc.* **2013**, *135*, 12608−12611.
(131) Chen, B.-C.; Legant, W. R.; Wang, K.; Shao, L.; Milkie, D. E.; Davidson, M. W.; Janetopoulos, C.; Wu, X. S.; Hammer, J. A.; Liu, Z.; English, B. P.; Mimori-Kiyosue, Y.; Romero, D. P.; Ritter, A. T.; Lippincott-Schwartz, J.; Fritz-Laylin, L.; Mullins, R. D.; Mitchell, D. M.; Bembenek, J. N.; Reymann, A.-C.; Böhme, R.; Grill, S. W.; Wang, J. T.; Seydoux, G.; Tulu, U. S.; Kiehart, D. P.; Betzig, E. *Science* **2014**, *346*, 346.
(132) Tanenbaum, M. E.; Gilbert, L. A.; Qi, L. S.; Weissman, J. S.; Vale, R. D. *Cell* **2014**, *159*, 635−646.
(133) Chung, H. S.; Eaton, W. A. *Nature* **2013**, *502*, 685−688.
(134) Chung, H. S.; Piana-Agostinetti, S.; Shaw, D. E.; Eaton, W. A. *Science* **2015**, *349*, 1504−1510.
(135) Speight, L. C.; Muthusamy, A. K.; Goldberg, J. M.; Warner, J. B.; Wissner, R. F.; Willi, T. S.; Woodman, B. F.; Mehl, R. A.; Petersson, E. J. *J. Am. Chem. Soc.* **2013**, *135*, 18806−18814.
(136) Wang, H.; Liu, J.; Han, A.; Xiao, N.; Xue, Z.; Wang, G.; Long, J.; Kong, D.; Liu, B.; Yang, Z. *ACS Nano* **2014**, *8*, 1475−1484.
(137) Lu, Y.; Lu, J.; Zhao, J.; Cusido, J.; Raymo, F. M.; Yuan, J.; Yang, S.; Leif, R. C.; Huo, Y.; Piper, J. A. *Nat. Commun.* **2014**, *5*, 5.
(138) Jahn, K.; Buschmann, V.; Hille, C. *Sci. Rep.* **2015**, *5*, 14334.
(139) Song, Y.; Zhu, S.; Xiang, S.; Zhao, X.; Zhang, J.; Zhang, H.; Fu, Y.; Yang, B. *Nanoscale* **2014**, *6*, 4676−4682.
(140) Penfold, T. J.; Karlsson, S.; Capano, G.; Lima, F. A.; Rittmann, J.; Reinhard, M.; Rittmann-Frank, M. H.; Braem, O.; Baranoff, E.; Abela, R.; Tavernelli, I.; Rothlisberger, U.; Milne, C. J.; Chergui, M. *J. Phys. Chem. A* **2013**, *117*, 4591−4601.
(141) Zhang, S.-R.; Du, D.-Y.; Qin, J.-S.; Bao, S.-J.; Li, S.-L.; He, W.-W.; Lan, Y.-Q.; Shen, P.; Su, Z.-M. *Chem. - Eur. J.* **2014**, *20*, 3589−3594.
(142) Li, Z.; Wang, Y.; Ni, Y.; Kokot, S. *Spectrochim. Acta, Part A* **2015**, *137*, 1213−1221.
(143) Ganiga, M.; Cyriac, J. *Anal. Methods* **2015**, *7*, 5412−5418.
(144) Galpothdeniya, W. I. S.; Das, S.; De Rooy, S. L.; Regmi, B. P.; Hamdan, S.; Warner, I. M. *RSC Adv.* **2014**, *4*, 17533−17540.
(145) Das, S.; Magut, P. K.; de Rooy, S. L.; Hasan, F.; Warner, I. M. *RSC Adv.* **2013**, *3*, 21054−21061.
(146) Palanimuthu, D.; Shinde, S. V.; Dayal, D.; Somasundaram, K.; Samuelson, A. G. *Eur. J. Inorg. Chem.* **2013**, *2013*, 3542−3549.
(147) Lin, W.; Buccella, D.; Lippard, S. J. *J. Am. Chem. Soc.* **2013**, *135*, 13512−13520.
(148) Liu, L.; Shao, Y.; Peng, J.; Huang, C.; Liu, H.; Zhang, L. *Anal. Chem.* **2014**, *86*, 1622−1631.
(149) Kumar, V.; Anslyn, E. V. *J. Am. Chem. Soc.* **2013**, *135*, 6338−6344.
(150) Wang, S.; Wang, X.; Zhang, Z.; Chen, L. *Colloids Surf., A* **2015**, *468*, 333−338.
(151) Guan, Y.-S.; Niu, L.-Y.; Chen, Y.-Z.; Wu, L.-Z.; Tung, C.-H.; Yang, Q.-Z. *RSC Adv.* **2014**, *4*, 8360−8364.
(152) Niu, L.-Y.; Guan, Y.-S.; Chen, Y.-Z.; Wu, L.-Z.; Tung, C.-H.; Yang, Q.-Z. *Chem. Commun. (Cambridge, U. K.)* **2013**, *49*, 1294−1296.
(153) Elbashir, A. A.; Ahmed, S.; Aboul-Enein, H. Y. *Luminescence* **2013**, *28*, 490−495.
(154) Shinde, M. A.; Divya, O. *Curr. Sci.* **2015**, *108*, 1348.
(155) Belal, T. S.; Mahrous, M. S.; Abdel-Khalek, M. M.; Daabees, H. G.; Khamis, M. M. *Luminescence* **2014**, *29*, 893−900.
(156) Divya, O.; Shinde, M. A. *Brazilian J. Anal. Chem.* **2013**, *10*, 468−475.
(157) Ragab, M. A.; Eman, I. *J. Fluoresc.* **2014**, *24*, 1745−1756.
(158) Sadrjavadi, K.; Shahlaei, M.; Bahrami, G.; Majnooni, M. B.; Mohebbi, M. *J. Iran. Chem. Soc.* **2015**, *12*, 967−977.
(159) Shcherbakova, E. G.; Minami, T.; Brega, V.; James, T. D.; Anzenbacher, P. *Angew. Chem., Int. Ed.* **2015**, *54*, 7130−7133.
(160) Jiao, L.; Deng, Q.; Wang, Y.; Li, H. *Anal. Lett.* **2013**, *46*, 831−843.
(161) Fakayode, S. O.; Taylor, A. M.; Myers, C. *Appl. Spectrosc.* **2012**, *66*, 999−1004.
(162) Sugisawa, E.; Miura, J.; Iwamoto, Y.; Uchigata, Y. *Diabetes Care* **2013**, *36*, 2339−2345.
(163) Spliethoff, J. W.; Evers, D. J.; Klomp, H. M.; van Sandick, J. W.; Wouters, M. W.; Nachabe, R.; Lucassen, G. W.; Hendriks, B. H.; Wesseling, J.; Ruers, T. J. *Lung cancer* **2013**, *80*, 165−171.
(164) Dankowska, A.; Małecka, M.; Kowalewski, W. *Dairy Sci. Technol.* **2015**, *95*, 413−424.
(165) Markechová, D.; Májek, P.; Sádecká, J. *Food Chem.* **2014**, *159*, 193−199.
(166) Liu, X.; Wan, Y. *Spectrochim. Acta, Part A* **2013**, *111*, 230−236.
(167) Vásquez, V.; Báez, M. E.; Bravo, M.; Fuentes, E. *Anal. Bioanal. Chem.* **2013**, *405*, 7497−7507.
(168) Verma, P.; Kumar, S. S.; Sawant, R.; Tomar, B.; Ramakumar, K. *J. Lumin.* **2014**, *153*, 162−168.
(169) Gidron, O.; Bendikov, M. *Angew. Chem., Int. Ed.* **2014**, *53*, 2546−2555.
(170) Everaerts, K.; Emery, J. D.; Jariwala, D.; Karmel, H. J.; Sangwan, V. K.; Prabhumirashi, P. L.; Geier, M. L.; McMorrow, J. J.; Bedzyk, M. J.; Facchetti, A. *J. Am. Chem. Soc.* **2013**, *135*, 8926−8939.
(171) Gather, M. C.; Yun, S. H. *Nat. Commun.* **2014**, *5*, 5722.
(172) Masai, H.; Terao, J.; Makuta, S.; Tachibana, Y.; Fujihara, T.; Tsuji, Y. *J. Am. Chem. Soc.* **2014**, *136*, 14714−14717.
(173) Mei, J.; Hong, Y.; Lam, J. W.; Qin, A.; Tang, Y.; Tang, B. Z. *Adv. Mater.* **2014**, *26*, 5429−5479.
(174) Anees, P.; Sreejith, S.; Ajayaghosh, A. *J. Am. Chem. Soc.* **2014**, *136*, 13233−13239.
(175) Abo, M.; Minakami, R.; Miyano, K.; Kamiya, M.; Nagano, T.; Urano, Y.; Sumimoto, H. *Anal. Chem.* **2014**, *86*, 5983−5990.
(176) Cao, S.-H.; Cai, W.-P.; Liu, Q.; Xie, K.-X.; Weng, Y.-H.; Huo, S.-X.; Tian, Z.-Q.; Li, Y.-Q. *J. Am. Chem. Soc.* **2014**, *136*, 6802−6805.
(177) Chen, T.; Hu, Y.; Cen, Y.; Chu, X.; Lu, Y. *J. Am. Chem. Soc.* **2013**, *135*, 11595−11602.
(178) McNeel, K. E.; Das, S.; Siraj, N.; Negulescu, I. I.; Warner, I. M. *J. Phys. Chem. B* **2015**, *119*, 8651−8659.
(179) Bollhorst, T.; Shahabi, S.; Wörz, K.; Petters, C.; Dringen, R.; Maas, M.; Rezwan, K. *Angew. Chem., Int. Ed.* **2015**, *54*, 118−123.
(180) Tian, J.; Ding, L.; Ju, H.; Yang, Y.; Li, X.; Shen, Z.; Zhu, Z.; Yu, J. S.; Yang, C. *Angew. Chem., Int. Ed.* **2014**, *53*, 9544−9549.
(181) Chen, L.-J.; Zhao, G.-Z.; Jiang, B.; Sun, B.; Wang, M.; Xu, L.; He, J.; Abliz, Z.; Tan, H.; Li, X. *J. Am. Chem. Soc.* **2014**, *136*, 5993−6001.
(182) Deshayes, S.; Cabral, H.; Ishii, T.; Miura, Y.; Kobayashi, S.; Yamashita, T.; Matsumoto, A.; Miyahara, Y.; Nishiyama, N.; Kataoka, K. *J. Am. Chem. Soc.* **2013**, *135*, 15501−15507.
(183) Duan, Q.; Cao, Y.; Li, Y.; Hu, X.; Xiao, T.; Lin, C.; Pan, Y.; Wang, L. *J. Am. Chem. Soc.* **2013**, *135*, 10542−10549.
(184) Guo, J.; Zhuang, J.; Wang, F.; Raghupathi, K. R.; Thayumanavan, S. *J. Am. Chem. Soc.* **2014**, *136*, 2220−2223.
(185) He, X.; Li, Z.; Chen, M.; Ma, N. *Angew. Chem., Int. Ed.* **2014**, *53*, 14447−14450.
(186) Chen, H.; Ma, X.; Wu, S.; Tian, H. *Angew. Chem., Int. Ed.* **2014**, *53*, 14149−14152.
(187) Pollock, J. B.; Schneider, G. L.; Cook, T. R.; Davies, A. S.; Stang, P. J. *J. Am. Chem. Soc.* **2013**, *135*, 13676−13679.
(188) Zhou, J.; Xu, X.; Liu, W.; Liu, X.; Nie, Z.; Qing, M.; Nie, L.; Yao, S. *Anal. Chem.* **2013**, *85*, 5746−5754.
(189) Zhou, Z.; Tan, C.; Zheng, Y.; Wang, Q. *Sens. Actuators, B* **2013**, *188*, 1176−1182.
(190) Zeigler, M. B.; Sun, W.; Rong, Y.; Chiu, D. T. *J. Am. Chem. Soc.* **2013**, *135*, 11453−11456.
(191) Yang, B.; Zhang, X.-B.; Kang, L.-P.; Shen, G.-L.; Yu, R.-Q.; Tan, W. *Anal. Chem.* **2013**, *85*, 11518−11523.
(192) Zhang, D.; Fu, R.; Zhao, Q.; Rong, H.; Wang, H. *Anal. Chem.* **2015**, *87*, 4903−4909.
(193) Huang, H.; Wei, H.; Zou, M.; Xu, X.; Xia, B.; Liu, F.; Li, N. *Anal. Chem.* **2015**, *87*, 2748−2754.
(194) Zhen, S. J.; Yu, Y.; Li, C. M.; Huang, C. Z. *Analyst* **2015**, *140*, 353−357.

DOI: 10.1021/acs.analchem.5b04109
Anal. Chem. 2016, 88, 170−202

(195) Lan, X.; Lu, X.; Shen, C.; Ke, Y.; Ni, W.; Wang, Q. *J. Am. Chem. Soc.* **2015**, *137*, 457−462.
(196) Amaral, N. B.; Zuliani, S.; Guieu, V.; Ravelet, C.; Perrier, S.; Peyrin, E. *Anal. Bioanal. Chem.* **2014**, *406*, 1173−1179.
(197) Pahari, B. P.; Chaudhuri, S.; Chakraborty, S.; Sengupta, P. K. *J. Phys. Chem. B* **2015**, *119*, 2533−2545.
(198) Wang, L.; Clifford, B.; Graybeal, L.; Tolley, L.; McCarroll, M. E. *J. Fluoresc.* **2013**, *23*, 881−888.
(199) Cohen, N.; Mechaly, A.; Mazor, O.; Fisher, M.; Zahavy, E. *J. Fluoresc.* **2014**, *24*, 795−801.
(200) Doeven, E. H.; Barbante, G. J.; Kerr, E.; Hogan, C. F.; Endler, J. A.; Francis, P. S. *Anal. Chem.* **2014**, *86*, 2727−2732.
(201) Zhou, Y.; Gao, H.; Wang, X.; Qi, H. *Inorg. Chem.* **2015**, *54*, 1446−1453.
(202) Azizi, S. N.; Shakeri, P.; Chaichi, M. J.; Bekhradnia, A.; Taghavi, M.; Ghaemy, M. *Spectrochim. Acta, Part A* **2014**, *122*, 482−488.
(203) Tang, Y.; Su, Y.; Yang, N.; Zhang, L.; Lv, Y. *Anal. Chem.* **2014**, *86*, 4528−4535.
(204) Dong, S.; Liu, F.; Lu, C. *Anal. Chem.* **2013**, *85*, 3363−3368.
(205) Ma, L.; Sun, Y.; Kang, X.; Wan, Y. *Biosens. Bioelectron.* **2014**, *61*, 165−171.
(206) Zhang, P.; Xue, Z.; Luo, D.; Yu, W.; Guo, Z.; Wang, T. *Anal. Chem.* **2014**, *86*, 5620−5623.
(207) Zhang, R.; Hu, Y.; Li, G. *Anal. Chem.* **2014**, *86*, 6080−6087.
(208) Wu, L.; Wang, J.; Ren, J.; Li, W.; Qu, X. *Chem. Commun.* **2013**, *49*, 5675−5677.
(209) Nepomnyashchii, A. B.; Parkinson, B. A. *ACS Appl. Mater. Interfaces* **2014**, *6*, 14881−14885.
(210) Wang, Z.; Teng, X.; Lu, C. *Anal. Chem.* **2015**, *87*, 3412−3418.
(211) Yu, Y.; Lu, C.; Zhang, M. *Anal. Chem.* **2015**, *87*, 8026−8032.
(212) Zhang, L.; He, N.; Lu, C. *Anal. Chem.* **2015**, *87*, 1351−1357.
(213) Dong, S.; Zhong, J.; Lu, C. *Anal. Chem.* **2014**, *86*, 7947−7953.
(214) Jang, J.; Lee, W.-Y. *J. Electroanal. Chem.* **2015**, *736*, 55−60.
(215) Fan, F.; Shen, H.; Zhang, G.; Jiang, X.; Kang, X. *Clin. Chim. Acta* **2014**, *431*, 113−117.
(216) Chen, Y.; Spiering, A.; Karthikeyan, S.; Peters, G. W.; Meijer, E.; Sijbesma, R. P. *Nat. Chem.* **2012**, *4*, 559−562.
(217) Lee, A.; Chin, J.; Park, O. K.; Chung, H.; Kim, J. W.; Yoon, S.-Y.; Park, K. *Chem. Commun.* **2013**, *49*, 5969−5971.
(218) Wang, J.; Chen, H.; Zhang, P.; Zhang, Z.; Zhang, S.; Kong, J. *Talanta* **2013**, *114*, 204−210.
(219) Khan, F.; Pickup, J. C. *Biochem. Biophys. Res. Commun.* **2013**, *438*, 488−492.
(220) Chen, Y.; Wang, J. *Anal. Biochem.* **2013**, *442*, 196−204.
(221) Yu, J.; Zhang, X.; Hao, X.; Zhang, X.; Zhou, M.; Lee, C.-S.; Chen, X. *Biomaterials* **2014**, *35*, 3356−3364.
(222) Kraft, J. C.; Ho, R. J. *Biochemistry* **2014**, *53*, 1275−1283.
(223) Cui, M.; Ono, M.; Watanabe, H.; Kimura, H.; Liu, B.; Saji, H. *J. Am. Chem. Soc.* **2014**, *136*, 3388−3394.
(224) Zhao, C.; Li, K.; Xie, N.; Zhao, M.; Peng, S. *J. Photochem. Photobiol., A* **2014**, *290*, 72−76.
(225) Liu, S.; Pang, S.; Huang, H.; Su, X. *Analyst* **2014**, *139*, 5852−5857.
(226) Ling, X.; Zhang, S.; Shao, P.; Li, W.; Yang, L.; Ding, Y.; Xu, C.; Stella, N.; Bai, M. *Biomaterials* **2015**, *57*, 169−178.
(227) Pennacchio, A.; Varriale, A.; Esposito, M. G.; Staiano, M.; D'Auria, S. *Anal. Biochem.* **2015**, *481*, 55−59.
(228) Hou, T.-C.; Wu, Y.-Y.; Chiang, P.-I.; Tan, K.-T. *Chem. Sci.* **2015**, *6*, 4643−4649.
(229) Pan, X.; Wang, X.; Wang, L.; Xu, K.; Kong, F.; Tang, B. *Anal. Chem.* **2015**, *87*, 7092−7097.
(230) Lu, L.; Lv, F.; Cao, B.; He, X.; Liu, T. *Molecules* **2014**, *19*, 525−537.
(231) Li, G.; Xing, Y.; Wang, J.; Conti, P. S.; Chen, K. *Amino Acids* **2014**, *46*, 1547−1556.
(232) Dinjaski, N.; Suri, S.; Valle, J.; Lehman, S. M.; Lasa, I.; Prieto, M. A.; García, A. J. *Acta Biomater.* **2014**, *10*, 2935−2944.
(233) Rüger, R.; Tansi, F. L.; Rabenhold, M.; Steiniger, F.; Kontermann, R. E.; Fahr, A.; Hilger, I. J. *J. Controlled Release* **2014**, *186*, 1−10.
(234) Wu, J. B.; Shao, C.; Li, X.; Shi, C.; Li, Q.; Hu, P.; Chen, Y.-T.; Dou, X.; Sahu, D.; Li, W. *Biomaterials* **2014**, *35*, 8175−8185.
(235) Taratula, O.; Schumann, C.; Duong, T.; Taylor, K. L.; Taratula, O. *Nanoscale* **2015**, *7*, 3888−3902.
(236) Li, Y.; Sun, Y.; Li, J.; Su, Q.; Yuan, W.; Dai, Y.; Han, C.; Wang, Q.; Feng, W.; Li, F. *J. Am. Chem. Soc.* **2015**, *137*, 6407−6416.
(237) Das, S.; Magut, P. K.; Zhao, L.; Hasan, F.; Karki, A. B.; Jin, R.; Warner, I. M. *RSC Adv.* **2015**, *5*, 30227−30233.
(238) Wang, C.; Wang, C.; Xu, L.; Cheng, H.; Lin, Q.; Zhang, C. *Nanoscale* **2014**, *6*, 1775−1781.
(239) Zhao, T.; He, X.-W.; Li, W.-Y.; Zhang, Y.-K. *J. Mater. Chem. B* **2015**, *3*, 2388−2394.
(240) Jia, X.; Yang, X.; Li, J.; Li, D.; Wang, E. *Chem. Commun.* **2014**, *50*, 237−239.
(241) Gao, X.; Lu, Y.; Liu, M.; He, S.; Chen, W. *J. Mater. Chem. C* **2015**, *3*, 4050−4056.
(242) Wang, C.; Cheng, H.; Sun, Y.; Lin, Q.; Zhang, C. *ChemNanoMat* **2015**, *1*, 27−31.
(243) Qing, Z.; He, X.; Qing, T.; Wang, K.; Shi, H.; He, D.; Zou, Z.; Yan, L.; Xu, F.; Ye, X. *Anal. Chem.* **2013**, *85*, 12138−12143.
(244) Chen, C.-A.; Wang, C.-C.; Jong, Y.-J.; Wu, S.-M. *Anal. Chem.* **2015**, *87*, 6228−6232.
(245) Shang, L.; Stockmar, F.; Azadfar, N.; Nienhaus, G. U. *Angew. Chem., Int. Ed.* **2013**, *52*, 11154−11157.
(246) Chen, X.; Essner, J. B.; Baker, G. A. *Nanoscale* **2014**, *6*, 9594−9598.
(247) Ghosh, S.; Das, N. K.; Anand, U.; Mukherjee, S. *J. Phys. Chem. Lett.* **2015**, *6*, 1293−1298.
(248) Bauch, M.; Toma, K.; Toma, M.; Zhang, Q.; Dostalek, J. *Plasmonics* **2014**, *9*, 781−799.
(249) Ganguly, M.; Mondal, C.; Chowdhury, J.; Pal, J.; Pal, A.; Pal, T. *Dalton Transactions* **2014**, *43*, 1032−1047.
(250) Deng, W.; Xie, F.; Baltar, H. T.; Goldys, E. M. *Phys. Chem. Chem. Phys.* **2013**, *15*, 15695−15708.
(251) Geddes, C. D. *Phys. Chem. Chem. Phys.* **2013**, *15*, 19537−19537.
(252) Mao, J.; Blair, S. *J. Phys. D: Appl. Phys.* **2015**, *48*, 184008.
(253) Martin, J.; Plain, J. *J. Phys. D: Appl. Phys.* **2015**, *48*, 184002.
(254) Gérard, D.; Gray, S. K. *J. Phys. D: Appl. Phys.* **2015**, *48*, 184001.
(255) Watson, A. M.; Zhang, X.; Alcaraz de la Osa, R.; Sanz, J. M.; González, F.; Moreno, F.; Finkelstein, G.; Liu, J.; Everitt, H. O. *Nano Lett.* **2015**, *15*, 1095−1100.
(256) Yoshida, R.; Matsumura, T.; Nakahodo, T.; Fujihara, H. *Chem. Lett.* **2015**, *44*, 135−137.
(257) Zhang, Z.-Y.; Wang, H.-Y.; Du, J.-L.; Zhang, X.-L.; Hao, Y.-W.; Chen, Q.-D.; Sun, H.-B. *IEEE Photonics Technol. Lett.* **2015**, *27*, 821−823.
(258) Abel, B.; Coskun, S.; Mohammed, M.; Williams, R.; Unalan, H. E.; Aslan, K. *J. Phys. Chem. C* **2015**, *119*, 675−684.
(259) Shtoyko, T.; Raut, S.; Rich, R. M.; Sronce, R. J.; Fudala, R.; Mason, R. N.; Akopova, I.; Gryczynski, Z.; Gryczynski, I. *ACS Appl. Mater. Interfaces* **2014**, *6*, 18780−18787.
(260) Kinoshita, T.; Nguyen, D. Q.; Nishino, T.; Nakao, H.; Shiigi, H.; Nagaoka, T. *Anal. Sci.* **2015**, *31*, 487−493.
(261) Karolin, J.; Geddes, C. *Appl. Phys. Lett.* **2014**, *105*, 063102.
(262) Hamo, H. B.; Karolin, J.; Mali, B.; Kushmaro, A.; Marks, R.; Geddes, C. D. *Appl. Phys. Lett.* **2015**, *106*, 081605.
(263) Dragan, A. I.; Mali, B.; Geddes, C. D. *Chem. Phys. Lett.* **2013**, *556*, 168−172.
(264) Prajapati, R.; Chatterjee, S.; Bhattacharya, A.; Mukherjee, T. K. *J. Phys. Chem. C* **2015**, *119*, 13325−13334.
(265) Abualnaja, K. M.; Šiller, L.; Horrocks, B. R. *Nanotechnology* **2015**, *26*, 145704.
(266) Schmitz, R. D.; Karolin, J. O.; Geddes, C. D. *Chem. Phys. Lett.* **2015**, *622*, 124−127.

DOI: 10.1021/acs.analchem.5b04109
Anal. Chem. 2016, 88, 170−202

(267) Sorokin, A. V.; Zabolotskii, A. A.; Pereverzev, N. V.; Bespalova, I. I.; Yefimova, S. L.; Malyukin, Y. V.; Plekhanov, A. I. *J. Phys. Chem. C* **2015**, *119*, 2743−2751.
(268) Sorokin, A. V.; Zabolotskii, A. A.; Pereverzev, N. V.; Yefimova, S. L.; Malyukin, Y. V.; Plekhanov, A. I. *J. Phys. Chem. C* **2014**, *118*, 7599−7605.
(269) Mishra, H.; Mali, B. L.; Karolin, J.; Dragan, A. I.; Geddes, C. D. *Phys. Chem. Chem. Phys.* **2013**, *15*, 19538−19544.
(270) Karolin, J.; Geddes, C. D. *Phys. Chem. Chem. Phys.* **2013**, *15*, 15740−15745.
(271) Hu, B.; Cao, X.; Nahan, K.; Caruso, J.; Tang, H.; Zhang, P. *J. Mater. Chem. B* **2014**, *2*, 7073−7081.
(272) Poorkazem, K.; Hesketh, A. V.; Kelly, T. L. *J. Phys. Chem. C* **2014**, *118*, 6398−6404.
(273) Wang, C.-Y.; Huang, K.-S.; Chang, S.-C.; Yang, C.-H. *Curr. Proteomics* **2014**, *11*, 86−91.
(274) Chang, Y.-F.; Tsao, K.-C.; Liu, Y.-C.; Chen, Y.-C.; Yu, P.-C.; Huang, Y.-C.; Chou, C. *J. Virol. Methods* **2015**, *213*, 151−156.
(275) Joshi, L. T.; Mali, B. L.; Geddes, C. D.; Baillie, L. *PLoS One* **2014**, *9* (8), e104334.
(276) Melendez, J. H.; Huppert, J. S.; Jett-Goheen, M.; Hesse, E. A.; Quinn, N.; Gaydos, C. A.; Geddes, C. D. *J. Clin. Microbiol.* **2013**, *51*, 2913−2920.

DOI: 10.1021/acs.analchem.5b04109
Anal. Chem. 2016, 88, 170−202